Wind turbine control algorithms

DOWEC-F1W1-EH-03-094/0

E.L. van der Hooft; P. Schaak; T.G. van Engelen

December 2003

Abstract

The objective of DOWEC task 3 of work package 1 has been defined as 'research and development of wind turbine (power) control algorithms to maximize energy yield and reduction of turbine fatigue load, and its optimisation for offshore operation'. In accordance with the DOWEC baseline turbine and the related DOWEC turbine all activities were focused on active pitch to vane, variable speed concept. The results of this task contribute to the:

- set-up of a modular control structure based on theoretical analysis and industrial needs;
- increase of turbine performance (power production, load reduction) by additional control features and actions.

It can be concluded that the control structure is superior to ordinary PD feedback control of the rotor speed. An independent comparison for the DOWEC turbine using an aerodynamic code, with a state-of-the-art control structure, has resulted in improvements concerning:

- extreme fore-aft tower bending moment (-40%);
- fatigue fore-aft tower bottom bending equivalent moment (-50%);
- variations in blade pitch rate (standard dev. -0.65 dg/s);
- tilt moment (-10%).

The mean power production (10min) in above rated wind speeds was over 99% of its rated value. Opposite to the improvements it has brought about larger variations in generator speed (standard dev. +0.5 rpm), increase of yaw moment (12%) and radial blade forces (14%).

The underlying approach of the control structure divides the multivariable wind turbine system into different independent scalar subsystems by band filtering. As a consequence the resulting setpoints, the pitch rate and electric torque, consist of additive contributions of the different control actions.

Concerning power control, ordinary rotor speed feedback has proved to be a robust core. However, valuable extensions were developed by wind speed feed forward control (pitch control) and optimisation around rated condition (electric torque control).

Promising results have been achieved on fore-aft tower damping by pitch control. Electric torque control has enabled considerable damping results of (collective) drive train resonances and possibilities for badly damped sideward tower vibrations.

Keywords:
DOWEC, Wind turbine control, Pitch Control, Power Control, Torque Control, Variable speed control

Acknowledgment

This report is issued within the framework of the DOWEC project, supported by the EET programme of the Dutch Ministry of Economic Affairs.

Unfortunately, only one author can be the first author of a report, in this case three would have been much better.

My colleague, Pieter Schaak, has contributed to a large extend to the results of this report, by performing the research and development on powerful optimisation around rated conditions (subsection 3.4.2), reduction of tower loading (section 5.2 and 5.3) and a final simulation case (chapter 4).

My other colleague, Tim van Engelen, has been involved intensely by drive train damping (section 5.1), and his contributions on turbine modelling, wind and wave dynamics (chapter 2) have been appeared to be indispensible.

As a task leader of DOWEC-WP1-task 3, my contributions were focussed on reporting, task management, supporting DOWEC control activities [3] and the development of wind speed feed forward control (subsection 3.2.5).

Finally, Ben Hendriks is acknowledged for DOWEC project management and his kind attitude towards wind turbine control.

Eric van der Hooft,
Petten, December 18th, 2003

.

CONTENTS

1 INTRODUCTION

The objective of DOWEC task 3 of work package 1 has been defined as 'research and development of wind turbine (power) control algorithms to maximize energy yield and reduction of turbine load fatigue, and its optimisation for offshore operation'. In accordance with the DOWEC baseline turbine all activities were focused on the active pitch to vane, variable speed concept. The workplan of this task define the following activities, from which the results will be decribed in this report:

- Development and evaluation of power control algorithms;
  - Active pitch control;
  - Torque setpoint control;
- Control strategies to reduce tower and drive train resonance;
- Verification of the algorithm with state-of-the-art control.

The last item has led to use a typical DOWEC turbine in this report for a comparision study by the DOWEC partner NEG-Micon Holland. Due to the confidentiality of this study, only general results related to the DOWEC algorithm will be reported. The modelling of this prevailing turbine concept and external influences is decribed in chapter 2.

Based on these (quasi) linear models, feedback control structures for power control (chapter 3) and load reduction (chapter 5) are developed. The power control results are verified in chapter 4.

As depicted in fig.(1.1), the control structure comprises *two control modes* (below and above rated wind speed) and *two actuation ports* (pitch rate and electric torque). Although, pitch

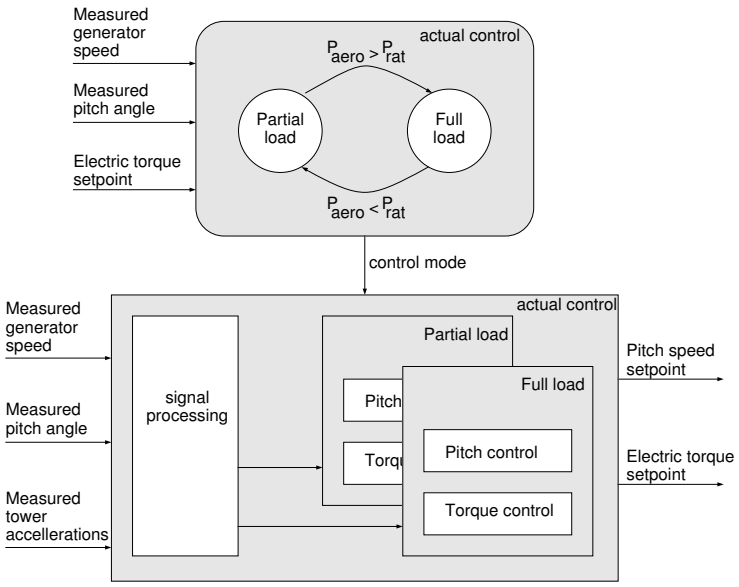

Figure 1.1: *Functional control structure*

and electric torque control are discussed in separated sections (section 3.2+3.3 and section 3.4 respectively), their mutual interaction appears to be an important issue (subsection 3.4.2).

In the underlying approach of the control structure, the multivariable wind turbine system is divided into different independent scalar subsystems by band filtering. As a consequence the resulting setpoints to the actuation systems, pitch rate and electric torque, consists of additive contributions of the different control actions (fig.(1.2)).

During full load operation, ordinary rotor speed feedback control by pitch actuation and constant (rated) power control by electric torque actuation, still remains a robust core of the control

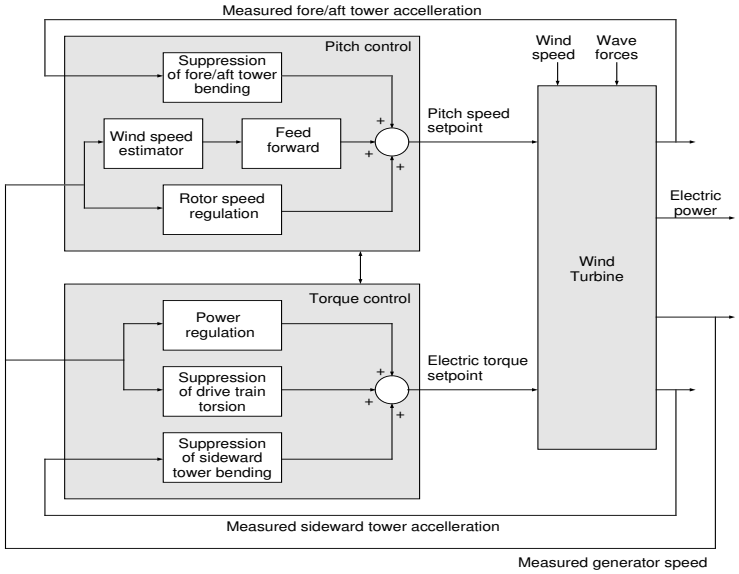

Figure 1.2: *Functional full load control structure*

structure. Improvements to power control will be achieved by additional control features (subsection 3.2.1 ... 3.2.4), estimated wind speed feed forward (subsection 3.2.5) and power optimisation around rated conditions (subsection 3.4.2). In order to reduce turbine loading, more high frequent *electric torque variations* can be used to reduce drive train resonances (section 5.1) and sideward tower vibrations (section 5.3), while *pitch speed variations* enable additional damping possibilities concerning fore-aft tower resonances (section 5.2).

2 MODELLING THE DOWEC TURBINE

This chapter will characterise and specify a typical DOWEC turbine in general terms (section 2.1) and describe the basis of a suitable turbine model for design of control algorithms (section 2.2). Models of disturbing phenomena, wind speed and wave forces, (section 2.3) are also described for the verification of dynamic behaviour by time domain simulations in chapter 4.

2.1 System description

In this section the DOWEC turbine is described in general terms. The DOWEC turbine is a three bladed variable speed turbine with pitch to vane actuation. This concept implies that electric torque and the pitch angle should set to suitable values in order to control electric power and rotor speed and to minimise loading.

Table(2.1) summarizes all relevant DOWEC data and constants. If not mentioned explicitly, these values have been used in the next chapters for turbine modelling (section 2.2) and design of control algorithms (chapter 3). Because of confidentiality reasons only general parameters and dimensions are listed. In case of other parameters or data, only normalised values or abstract variables will be used.

2.2 Wind turbine subsystems

In this section a suitable general model for the development of control algorithms of a variable speed, active pitch to vane turbine (as the DOWEC turbine) is derived. Fig.(2.1), shows the mutual relationships of five physical sub-systems which will be discussed separately in more detail in the next sub-sections:

- rotor aerodynamic conversion (2.2.1);
- rotating mechanical system (2.2.2);
- tower dynamics (2.2.3);
- electric conversion system (2.2.4);
- pitch actuation system (2.2.5).

Fig.(2.1) shows two actuation ports (pitch speed and electric torque) for control purposes, two external disturbing influences (wind speed and wave forces) and five measurable output ports (tower top acceleration in fore-aft and sideward direction, rotor speed, electric power, pitch angle).

2.2.1 Rotor aerodynamics

In addition the conversion process from wind speed to aerodynamic torque and thrust force (aerodynamic conversion), it is proven that the behaviour of the rotor wake is also of importance for control design (dynamic inflow).

Aerodynamic conversion The aerodynamic conversion proces of the turbine rotor is approximated with quasi stationary non linear equations for aerodynamic torque and thrust force

$$T_{\mathrm{a}} = C_{\mathrm{q}}(\lambda,\theta)\cdot\tfrac{1}{2}\rho_{\mathrm{air}}\pi R_{\mathrm{b}}^3\cdot(V_{\mathrm{w}}-\dot{x}_{\mathrm{nd}})^2 \quad (2.1)$$

$$F_{\mathrm{a}} = C_{\mathrm{t}}(\lambda,\theta)\cdot\tfrac{1}{2}\rho_{\mathrm{air}}\pi R_{\mathrm{b}}^2\cdot(V_{\mathrm{w}}-\dot{x}_{\mathrm{nd}})^2 \quad (2.2)$$

with the tip to wind speed ratio, λ :

$$\lambda = \frac{\Omega_{\mathrm{r}}\cdot R_{\mathrm{b}}}{(V_{\mathrm{w}}-\dot{x}_{\mathrm{nd}})} \quad (2.3)$$

Table 2.1: *DOWEC turbine data and constants used for pitch control design*

General design and operational data				
Description	Symbol	Value	Unit	Remarks
Design wind class	WTGS	3	-	IEC 61400-1
Turbulence intensity	I_{15}	16	-	IEC 61400-1
Wind shear coefficient	$\alpha_{\rm sh}$	0.1	-	IEC 61400-1
Rated electric power	$P_{\rm e}^{\rm rat}$	2750	W	
Rated wind speed	$V_{\rm w}^{\rm rat}$	12.3	$\rm m/s$	
Rated rotor speed	$\Omega_{\rm r}^{\rm rat}$	15.57	$\rm m/s$	
Annual wind speed	$V_{\rm w}^{\rm annual}$	9.5	$\rm m/s$	at hub height
Cut in wind speed	$V_{\rm w}^{\rm ci}$	4	$\rm m/s$	
Cut out wind speed	$V_{\rm w}^{\rm co}$	25	$\rm m/s$	10 min. average
Gravity constant	g	9.83	$\rm m/s^2$	
Air density	$\rho_{\rm air}$	1.225	$\rm kg/m^3$	
Steel density	$\rho_{\rm steel}$	8e3	$\rm kg/m^3$	
Steel elasticity modulus	$E_{\rm steel}$	210e9	$\rm N/m^2$	
Rotor data				
Number of blades	B	3	-	
Rotor radius	$R_{\rm b}$	46	m	tip to center
Rotor inertia	$J_{\rm r}$	12.6e6	$\rm kgm^2$	
Rotor tilt angle	$\alpha_{\rm tilt}$	5	$^{\rm o}$	
Rotor cone angle	$\alpha_{\rm cone}$	0	$^{\rm o}$	
Power coefficient curves	$C_{\rm p}(\lambda,\theta)$	fig.(2.2)	-	
Thrust coefficient curves	$C_{\rm t}(\lambda,\theta)$	fig.(2.2)	-	
Shaft efficiency	$\eta_{\rm sh}$	0.97 n	-	bearing effcy
Generator and nacelle data				
Generator inertia	$J_{\rm g}$	239	$\rm kgm^2$	
Synchrounous speed	$\Omega_{\rm g}^{\rm syn}$	14.155	rpm	slow shaft eq
Maximum generator speed	$\Omega_{\rm g}^{\rm max}$	18.402	rpm	
Minimum generator speed	$\Omega_{\rm g}^{\rm min}$	9.909	rpm	
Total nacelle weight	$m_{\rm nac}$	1.2e5	kg	incl rotor
Transmission data				
Gearbox ratio	$i_{\rm gb}$	70.65	-	
Collective res frequency	$\omega_0^{\rm d}$	2.3	Hz	Phatas
Tower data				
Hub height	$Z_{\rm t}$	94	m	
Tower top diameter	$d_{\rm tw}^{\rm top}$	2.52	m	
Tower base diameter	$d_{\rm tw}^{\rm base}$	4.2	m	
Tower resonance frequency	$f_{\rm 0t}$	0.35	Hz	
Pitch control data				
Cycle time	$T_{\rm c}$	0.1	s	
Pitching speed at start-up	$\dot{\theta}^{\rm strt}$	0.5	$^{\rm o}/\rm s$	
Max. pitch speed full	$\dot{\theta}^{\rm full}$	4.0	$^{\rm o}/\rm s$	
Max. pitch speed emergency	$\dot{\theta}^{\rm emg}$	10.0	$^{\rm o}/\rm s$	
Maximum pitch angle	$\theta_{\rm wtb}^{\rm max}$	90	$^{\rm o}$	
Minimum pitch angle	$\theta_{\rm wtb}^{\rm min}$	-2.5	$^{\rm o}$	

In eq.(2.1) the reference of the tower top displacement speed, $\dot{x}_{\rm nd}$, is related to the mean wind speed, $\overline{V}_{\rm w}$ in longitudinal sense.
The torque coefficient $C_{\rm q}$ can be derived from the power coefficient $C_{\rm p}$ by

$$C_{\rm q}(\lambda,\theta) = C_{\rm p}(\lambda,\theta)/\lambda. \tag{2.4}$$

Both $C_{\rm p}$, $C_{\rm t}$ and $C_{\rm q}$ are dependent of the tip to wind speed ratio λ and the pitch angle θ . For the DOWEC rotor, the power and thrust coefficient characteristics are shown in fig.(2.2).

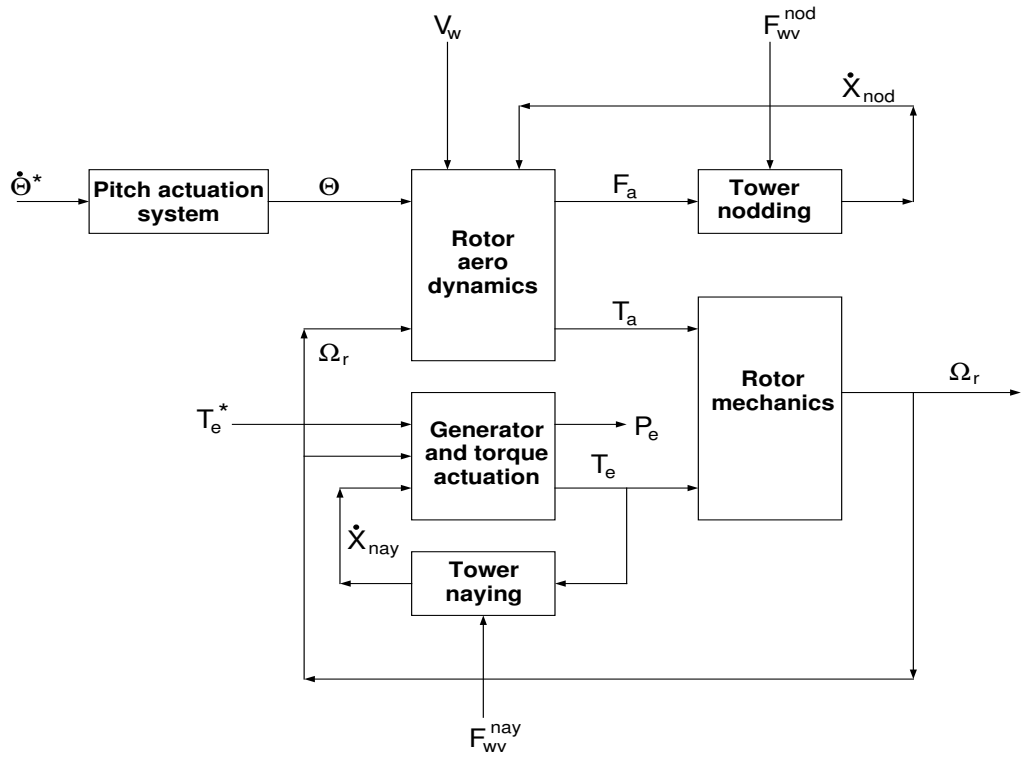

Figure 2.1: *Sub-systems of wind turbine model*

Dynamic inflow To deal with dynamic wake effects the quasi stationary approach as described before has to be extended. Due to wake effects or 'dynamic inflow effects', each variation in the pitch angle θ , the rotor speed $\Omega_{\rm r}$ or the wind speed $V_{\rm w}$ will temporarily cause different aerodynamic torque $T_{\rm a}$ and thrust force values $F_{\rm a}$, than those calculated from the power- and thrust coefficients $C_{\rm p}$, $C_{\rm t}$ in eq.(2.1) and (2.2).

The physical background of this phenomenon is found in the conservative nature of the rotor wake. The axial induction speed along the rotor radius is mainly responsible for the behaviour to maintain the current wake state. Therefore, each variation in the pitch angle, the rotor speed or the wind speed will result in a dynamic transition from the old 'frozen wake state' to its equilibrium wake state [7].

Based on the 'ECN cylindrical wake model' as presented in [7], a linearised correction principle has been derived in [8] to correct the stationary power and the thrust coefficients curves for dynamic inflow effects. This correction consists of a so called 'lead-lag' filter which affects the actual pitch angle [1] such, that the 'lead-lag filtered value of the pitch angle' causes an approximately similar effect on both the aerodynamic torque and the axial force as should be achieved if momentum wake effects were calculated by axial momentum theory. Therefore, eq.(2.1) and (2.2) are modified as shown in eq.(2.5) and (2.6),

$$T_{\rm a} = C_{\rm q}(\lambda, \theta^{\rm DI}_{\rm T_a}) \cdot \tfrac{1}{2}\rho_{\rm air}\pi R_{\rm b}^3 \cdot (V_{\rm w} - \dot{x}_{\rm nd})^2 \quad (2.5)$$

$$F_{\rm a} = C_{\rm t}(\lambda, \theta^{\rm DI}_{\rm F_a}) \cdot \tfrac{1}{2}\rho_{\rm air}\pi R_{\rm b}^2 \cdot (V_{\rm w} - \dot{x}_{\rm nd})^2 \quad (2.6)$$

in which $\theta^{\rm DI}_{\rm T_a}$ and $\theta^{\rm DI}_{\rm F_a}$ are respectively the lead-lag filtered values of the pitch angle for aerodynamic torque and axial force. The lead-lag filter dynamics are described by eq.(2.7) and (2.8).

$$\tau^{\rm DI}_{\rm lg} \cdot \dot{\theta}^{\rm DI}_{\rm T_a} + \theta^{\rm DI}_{\rm T_a} = \tau^{\rm DI}_{\rm ld,T_a} \cdot \dot{\theta} + \theta \quad (2.7)$$

[1] Only dynamic effects caused by the variations of the pitch angle are taken into account, it can be proven that effects due to rotor speed and wind speed variations are negligible with respect to pitch angle variations

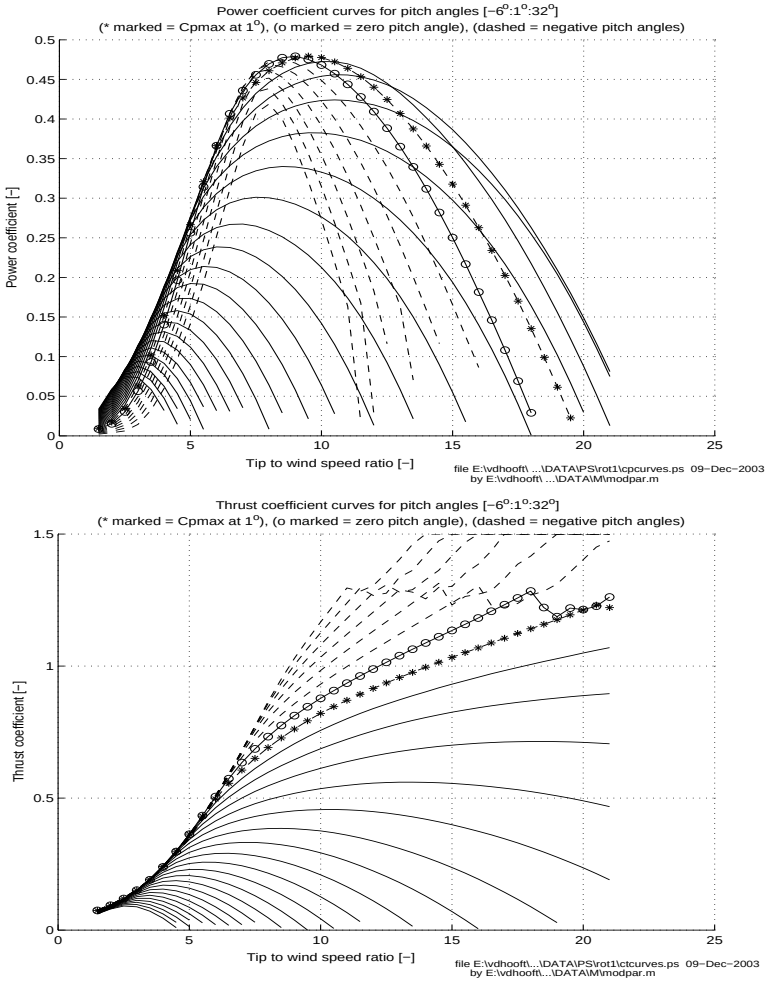

Figure 2.2: *Power- en thrust coefficient curves of the DOWEC turbine*

$$\tau_{\rm lg}^{\rm DI} \cdot \dot{\theta}_{\rm F_a}^{\rm DI} + \theta_{\rm F_a}^{\rm DI} \quad = \quad \tau_{\rm ld,F_a}^{\rm DI} \cdot \dot{\theta} + \theta \tag{2.8}$$

The non linear behaviour of the dynamic inflow effects are incorporated by scheduling of the time constants $\tau_{\rm lg}^{\rm DI}$, $\tau_{\rm ld,T_a}^{\rm DI}$ and $\tau_{\rm ld,F_a}^{\rm DI}$ to the 'rotor uniform wind speed' (see 2.3.1). The lagging time constant, $\tau_{\rm lg}^{\rm DI}$, is equal for both the aerodynamic torque and the axial force filtering. Fig.(2.3) shows that the value of these time constants are considerable in the low wind speed region.

The initial gain for stepwise pitch angle variations varies between $\tau_{\rm ld,T_a}^{\rm DI}/\tau_{\rm lg}^{\rm DI} \sim 1.1 \ldots 1.6$ for the aerodynamic torque and between $\tau_{\rm ld,F_a}^{\rm DI}/\tau_{\rm lg}^{\rm DI} \sim 1.1 \ldots 1.3.$ for the axial force. Especially, in the low speed region the dynamic inflow effect is considerable, this is shown in fig.(2.4)

2.2.2 Rotating mechanical system

The turbine rotor will accelerate or decelerate if there's a difference between aerodynamic torque, $T_{\rm a}$ and electric torque, $T_{\rm e}$. The rotor is assumed to be stiff connected to the low-speed main shaft, which is elastically coupled via the gearbox with the high-speed generator-side.

In [8] the mechanical equations of this rotating system were described by a second order equation for shaft torsion and a first order equation for rotor speed, eq.(2.10)

$$\frac{J_{\rm r} \cdot J_{\rm g}}{J_{\rm r} + J_{\rm g}} \cdot (\ddot{\gamma}_{\rm sh}) \quad = \quad -c_{\rm d} \cdot \gamma_{\rm sh} - k_{\rm d} \cdot \dot{\gamma}_{\rm sh} + \frac{J_{\rm g}}{J_{\rm r} + J_{\rm g}} \cdot (T_{\rm a} - T_{\rm l}) + \frac{J_{\rm r}}{J_{\rm r} + J_{\rm g}} \cdot T_{\rm e} \tag{2.9}$$

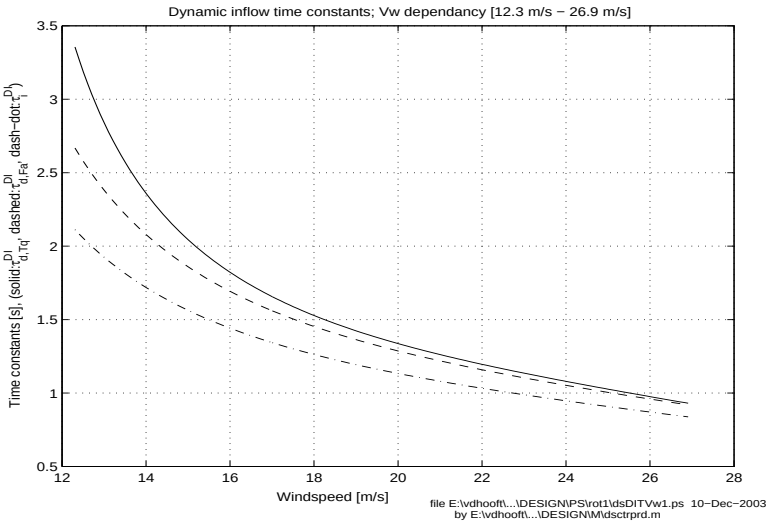

Figure 2.3: *Non linear dependency of the lead-lag time constants to the wind speed, solid line:* $\tau^{\mathrm{DI}}_{\mathrm{ld,T_a}}$ *; dashed line:*$\tau^{\mathrm{DI}}_{\mathrm{ld,F_a}}$ *; dotted line:* $\tau^{\mathrm{DI}}_{\mathrm{lg}}$

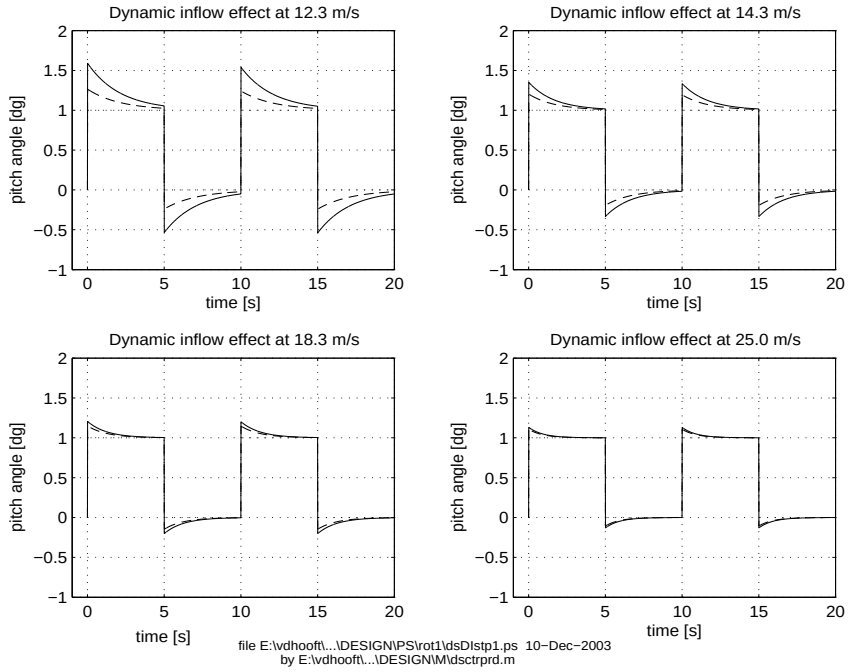

Figure 2.4: *Dynamic inflow effect on aerodynamic torque (solid line) and thrust force (dashed line) on 0.1Hz unity step shaped pitch angle excitation at wind speeds of 12.3 m/s (upper left), 14.3 m/s (upper right), 18.3 m/s (lower left) and 25 m/s (lower right)*

$$J_{\mathrm{g}} \cdot \dot{\Omega}_{\mathrm{g}} \quad = \quad c_{\mathrm{d}} \cdot \gamma_{\mathrm{sh}} + k_{\mathrm{d}} \cdot \dot{\gamma}_{\mathrm{sh}} - T_{\mathrm{e}}, \tag{2.10}$$

where γ_{sh} , $\dot{\gamma}_{\mathrm{sh}}$, $\ddot{\gamma}_{\mathrm{sh}}$ are shaft torsion angle, -speed, -acceleration respectively. The torsion angle is defined as $\gamma_{\mathrm{sh}} = \int(\Omega_{\mathrm{r}} - \Omega_{\mathrm{g}})\mathrm{d}t$. The moments of inertia J_{g} and J_{r} are related to the slow shaft side. Aerodynamic losses consist of a constant part ('Coulomb friction') and a speed dependent part ('rotation losses'):

$$T_{\mathrm{l}} = C_{\mathrm{c}} + C_{\Omega_{\mathrm{r}}} \cdot \Omega_{\mathrm{r}} \tag{2.11}$$

For the DOWEC turbine, only the rotation losses were determined, C_{Ω_r} = 32 kNm/(rad/s) by using the overall efficiency at rated conditions.

The resonance frequency $\omega_0^{\rm d}$ and the damping rate $\beta_{\rm d}$ of the drive train are linked to the torsion stiffness $c_{\rm d}$ and the damping constant $k_{\rm d}$ as given in eq.(2.12) and 2.13:

$$\omega_0^{\rm d} = \sqrt{\frac{c_{\rm d}}{J_{\rm r} \cdot J_{\rm g}/(J_{\rm r}+J_{\rm g})}} \tag{2.12}$$

$$\beta_{\rm d} = \frac{k_{\rm d}}{2\sqrt{c_{\rm d} \cdot J_{\rm r} \cdot J_{\rm g}/(J_{\rm r}+J_{\rm g})}} \tag{2.13}$$

The stiffness and damping parameter $c_{\rm d}$ and $k_{\rm d}$ can be chosen such that they represent the first coupled drive-train / collective lead-lag blade vibration mode. This coupled mode appears to dominate the inplane vibration behaviour (subsection 5.1.1).

Because the generator stator and the gearbox-housing are assumed to be rigid connected to the nacelle frame, there will be a reaction torque. Based on conservation of energy just before the rotor-side gearbox through the generator, in [8] it was derived that:

$$T_{\rm nac} = \frac{i_{\rm gb} \pm 1}{i_{\rm gb}} \cdot J_{\rm g} \cdot \dot{\Omega}_{\rm g} + T_{\rm e} \tag{2.14}$$

All quantities in eq.(2.14) are slow-scale related. The gearbox ratio is introduced by $i_{\rm gb}$. The minus-sign shall be used if both shafts are designed to rotate in the same direction.

If a stiff coupling is assumed between rotor and generator, then $\Omega_{\rm r}$ = $\Omega_{\rm g}$ and the mechanical equation of the drive system can be simplified considerably to (eq.(2.15))

$$J_{\rm t} \cdot \dot{\Omega}_{\rm r} = T_{\rm a} - T_{\rm l} - T_{\rm e} \tag{2.15}$$

in which $J_{\rm t}$ is defined as total 'slow speed shaft equivalent' inertia:

$$J_{\rm t} = J_{\rm r} + i_{\rm gb}^2 \cdot J_{\rm g}; \tag{2.16}$$

2.2.3 Tower dynamics

For controller design purposes, it was considered to use a simplified axisymmetric tower model [8]. Tower top equivalent displacements of only the first bending mode, in both the fore-aft direction ('nodding') and the sideward direction ('naying') are modelled by two equal common mass-spring-damper systems. As a consequence, the tower top rotation, the torsion deformation, the yawing effects and higher bending modes are neglected. Additionally, tilt related influences are ignored.

The first bending mode of both naying and nodding is modelled by the differential equations of a common mass-spring system (eq.(2.17), (2.18)):

$$m_{\rm t} \cdot \ddot{x}_{\rm nd} + k_{\rm t} \cdot \dot{x}_{\rm nd} + c_{\rm t} \cdot x_{\rm nd} = F_{\rm nd}^{\rm top_{eq}} \tag{2.17}$$

$$m_{\rm t} \cdot \ddot{x}_{\rm ny} + k_{\rm t} \cdot \dot{x}_{\rm ny} + c_{\rm t} \cdot x_{\rm ny} = F_{\rm ny}^{\rm top_{eq}} \tag{2.18}$$

In fore-aft sense, tower top displacement position, speed and acceleration are defined as $x_{\rm nd}$, $\dot{x}_{\rm nd}$ and $\ddot{x}_{\rm nd}$ respectively. In the same way, in sideward sense as $x_{\rm ny}$, $\dot{x}_{\rm ny}$ $\ddot{x}_{\rm ny}$.

The tower top effective mass, $m_{\rm t}$, is determined by the sum of tower top mass (nacelle mass including rotor) and a top equivalent tower mass (tower mass which is assumed to be virtual concentrated at the tower top). For the DOWEC turbine the top equivalent tower mass was determined to 144.9 tons, therefore $m_{\rm t}$ equals 264.7 tons. The structural damping $k_{\rm t}$ and spring stiffness $c_{\rm t}$ are determined by eq.(2.19) as 5.8 kN/(m/s) and 1280 kN/m respectively, using the tower resonance frequency $\omega_0^{\rm t}$ and a modified damping ratio [2] of 0.005

$$\begin{aligned} (\omega_0^{\rm t})^2 = c_{\rm t}/m_{\rm t} &\Leftrightarrow c_{\rm t} = (\omega_0^{\rm t})^2 \cdot m_{\rm t} \\ 2\beta_{\rm t}/\omega_0^{\rm t} = k_{\rm t}/c_{\rm t} &\Leftrightarrow k_{\rm t} = 2\beta_{\rm t} \cdot \omega_0^{\rm t} \cdot m_{\rm t} \end{aligned} \tag{2.19}$$

[2] normally, a damping ratio, $\beta_{\rm t}$, of 0.009 is assumed for a free vibrating steel structure, but taking a top mass (nacelle, rotor) into account this will reduce both the resonance frequency and damping with a factor 25-50%

The nodding excitation force, $F_{\rm nd}^{\rm top_{eq}}$, eq.(2.17), consists of tower top equivalent components caused by the turbine thrust force $F_{\rm a}$, eq.(2.2), and the external (hydrodynamic) fore-aft forces $F_{\rm nd}^{\rm hyd}$. From bending theory of slender beams [8] , it has been derived that the exitation force components of $F_{\rm nd}^{\rm top_{eq}}$ appear as given in eq.(2.20)

$$\begin{aligned} F_{\rm nd}^{\rm top_{eq}} &= F_{\rm a} + F_{\rm nd}^{\rm hyd} \\ &= F_{\rm a} + \tfrac{3}{2} \sum_{\rm k=1}^{\rm N_{t,wave}} \left(\frac{d - z_{\rm k}}{Z_{\rm t}} \right)^{\frac{3}{2}} \cdot F_{\rm nd}^{\rm hyd,k} \end{aligned} \tag{2.20}$$

The variables d and $z_{\rm k}$ are related to the tower part below the water surface and defined as the waterdepth and the distance to the water surface at element k, respectively (see 2.3.2).

The naying excitation force, $F_{\rm ny}^{\rm top_{eq}}$,eq.(2.18), consists of a nacelle force caused by the drive train reaction torque on the tower $F_{\rm nac}^{\rm top_{eq}}$ and the external sideward (hydrodynamic) forces $F_{\rm ny}^{\rm hyd}$. From bending theory of slender beams [8] , it has been derived that the exitation force components of $F_{\rm ny}^{\rm top_{eq}}$ appear as given in eq.(2.21)

$$\begin{aligned} F_{\rm ny}^{\rm top_{eq}} &= F_{\rm nac}^{\rm top_{eq}} + F_{\rm ny}^{\rm hyd} \\ &= \tfrac{3}{2} \tfrac{T_{\rm nac}}{Z_{\rm t}} + \tfrac{3}{2} \sum_{\rm k=1}^{\rm N_{t,wave}} \left(\frac{d - z_{\rm k}}{Z_{\rm t}} \right)^{\frac{3}{2}} \cdot F_{\rm ny}^{\rm hyd,k} \end{aligned} \tag{2.21}$$

The definitions of d and $z_{\rm k}$ are equal as in eq.(2.20), $T_{\rm nac}$ is the reaction torque of the drive train as given in eq.(2.14)

Rotation effects in sideward direction will disturb the (measured) rotor speed. A rough (linear) approximation of this rotation angle is given in eq.(2.22).

$$\phi_{\rm ny} = \frac{2 \cdot x_{\rm ny}}{Z_{\rm t}} \tag{2.22}$$

Both in eq.(2.20) and eq.(2.21), simple addition is allowed, because the tower is assumed to have a cilindrical shape and the angle of attack of the waves is assumed to be in line with the axial force.

2.2.4 Electric conversion

The electric conversion part of the DOWEC turbine consists of a voltage source back-to-back converter, which controls the rotor voltages of a doubly fed asynchronous generator using a dedicated 'field oriented control' algorithm. The stator of the generator is directly connected to the grid. This topology is able to realise cost-effective variable speed control for a limited speed range (+/- 30%), determined by the capacity of the inverter. High speed switching power electronics are able to set electric generator torque almost instantaneously with respect to the mechanical dynamics. For the proposed control design purposes, only the generator side inverter of the converter is relevant and dynamic behaviour above 5-10Hz (suppression of shaft torsion resonance 2-3Hz) are neglected. Therefore, a well fitted second order torque-servo approach as given in eq.(2.23), represents the overall dynamic behaviour from setpoint to actual torque, sufficiently.

$$T_{\rm e}^{*} = \frac{1}{\left(\omega_0^{\rm g}\right)^2} \cdot \ddot{T}_{\rm e} + \frac{2\beta_{\rm g}}{\omega_0^{\rm g}} \cdot \dot{T}_{\rm e} + T_{\rm e} \tag{2.23}$$

The used bandwidth amounted to 6Hz ($\omega_0^{\rm g}$ = $\pm$ 38 $\mathrm{rad/s}$), which is quite conservative, the damping rate $\beta_{\rm g}$ was set to 0.7 which implicates a just critical damped system. The electric torque servo controlequuipment will certainly be capable to achieve these requirements.

Further simplification can be achieved by ignoring second order dynamics and take only a first order dynamics into consideration:

$$T_{\rm e}^{*} = \tau_{\rm T_e} \cdot \ddot{T}_{\rm e} + T_{\rm e} \tag{2.24}$$

A conservative value for the time constant $\tau_{\mathrm{T_e}}$ will be 0.1s.

Basically the electric torque setpoint consists of the stationary relation for power production (subsection 3.4.1). Sideward tower movements ('naying') will slightly affect the electric torque. Additional (dynamic) torque setpoint components $T^*_{\mathrm{e,ctrl}}$ can be added to achieve improved turbine control (subsection 3.4.2 and 3.4.3) or reduction of resonances (section 5.1, section 5.3).

$$T^*_{\mathrm{e}} = T^*_{\mathrm{e}}(\Omega_{\mathrm{r}} - 2\frac{\dot{x}_{\mathrm{ny}}}{Z_{\mathrm{t}}}) + T^*_{\mathrm{e,ctrl}} \tag{2.25}$$

2.2.5 Pitch actuation system

The calculated pitch speed setpoint of the control algorithm will be applied to the blades by pitch actuation. For the DOWEC turbine, three independent but simultaneous acting electric pitch actuators will change the pitch angle of the blades each control step.

The speed control equipment of the electric drive system usually acts as a servo system with respect to its commanded (pitch)speed, by separation of field and torque control. The dynamics of electric components are usually small with respect to the mechanical loading behaviour. The pitch motor load is determined by the pitch system inertia and a (disturbing) torque due to friction of the blade bearing. This friction consists of a component which is proportional to the pitch speed and a constant component (Coulomb friction), which changes of sign at pitch speed reversal. Bending of the blades are mainly responsible for the friction behaviour of pitch bearings.

In [8] it has been proved that a delayed second order system fits the pitch actuator dynamics sufficiently for control analysis purposes and that the Coulomb friction behaviour can be modelled by adding additional actuation delay in case of pitch speed reversal (in Laplace domain):

$$\begin{aligned} \dot{\theta}(s) &= H_{\mathrm{pt}}(s) \cdot \dot{\theta}^*(s) \\ H_{\mathrm{pt}}(s) &= \frac{\mathrm{e}^{-(T^{\mathrm{ptv}}_{\mathrm{d}} + T^{\mathrm{ptx}}_{\mathrm{d}}) \cdot s}}{\left(\frac{1}{(\omega^{\mathrm{pt}}_0)^2} \cdot s^2 + \frac{2 \cdot \beta_{\mathrm{pt}}}{\omega^{\mathrm{pt}}_0} \cdot s + 1 \right)} \cdot \dot{\theta}^*(s), \end{aligned} \tag{2.26}$$

in which $T^{\mathrm{ptx}}_{\mathrm{d}}$ is defined as the conditional delay time to overcome Coulomb friction. $T^{\mathrm{ptv}}_{\mathrm{d}}$, ω^{pt}_0 , β_{pt} , are equivalent system parameters which represent the overall pitch actuation delay during normal operation: pitch delay time, pitch system eigen frequency, damping rate.

Usual values for $T^{\mathrm{ptv}}_{\mathrm{d}}$, ω^{pt}_0 and β_{pt} are respectively: 1-3 ms, 80-100 rad/s and 0.3-0.5. The representive delay for Coulomb friction is relative large, $\pm$ 100 ms. This means well damped dynamic behaviour with a bandwidth of approximately 10-15 Hz and a dominating conditional delay.

2.3 External phenomena

As mentioned before in fig.(2.1), two external disturbing influences are relevant for an offshore turbine: wind speed and wave forces. Both comprises stochastic properties. In subsection 2.3.1, wind speed will be modelled 'rotor wide'; on the one hand side as a driving quantity (to produce power from aerodynamic torque) and on the other hand side as a disturbing quantity (fluctuations by turbulences). In subsection 2.3.2, wave forces will be modelled as force effective wave accellerations, which excite the tower (disturbing quantity).

2.3.1 Rotor effective windspeed

To verify the performance of a control algorithm by time domain simulations, a representative wind speed signal is necessary. Therefore, 'rotor effective wind speed' is defined as [8]:

'a single point wind speed signal which will cause wind torque variations through rotor power and thrust coefficients, that will be stochastically equivalent to those calculated with blade element momentum theory in a turbulent wind field'.

The stochastic wind speed signal is derived from the autopower spectrum of the longitudinal wind speed variations and lateral coherence in the rotor plane, according to IEC class IIB with turbulence intensity 16% [1]. The rotor effective wind speed signal has been normalised by the mean value of wind speed and comprises:

- tower shadow influences;
- wind shear variations;
- 0p mode of the turbulent windfield;
- 3p- and 6p effects of the rotationally sampled wind field.

Fig.(2.5) shows these components in detail during 20 seconds. In the upper plot of fig.(2.5),

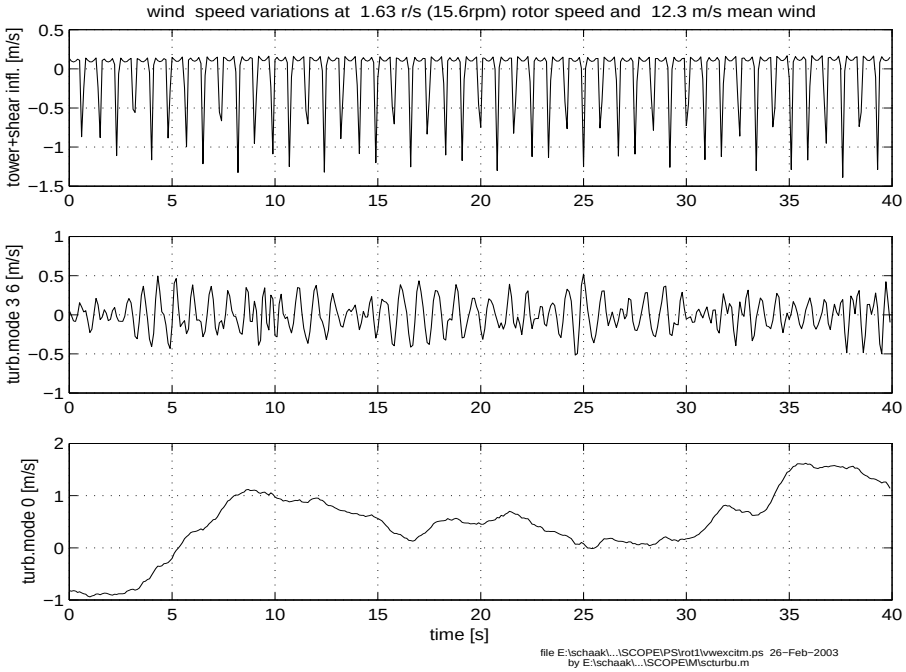

Figure 2.5: *Details of contributions to rotor effective windspeed; tower and shear, rotational sampling, 0p mode*

tower shadow influences are clearly visible as 3p periodical notches. Wind shear is nearly negligible. The middle plot shows the 3p and 6p rotational wind field sampling effects of the blades. Because these effects considerably affect the rotor acceleration, incorporating them is significant to verify filtering performance during rotor speed control. The lower plot shows 'low frequent' wind speed variations (0p) determined by the stochastic properties of wind and turbulence intensity.

For simulation purposes the actual wind speed is determined from a prior calculated wind file comprising normalised periodic and turbulent components for actual rotor azimuth, $\Psi_{\rm r}$ and desired mean wind speed, $\overline{V}_{\rm w}$.

$$\begin{array}{rl} \Psi_{\rm r} = & \int^t \Omega_{\rm r} \cdot {\rm d}t \\ V_{\rm w} = & \overline{V}_{\rm w} \cdot [1 + v_{\rm w}^{\rm tur}(\Psi_{\rm r})] + \\ & \overline{V}_{\rm w} \cdot [1 + v_{\rm w}^{\rm tur_{0p}}(\Psi_{\rm r})] \cdot [v_{\rm w}^{\rm tow}(\Psi_{\rm r} {\rm mod} 2\pi) + v_{\rm w}^{\rm shr}(\Psi_{\rm r} {\rm mod} 2\pi)] \end{array} \tag{2.27}$$

In eq.(2.27), both tower shadow and wind shear variations are periodic effects in the range $[0, 2\pi]$ of the rotor azimuth, and scalable with 'rotor uniform wind', $V_{\rm w}^{\rm unif}$. Turbulence is approximately proportional with mean wind speed, $\overline{V}_{\rm w}$. In eq.(2.27), the components $v_{\rm w}^{\rm tur}$, $v_{\rm w}^{\rm tur_{0p}}$,$v_{\rm w}^{\rm tow}$ and $v_{\rm w}^{\rm shr}$ are normalised variations with respect to the mean windspeed $\overline{V}_{\rm w}$.

Finally, fig.(2.6) shows simulation time series of the rotor uniform wind speed and rotor effective wind speed, respectively.

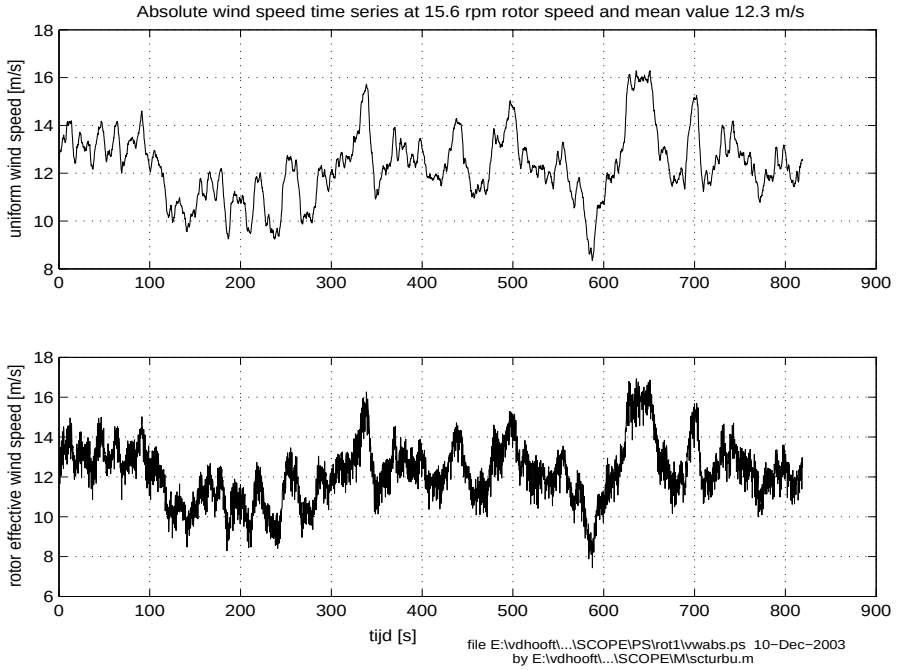

Figure 2.6: *Time series of uniform wind speed and rotor effective wind speed signals*

2.3.2 Towertop effective wave forces

The stochastic properties of linear waves are described by spectral density functions like the one of Pierson-Moskowitz. Specifically, the model for wind turbine simulation should describe the impacts on the tower base structure and its foundation. These wave disturbances (diffraction) are described by the MacCamy Fuchs correction. Modelling of waves has been restricted by taking the following assumptions into account:

- the considered waves pertain to a specific mean wind speed value;
- the propagation of the waves are horizontal and uni-directional;
- 'low waves', which means that the wave heights are small with respect to their length and depth;

Below the modelling approach of wave impact on the turbine tower is discussed shortly, more detailed analysis can be found in [8] and fundamental theory in [10].

Horizontal wave velocity and acceleration: In case of 'low waves' it is allowed to use theory for linear waves (Airy's theory), which describes two important issues:

1. both the water velocity w and acceleration $\dot{w}$, for any arbitrary distance to the surface of the water z, is fully determined by surface raisings (elevation, η) via a scaling factor, which depends on the distance to the surface, the wave length λ and the wave frequency ω;
2. the so called relation of dispersion, which unambigiously establishes the relationship between wave length, water depth d and wave frequency ω

$$\omega^2 = \frac{2\pi g}{\lambda} \cdot \tanh\left(\frac{2\pi d}{\lambda}\right). \tag{2.28}$$

It appears, that high frequent waves have the strongest effects below the surface of the water. The stochastic properties of waves are usually described by the Pierson-Moskowitz spectrum for wave elevation. This single sided spectrum incorporates dependency on the (mean) wind speed, which has a direct relationship to the significant wave height H_{s} by means of the gravitation g

$$G_{\eta}(\omega) = \frac{8.1 \cdot 10^{-3} \cdot g^2}{\omega^5} \cdot e^{-B/\omega^4}, \tag{2.29}$$

in which the constant B has been defined as:

$$B = 0.74 \cdot \left(\frac{g}{\overline{V}_{\mathrm{w}}} \right)^4 = \frac{3.11}{H_{\mathrm{s}}^2} \tag{2.30}$$

A time domain realisation of this spectrum results in a series of real harmonic elevation components with random phase angles, as a consequence of its stochastic nature. Based on the linear wave theory, it is now possible to derive elevation dependent expressions for water velocity w and accelleration $\dot{w}$ (eq.(2.31)), by means of (real) harmonic time series and the pertaining spectral functions (APSD). The wave speed and acceleration spectra depends as follows on the elevation spectrum:

$$\begin{aligned} G_{\mathrm{w(z)}}(\omega_{\mathrm{l}}) &= \omega_{\mathrm{l}}^2 \cdot \left(\frac{\cosh\left(\frac{2\pi}{\lambda_{\mathrm{l}}} \cdot (d-z)\right)}{\sinh\left(\frac{2\pi}{\lambda_{\mathrm{l}}} \cdot d\right)} \right)^2 \cdot G_{\eta}(\omega_{\mathrm{l}}) \\ G_{\dot{\mathrm{w}}(\mathrm{z})}(\omega_{\mathrm{l}}) &= \omega_{\mathrm{l}}^4 \cdot \left(\frac{\cosh\left(\frac{2\pi}{\lambda_{\mathrm{l}}} \cdot (d-z)\right)}{\sinh\left(\frac{2\pi}{\lambda_{\mathrm{l}}} \cdot d\right)} \right)^2 \cdot G_{\eta}(\omega_{\mathrm{l}}) \end{aligned} \tag{2.31}$$

where z is the distance to surface.

Fig.(2.7) shows spectral realisations of eq.(2.31) for wave velocity at different heights above the soil and a waterdepth of 20m in case of two different wind speeds: 12 m/s and 20 m/s.

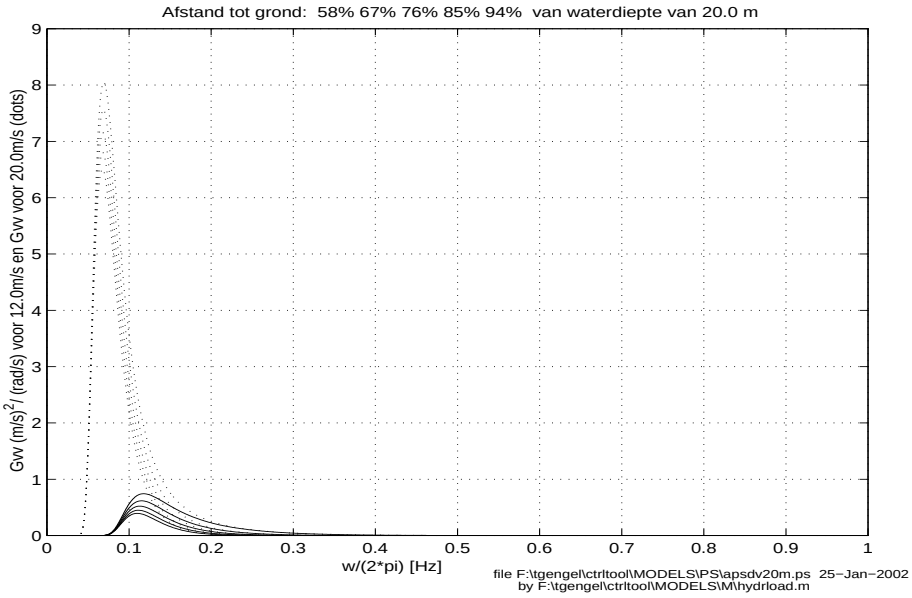

Figure 2.7: *Single sided spectrum for the amplitude of horizontal wave velocity of Pierson-Moskowitz spectrum for mean wind speeds of 12 m/s (solid line, 3.1m wave height) and 16 m/s (dotted line, 5.4m wave height), different distances to the water surface (1,3,5,7 and 9m) and a total depth of 20m*

Force effective wave acceleration: The waves as described in eq.(2.31) will collide with the tower (diffraction). Concerning the 'wave velocity which deals with friction forces', it is allowed to use the spectrum of eq.(2.31) without modifications. Although, for 'wave velocity which deals with mass forces', the tower will disturb the wave acceleration. The amount of disturbance is mainly determined by the relationship between tower diameter d_{t} and wave length and thus, via eq.(2.28), by the wave frequency.

In eq.(2.31), diffraction effects can be taken into account by means of the frequency dependent mass coefficients $C_{\mathrm{m}}(\omega_{\mathrm{l}})$, which results in a power spectrum eq.(2.32) for *force effective wave accelerations* $\dot{w}^{\mathrm{eff}}$.

$$G_{\dot{\mathrm{w}}^{\mathrm{eff}}(\mathrm{z})}(\omega_{\mathrm{l}}) = C_{\mathrm{m}}(\omega)^2 \cdot G_{\dot{\mathrm{w}}(\mathrm{z})}(\omega_{\mathrm{l}}) \tag{2.32}$$

For this correction, the non linear relation of MacCamy Fuchs has been used. This correction gives for waves larger than 10 times the tower diameter a mass coeffient of 2, while it decreases to 0.4 at wave lengths equal to the tower diameter. The corrected spectral function for acceleration (force effective wave acceleration) is shown with respect to the 'not disturbed' spectrum in fig.(2.8). Finally, time domain realisations for force effective wave velocity and

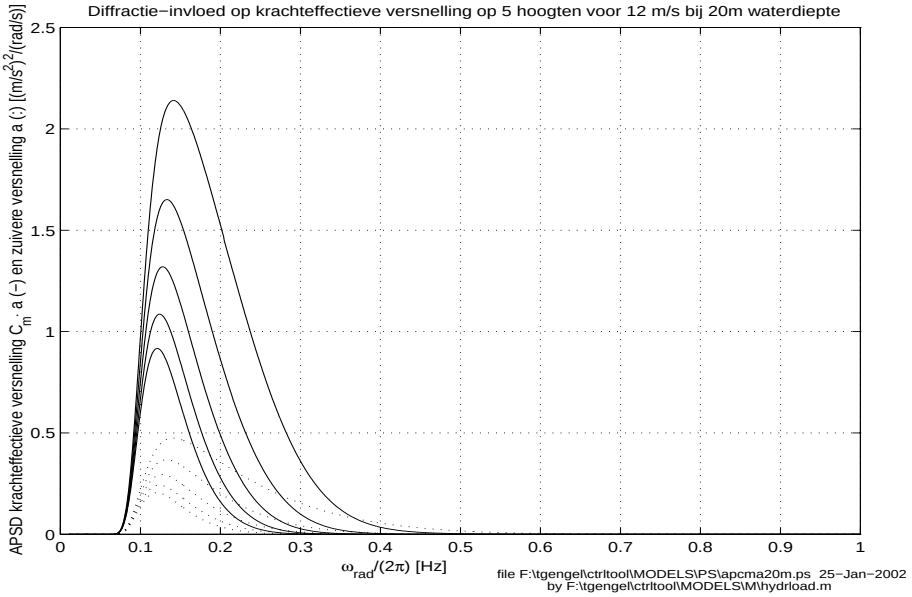

Figure 2.8: *Single sided spectrum of the amplitude of 'not disturbed (dotted) and corrected for diffraction (solid), wind speed of 12 m/s, 3.1m wave height), different distances to the water surface (1,3,5,7 and 9m) and a total depth of 20m*

acceleration are shown in fig.(2.9) for a wind speed of 12 m/s and five different distances to the water surface.

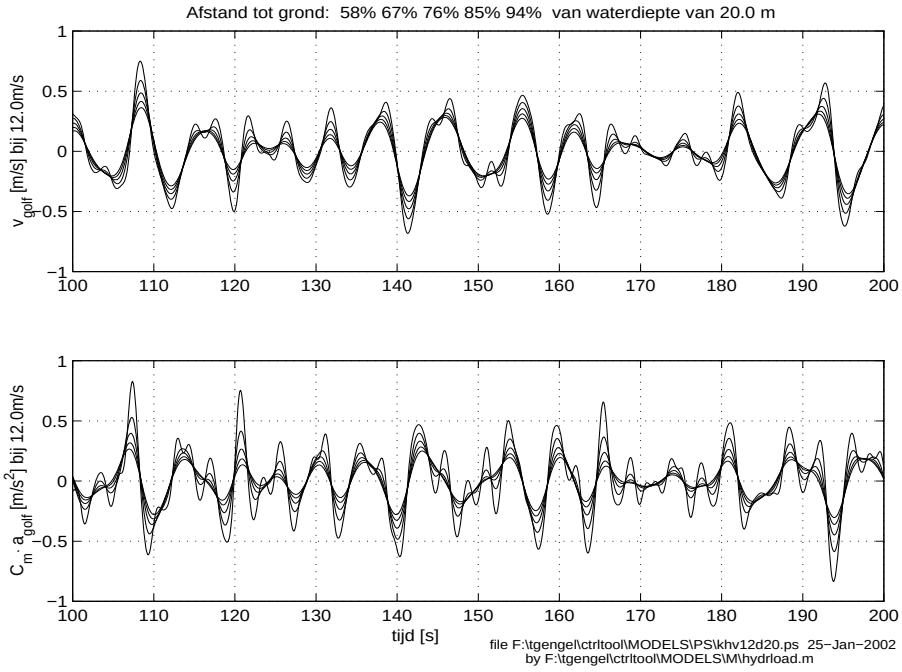

Figure 2.9: *Time domain realisations for wave velocity (upper plot) and force effective acceleration (lower plot) for a wind speed of 12 m/s and five different distances to the water surface*

3 DESIGN OF POWER CONTROL ALGORITHM

In this chapter the design of a power control algorithm is discussed for the DOWEC turbine as specified in the previous chapter. Power will be controlled by pitch angle control and generator torque control and operation can be separated in below rated (partial load) and above rated (full load control) operation. The power control approach and pertaining control principles are discussed in section 3.1, while control algorithms are discussed in three sections: Pitch control algorithm at full load operation (section 3.2), Pitch control algorithm at partial load operation (section 3.3) and Torque setpoint control (section 3.4).

3.1 Power control approach

In this chapter a *functional* description of the DOWEC power control approach is given. Power control is achieved by both pitch control and electric torque control, both below rated wind speed and above rated wind speed conditions. Fig.(3.1) shows a functional overview of turbine power control. Principles of the 'shaded' blocks are discussed shortly in this section, In the next sections design features and more detail will be discussed.

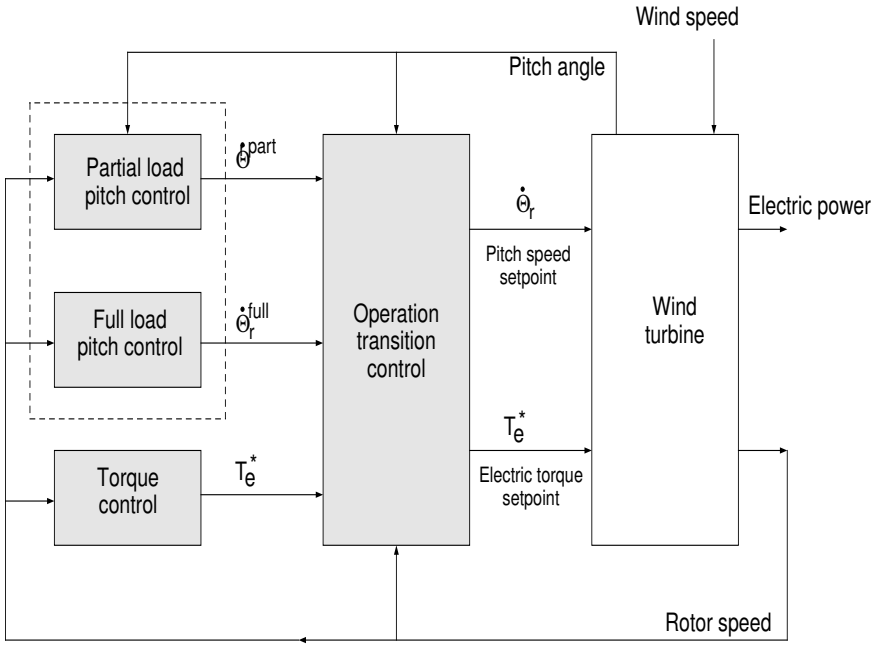

Figure 3.1: *Functional overview of turbine power control*

Control objectives: Due to its variable speed, active pitch to vane concept, the DOWEC turbine is able to operate below rated wind speed at below rated rotor speed values, obviously producing less than rated electric power. In the below rated region the pitch position of the rotor blades has to be set optimal for power production, while rotor speed is varying freely.

During full load operation the pitch control objective is defined as:

'Rotor speed regulation at rated rotor speed and yield of rated power, by controlling the blade pitch angle in such a manner, that the lift coefficient lowers by decreasing the angle of attack and oppositely ('pitch to vane control')',

While the electric torque control objective is defined as:

'Production of constant rated electric power and optimised interaction in relation to pitch control',

Pitch and torque control below rated conditions: To ensure as much as possible energy yield, during partial load the electric torque setpoint is set such that the tip speed ratio, λ , is maintained at its optimal value, $\lambda_{\rm opt}$.

$$P_{\rm a}^{\rm part} = C_{\rm p,max}(\theta, \lambda_{\rm opt}) \cdot \tfrac{1}{2}\rho_{\rm air}\pi R_{\rm b}^2 \cdot (V_{\rm w})^3 \tag{3.1}$$

with the optimal tip speed ratio, $\lambda_{\rm opt}$:

$$\lambda_{\rm opt} = \lambda|_{C_{\rm p}=C_{\rm p,max}} \tag{3.2}$$

The pitch angle is set to an optimal pitch angle $\theta_{\rm opt}$ where maximal lift is found. Design of partial load pitch control will be subject of section 3.3.

Pitch and torque control above rated conditions: From rated speed through maximum (generator)speed, rated power production is aimed by means of pitch regulated rotor speed and following the constant power curve by generator control. The variable speed, active 'pitch to vane' concept gives advantageous properties, like well known aerodynamic behaviour due to small angle of attack and good power quality due to allowed rotor speed fluctuation.

Fig.(3.2) shows a cross section of a rotor blade element at a distance r from the rotor center and seen from tip to root for a clockwise rotor rotation. To give sense a typical aerofoil characteristic is also shown.

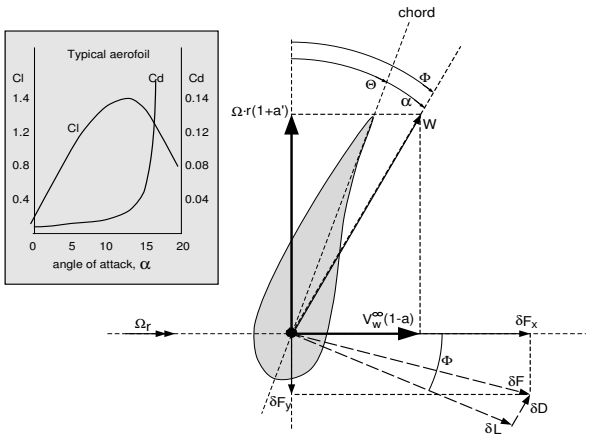

Figure 3.2: *Cross section of a rotor blade as seen from tip to root and clockwise rotor rotation in normal position*

The inflow angle, ϕ, is equal to the sum of the pitch angle, θ , and the angle of attack, α and separated by the chord line of the blade section (chord line will differ for other blade sections). The effective windspeed, W, is constructed from the undisturbed wind speed, $V_{\rm w}^{\infty}$, and wind speed due to rotation, $\Omega_{\rm r} \cdot r$ (both a and a' reflect induction effects). A decomposition of the force contribution of the blade section, δF, which has been constructed from the lift contribution, δL, and drag contribution, δD, results in a thrust force component, $\delta F_{\rm x}$, and a torque component, $\delta F_{\rm y}$.

Despite of the simplicity of the model and neglecting induction variation in fig.(3.3) it is clear that rotor speed increase can be avoided by enlarging the pitch angle ('pitch to vane'), θ, at high wind speed level.

Due to reduction of the the lift coefficient $C_{\rm l}$, the torque component, $\delta F_{\rm y}$ is kept at equal level as shown in fig.(3.2). In both cases the angle of attack, α, is small and stall effects will be avoided.

Design of an algorithm to control rotor speed and to optimise power production using the active 'pitch to vane' principle, will be subject of section 3.2

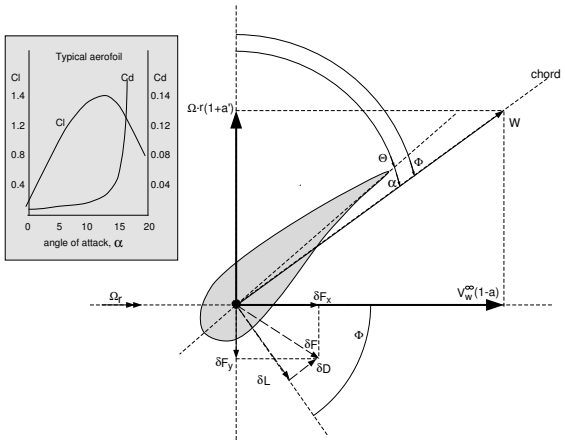

Figure 3.3: *Cross section of a rotor blade as seen from tip to root and clockwise rotor rotation in feathered position*

Operation transition control: Smooth transition control between full load operation and partial load operation is necessary to cover the whole operation range of the turbine. Obviously, transition will take place around rated conditions. A wind turbine will be designed for rated wind conditions, therefore most of the time (more than 50% of the production time) it is operating around rated speed. A smooth transition mechanism, which deals with the interaction between pitch and generator control will be very important to achieve energy yield design targets. Generator torque control and its interaction with pitch control will be subject of section 3.4.

3.2 Pitch control algorithm at full load operation

As mentioned in subsection 3.1, during full load operation the excess of aerodynamic power is reduced by pitching the rotor blades simultaneously in feathering direction. The 'constant power' control of the generator and the rotor inertia (fly wheel) will then establish good power quality. For this reason aerodynamic torque variations will result in rotor speed variations. The amount of rotor speed variation above its rated value, to maintain rated power, is restricted both by the maximum speed of the generator and perhaps by the tower eigen frequency to avoid tower resonance. In fig.(3.4) the (functional) overall structure of the proposed pitch controller at full load operation is shown. All 'shaded' blocks will be discussed in the next subsections.

3.2.1 Rotor speed feedback control

The 'core' of the full load pitch controller is based on a linear rotor speed and -acceleration feed back structure for the wind turbine operating area. The measured rotor speed is filtered accurately and the rotor acceleration is calculated numerically. To cope with non linear turbine behaviour caused by aerodynamics, the controller gains have been scheduled dependent on the pitch angle. Rotor speed setpoint adaptation is a possibility to utilise the allowed rotor speed fluctuation for maintaining rated power at sudden negative wind gusts (kinetic energy storage in rotor inertia).

Linearised transfer model: A linear transfer model as depicted in fig.(3.5) in Laplace domain (s is defined as Laplace operator) between pitching speed and rotor speed has been derived by linearising the non linear aerodynamic rotor equations eq.(2.1) and (2.2) around a certain operation point determined by θ ,Ω_{r} , V_{w} and $\dot{x}_{\mathrm{nd}}$.

$$\delta X = \sum_{\forall y} \left.\frac{\partial X}{\partial y}\right|_{\bar{y}} \cdot \delta y = \sum_{\forall y} (X)'_{\mathrm{y}} \cdot \delta y \qquad (3.3)$$

with X $\epsilon\{T_{\mathrm{a}}, F_{\mathrm{a}}\}$ and y $\epsilon\{\theta, \Omega_{\mathrm{r}}, V_{\mathrm{w}}, \dot{x}_{\mathrm{nd}}\}$

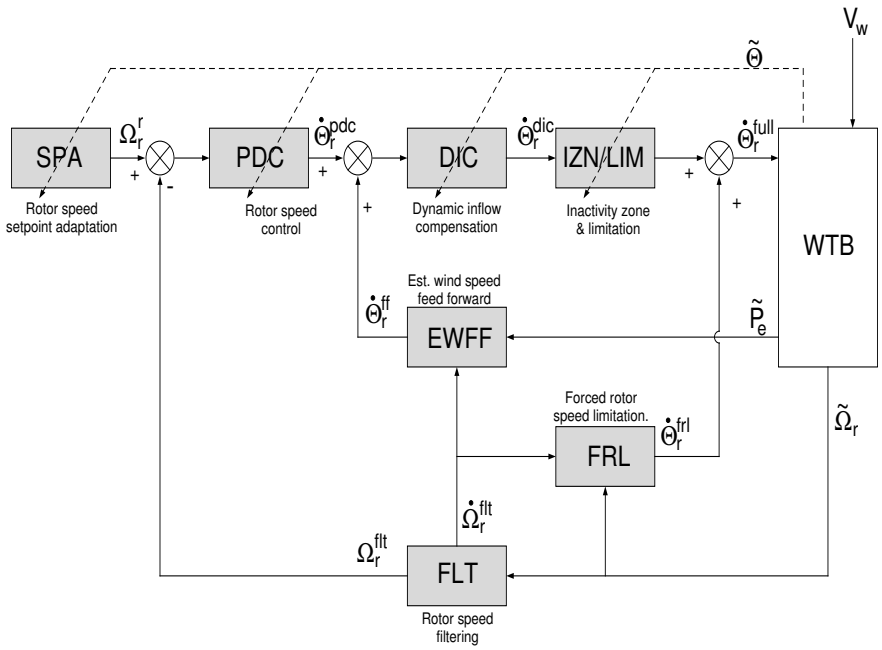

Figure 3.4: *functional overall structure of the proposed pitch controller at full load operation*

Each partial derivative can be interpreted as 'the sensitivity of X for small variations of y in a specific operation point defined by $\overline{\theta}$, $\overline{\Omega}_{\rm r}$, $\overline{V}_{\rm w}$ and $\overline{\dot{x}}_{\rm nd}$.

The fore-aft tower bending is incorporated in conformity with eq.(2.17), while nodding speed variations $\dot{x}_{\rm nd}$ are assumed opposite to wind speed variations.

Aerodynamic torque fluctuations $T_{\rm a}$ are then caused by *direct effects* (through $(T_{\rm a})'_{\theta}$, $(T_{\rm a})'_{\Omega_{\rm r}}$ and $(T_{\rm a})'_{\rm V_w}$) and *indirect effects* ('through $(F_{\rm a})'_{\theta}$, $(F_{\rm a})'_{\Omega_{\rm r}}$, $(F_{\rm a})'_{\rm V_w}$ and tower dynamics'), due to fluctuations of θ , $\Omega_{\rm r}$ and $V_{\rm w}$.

Wind speed disturbances, $\delta V_{\rm w}$ will affect rotor speed, which has to be cancelled by actuation of the pitch angle θ (this section) and the electric torque setpoint $T_{\rm e}^*$ (section 3.4).

Rotor speed filtering: The quality of the measured rotor speed is crucial for rotor speed feed back control. The following turbine effects are disturbing the rotor speed and should be suppressed sufficiently by means of digital filtering:

- 3p effects (see 2.3.1);
  - tower shadow;
  - 3p and 6p rotational sampling effects;
- collective lead-lag bending effects of the blades;
- sideward tower motion.

Because rotor acceleration is numerical calculated using the backward difference approach, all disturbances above the pitch control bandwidth have to be reduced to avoid amplification by the controller (differential) gain. If no filtering should be applied, then from eq.(3.4) it follows that typical 3p wind speed fluctuations of 0.8 m/s (fig.(2.5)), would cause (undesired) pitching speed amplitude fluctuations of order 0.4 $^{\rm o}/{\rm s}$ (using typical values: $(T_{\rm a})'_{\rm V_w} \sim$ 370kNm/(m/s),

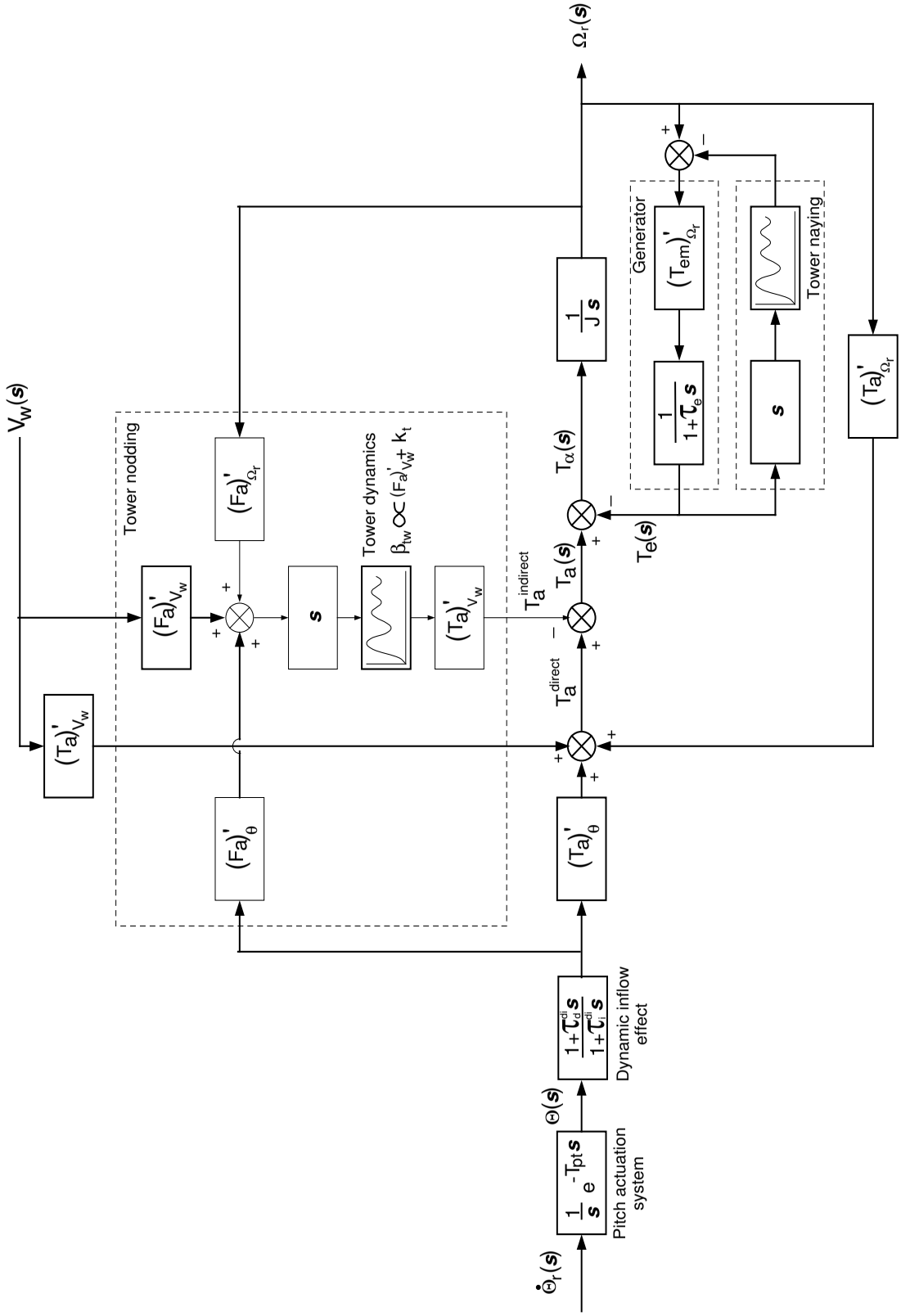

Figure 3.5: *Linearised transfer model of a wind turbine*

$K_{\mathrm{D}}^{\Omega_{\mathrm{r}}} \sim 17\ ^{\mathrm{o}}/\mathrm{s}/\mathrm{rad}/\mathrm{s}^2$).

$$\left|\dot{\theta}^*\right| \sim \Delta V_{\mathrm{w}}^{3\mathrm{p}} \cdot \frac{(T_{\mathrm{a}})'_{\mathrm{V_w}}}{J_{\mathrm{t}}} \cdot |K_{\mathrm{D}}^{\Omega_{\mathrm{r}}}| \tag{3.4}$$

Forseeing a smallest pitch inactivity zone of about $0.1^{\mathrm{o}}/\mathrm{s}$, a reduction factor of at least 5 to 10 would be required for 3p frequencies and higher.

A cascade filter consisting of a fourth order inverse Chebychev low pass filter (3p effects), a fourth order elliptic band notch filter (collective blade mode) and a second order elliptic band notch filter (sideward tower) as given in eq.(3.5) and specified in table(3.1) achieves sufficient reductions at least phase shift ($\sim 60\ ^{\mathrm{o}}$ at $\omega_{\mathrm{nq}} = 1.18\ \mathrm{rad}/\mathrm{s}$).

$$H_{\Omega_{\mathrm{r}}}^{\mathrm{filt}}(s) = H_{\Omega_{\mathrm{r}}}^{\mathrm{filt,3p}}(s) \cdot H_{\Omega_{\mathrm{r}}}^{\mathrm{filt,cb}}(s) \cdot H_{\Omega_{\mathrm{r}}}^{\mathrm{filt,tow}}(s) \tag{3.5}$$

Table 3.1: *Rotor speed filter specifications*

Filtersection	1	2	3
Type	Inverse Chebychev low pass	Elliptic band notch	Elliptic band notch
Behaviour	Low pass	Band notch	Band notch
Order	4	4	2
Reduction	30 dB	19 dB	29 dB
Pass ripple	-	1 dB	1 dB
cut-off	($\omega_0^{3\mathrm{p}}$-0.3) rad/s	-	-
notch	-	[0.625 1.125]ω_0^{col}	[0.85 1.15]ω_0^{t}

In figure 3.6 the amplitude and phase characteristic of this filter are shown.

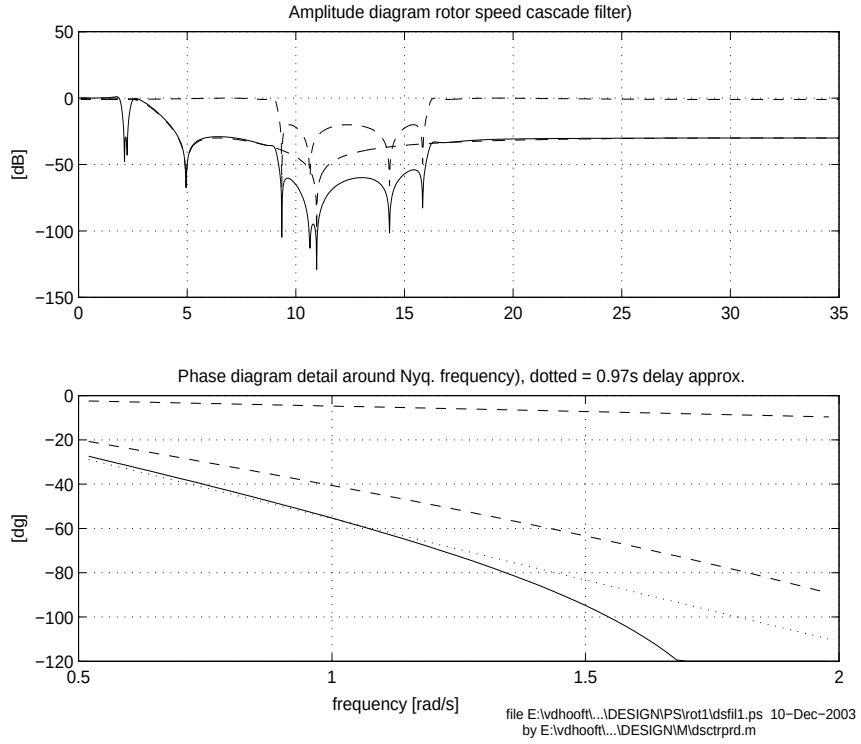

Figure 3.6: *Bode diagrams of rotor speed cascade filter (solid lines*

Below 1.25 rad/s a delay time, $T_{\mathrm{d}}^{\mathrm{filt}}$ = 0.97s, appears to be an accurate phase approximation for further linear analysis.

Linear PD controller: Further simplification of the linearised wind turbine model of fig.(3.5) results in 'a delayed double integrator' process. Therefore, a rotor speed feed back structure using a linear proportional/differential controller (PD-controller) is able to set the pitching speed setpoint such, that the rotor speed deviation between measured rotor speed and rotor speed setpoint will be eliminated.

The linear design is restricted to an operation range defined for aerodynamic torque levels between 90% and 140% with respect to rated torque, a rotor speed range between 14.57 rpm and 17.57 rpm and a windspeed range between 11.25 m/s and 26m/s. The linearised wind turbine model of fig.(3.5) is simplified to:

- data processing delay which represents computer calculation, measurement and actuation delay time: $2T_{\mathrm{c}}$;
- rotor speed filter delay $T_{\mathrm{d}}^{\mathrm{filt}}$;
- maximum value of aerodynamic torque to pitch angle sensitivity, $\left[(T_{\mathrm{a}})'_{\theta}\right]^{\max}$;
- delayed integrator representing pitching speed to pitch angle transfer (subsection 2.2.5)
- integrator representing acceleration of the rotor inertia, J_{t}= (J_{r}+J_{g}), eq.(2.15);
- neglection of dynamic inflow effects.

The process transfer function $H_{\Omega_{\mathrm{r}}}^{\dot{\theta}^*}$ from $\dot{\theta}^*$ to Ω_{r} can be written as eq.(3.6):

$$H_{\Omega_{\mathrm{r}}\,\dot{\theta}^*}(s) = \frac{\left[(T_{\mathrm{a}})'_{\theta}\right]^{\max}}{J_{\mathrm{t}} \cdot s^2} \cdot \mathrm{e}^{-\mathrm{T}_{\mathrm{d}}^{\Omega_{\mathrm{r}}} \cdot \mathrm{s}} \tag{3.6}$$

The overall loop delay,

$$T_{\mathrm{d}}^{\Omega_{\mathrm{r}}} = T_{\mathrm{d}}^{\mathrm{ptv}} + T_{\mathrm{d}}^{\mathrm{ptx}} + 2 \cdot T_{\mathrm{c}} + T_{\mathrm{d}}^{\mathrm{filt}} \tag{3.7}$$

was determined to 1.3s.

The pitch angle sensitivity of aerodynamic torque,$(T_{\mathrm{a}})'_{\theta}$, is non-linear in nature. It strongly dependents on the pitch angle, θ and also on the rotor speed Ω_{r} . Fig.(3.7) shows this sensitivity function within the defined operational envelope.

The maximum (negative) sensitivity value for controller design is determined to $\left[(T_{\mathrm{a}})'_{\theta}\right]^{\max}$ = 392 $\mathrm{kNm/^o}$.

Using a PD compensator, eq.(3.8),

$$\begin{aligned} H_{\Omega_{\mathrm{r}}}^{\mathrm{c}}(s) &= \frac{\dot{\theta}^*_{\Omega_{\mathrm{r}}}}{\Omega_{\mathrm{r}}^* - \tilde{\Omega}_{\mathrm{r}}^{\mathrm{f}}} = K_{\mathrm{P}}^{\Omega_{\mathrm{r}}} \cdot (1 + \tau_{\mathrm{D}}^{\Omega_{\mathrm{r}}} \cdot s) \\ &= K_{\mathrm{P}}^{\Omega_{\mathrm{r}}} + K_{\mathrm{D}}^{\Omega_{\mathrm{r}}} \cdot s \end{aligned} \tag{3.8}$$

the open loop transfer function becomes

$$\mathring{H}_{\Omega_{\mathrm{r}}}(s) = H_{\Omega_{\mathrm{r}}}^{\mathrm{c}}(s) \cdot H_{\Omega_{\mathrm{r}}\,\dot{\theta}^*}(s) \tag{3.9}$$

To achieve sufficient stability and robustness the stability criterion of Bode is used for a gain margin (GM) of 0.5 and a phase margin (PM) of 45 $^{\mathrm{o}}$. By solving eq.(3.10) ($s = j\omega$),

$$\begin{cases} \left|\mathring{H}_{\Omega_{\mathrm{r}}}(\omega_{\mathrm{nq}})\right| & = 1 - \mathrm{AM} \\ \arg\left(\mathring{H}_{\Omega_{\mathrm{r}}}(\omega_{\mathrm{nq}})\right) & = -\pi \\ \left|\mathring{H}_{\Omega_{\mathrm{r}}}(\omega_{\phi})\right| & = 1 \\ \arg\left(\mathring{H}_{\Omega_{\mathrm{r}}}(\omega_{\phi})\right) & = -\pi + \mathrm{PM} \end{cases} \tag{3.10}$$

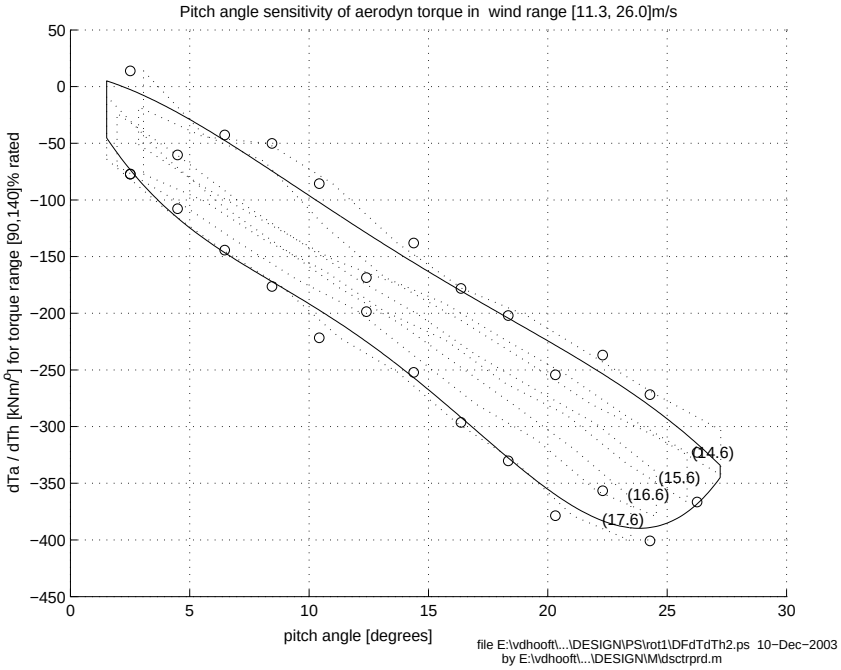

Figure 3.7: *Pitch angle sensitivity of aerodynamic torque,* $(T_{\rm a})'_\theta$ *for turbine operation range*

the proportional gain, $K_{\rm P}^{\Omega_{\rm r}}$, and differential gain $K_{\rm D}^{\Omega_{\rm r}}$ are dimensioned as:

$$\begin{aligned} K_{\rm P}^{\Omega_{\rm r}} &= 1.14(^{\rm o}/{\rm s})/({\rm rad/s}) \\ K_{\rm D}^{\Omega_{\rm r}} &= 17.33(^{\rm o}/{\rm s})/({\rm rad/s^2}) \\ \tau_{\rm D}^{\Omega_{\rm r}} = K_{\rm D}^{\Omega_{\rm r}}/K_{\rm P}^{\Omega_{\rm r}} &= 15.19{\rm s} \end{aligned} \tag{3.11}$$

at a value $\omega_{\rm nq}$ = 1.18 $\rm rad/s$ and ω_ϕ = 0.64 $\rm rad/s$ for a phase margin of 45 $^{\rm o}$.

Gain scheduling: Because the largest value of $(T_{\rm a})'_\theta$ which occurred at $\theta \sim 24$ $^{\rm o}$ and $\Omega_{\rm r}$ = 17.6 rpm was used during controller design, the 'weakest' PD controller was dimensioned. Therefore, the pitch angle sensitivity of the aerodynamic torque, $(T_{\rm a})'_\theta$ (fig.(3.7)), is used to amplify the designed controller gains of eq.(3.11) in the region of 'lower' pitch angles (below 20-23 $^{\rm o}$) and rotor speed values (below 17.6 rpm) by a numerically fitted two dimensional *gain scheduling polynomial*, eq.(3.12):

$$\mu_{\rm PD}(\theta,\Omega_{\rm r}) = \sum_{\rm i=1}^{{\rm N}_\theta+1} \sum_{\rm j=1}^{{\rm N}_{\Omega_{\rm r}}+1} C_{\mu_{\rm PD}}(i,j)\cdot\theta^{i-1}\cdot\Omega_{\rm r}^{j-1} \tag{3.12}$$

Sufficient accuracy was achieved for N_θ=2 and $N_{\Omega_{\rm r}}$=1. The scheduling factor $\mu_{\rm PD}$is shown in fig.(3.8). The lower curves pertain to higher rotor speed values. It is shown that inclusion of the rotor speed dependancy is of importance (gain increase for lower rotor speeds up to a factor 1.5). The scheduling factor is bounded between a maximum value of 7 to avoid extreme gain sensitivity in the low θ region, and a minimum value of 1, that maintains the design values of the PD controller in the higher θ region.

Stability analysis: The validity of the simplified model that has been used for controller design (section 3.2.1) will be checked for stability. Therefore, the transfer function $\mathring{H}_{\Omega_{\rm r}}({\rm s})$ in the *stability analysis* incorporates the following modelling aspects, which are in linearised format over the whole operational envelope:

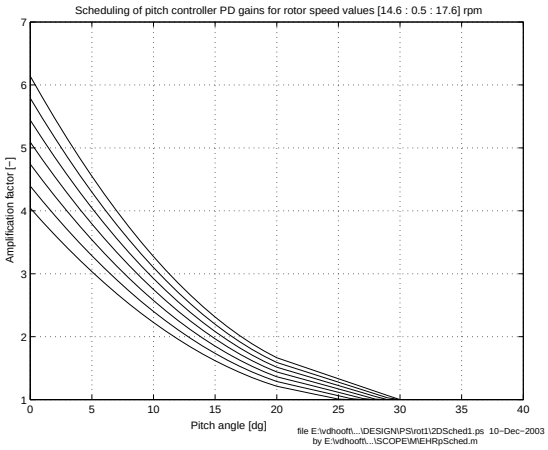

Figure 3.8: *Bode diagrams of rotor speed cascade filter (solid lines)*

1. basic drive-train dynamics, eq.(2.15);
2. direct aerodynamic torque influence by pitch angle, $(T_{\rm a})'_{\theta}$;
3. 2D scheduled PD-compensator eq.(3.8) and (3.12);
4. rotor speed cascade filter, eq.(3.5);
5. pitch actuator dynamics eq.(2.26);
6. electric torque influence by generator through speed/torque curve $(T_{\rm e}^*)'_{\Omega_{\rm r}}$;
7. direct aerodynamic torque influence by rotor speed $(T_{\rm a})'_{\Omega_{\rm r}}$;
8. indirect aerodynamic torque influence by pitch angle through fore-aft tower movement, $\partial T_{\rm a}/\partial \dot{x}_{\rm nd} \cdot \partial \dot{x}_{\rm nd}/\partial \theta$;
9. indirect aerodynamic torque influence by rotor speed through fore-aft tower movement, $\partial T_{\rm a}/\partial \dot{x}_{\rm nd} \cdot \partial \dot{x}_{\rm nd}/\partial \Omega_{\rm r}$.

For clarity, the influence of in plane motion to the electric torque is NOT taken into account.

The latter two modelling aspects cater for the affection of the effective wind speed by the tower motion as caused by axial forces from pitch angle and rotor speed variation (see fig.(3.5)). The indirect torque sensitivity to pitching is modelled as follows :

$$\frac{\partial T_{\rm a}}{\partial \dot{x}_{\rm nd}} \cdot \frac{\partial \dot{x}_{\rm nd}}{\partial \theta} = -(T_{\rm a})'_{\rm V_w} \cdot \frac{(F_{\rm a})'_{\theta}}{c_{\rm t}} \cdot \frac{s}{\frac{m_{\rm t}}{c_{\rm t}} s^2 + \frac{(k_{\rm t}+(F_{\rm a})'_{\rm V_w})}{c_{\rm t}} s + 1} \tag{3.13}$$

The indirect torque sensitivity to rotor speed variations is modelled as

$$\frac{\partial T_{\rm a}}{\partial \dot{x}_{\rm nd}} \cdot \frac{\partial \dot{x}_{\rm nd}}{\partial \Omega_{\rm r}} = -(T_{\rm a})'_{\rm V_w} \cdot \frac{(F_{\rm a})'_{\Omega_{\rm r}}}{c_{\rm t}} \cdot \frac{s}{\frac{m_{\rm t}}{c_{\rm t}} s^2 + \frac{(k_{\rm t}+(F_{\rm a})'_{\rm V_w})}{c_{\rm t}} s + 1} \tag{3.14}$$

Fig.(3.9) shows the magnitude of the direct and indirect torque influences by pitch angle and rotor speed variations in 'comparable terms' in the frequency range around the Nyquist frequency of 1.2 $\rm rad/s$ ($|s| = 1.2$). This implies that the pitch angle influences are 'scaled to *actively* fed back rotor speed variations' through the gain-scheduled D-action of the PD-compensator [3]. The lower left graph in fig.(3.9) shows the impact of the destabilising behaviour of the gener-

[3] Near the Nyquist frequency the D-action dominates the P-actions by far.

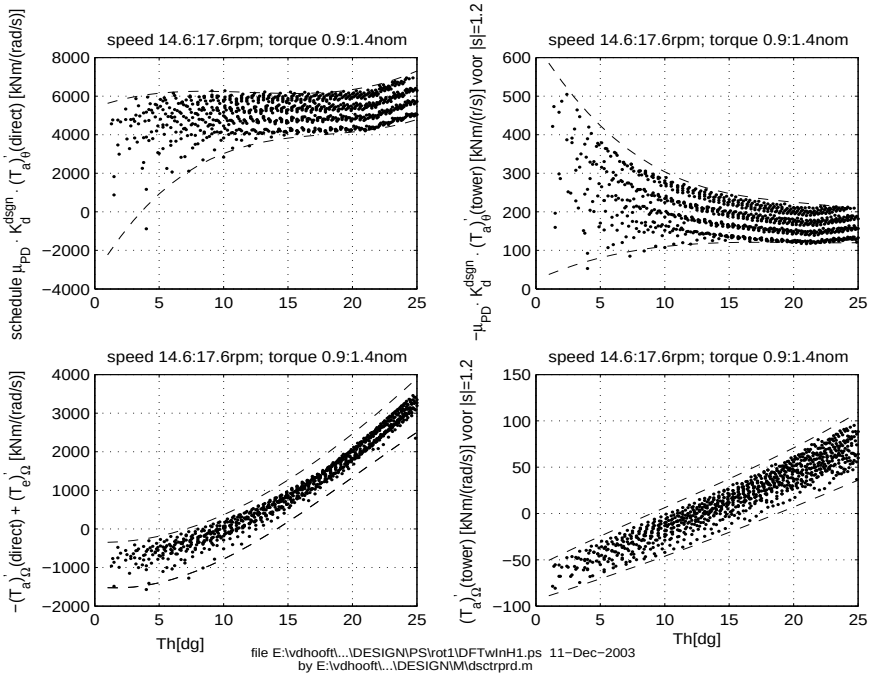

Figure 3.9: *Magnitude over the whole operational range of the four rotor speed feedback terms in the open loop transfer function model for stability analysis in the Nyquist frequency (1.2 rad/s)*

ator above rated speed (constant power production). As for working points above pitch angle values of 10 ^{o}s the (negative) values are compensated by the corresponding (positive) values in the upper left plot.

Four conclusions can be drawn:

- for pitch angles beyond 10 ^{o}, the direct PD-influence on the aerodynamic torque largely dominates, thus guaranteeing closed loop stability;
- for pitch angles below 5 ^{o}, the direct PD-influence is in some cases of the same magnitude as the destabilising direct speed influence for over-rated rotor speeds and the indirect torque influence by pitching may be an additional destabilising factor;
- the indirect torque influence by pitch angle is of relevance, through still small, for pitch angles below 5 ^{o} (upper right plot);
- the indirect torque influence by the rotor speed is negligeable (lower right plot).

To check stability, in fig.(3.10), the Nyquist diagrams show the magnitude and phase of the open loop transfer function in the defined operation range (sinusoidal transfer performance) for *four classified blade angle areas centered* around 2.5^{o}, 7.5^{o}, 14.5^{o} and 21.5^{o}. The phase shift and amplitude information in the Nyquist diagram yield the basic amplitude and phase margins of the system considered when the loop is closed. The 'upper left' plot proves 'passing from the wrong side' of the instability determining point (-1,0). This only concerns one specific working point and potential instability will be smoothed out by the 'overall time domain reality' in which is continuously crossed over from one to another working point. This effect is confirmed by time domain simulation results in chapter 4.

The encircling in the Nyquist diagrams of the point (0,0) visualises the indirect torque influence by pitching *in and around the tower eigenfrequency* ω_0^t. As eigenfrequency ω_0^t lays above the Nyquist frequency (1.2 rad/s), the encircling of the point (0,0) occurs without problems. In addition a tower filter will avoid any influence of the tower in this region.

The overall stability behavior is illustrated through fig.(3.11). The figure shows in the upper left graph the open loop gain in the Nyquist frequency in the whole operational range. All

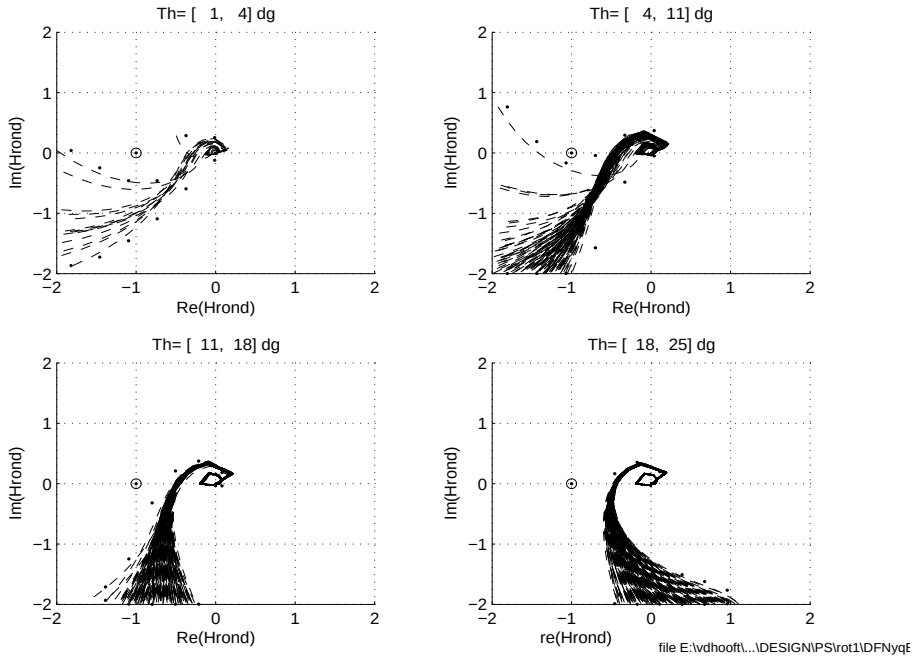

Figure 3.10: *Nyquist diagrams for the windturbine with scheduled PD-feedback and rotor speed filter; aerodynamic torque levels between 90% and 140% of the rated value; wind speed range [11.25m/s - 26m/s]; rotor speed range [14.6rpm - 17.6 rpm]*

gains are around the controller design target of 0.5 (eq.(3.10)). The upper right graph shows the phase lag in the open loop in the frequency beyond which the magnitude of $\mathring{H}_{\Omega_{\rm r}}$ becomes smaller than 1. Both the amplitude margin criterion (0.5) and the phase margin criterion (45 $^{\rm o}$) are amply met in all working points. So there is no risc for oscillating instability in the Nyquist frequency. The lower left graph shows the accompanying Nyquist frequencies, $\omega_{\rm nq}$ and 'phase margin frequencies',ω_ϕ . The former determine the oscillation frequency of the controlled system if the amplitude margin would be 0, that is to say if the open loop gain would be equal to 1 in this frequency; the latter are indicative for the control bandwidth, that is to say the maximum frequency in wind gusts of which the effect on the rotor speed still can be rejected. Dependent of the working point the value of the Nyquist and phase margin frequencies are around 1.2 rad/s and 0.4 rad/s respectively.

The lower right graph shows the so called 'destabilisation factor' $\eta_{\rm destab}$. This factor represents the ratio between *stabilising feedback* through the PD-compensator and *destabilising feedback* through the rotor speed; the latter occurs when the generator torque decreases at increasing rotor speed. For $\eta_{\rm destab} > 1$ the closed loop behaviour is exponentially instable. The graphs show that this holds one working point (fat dot at 17.6 rpm). This point corresponds with the 'upper envelope' in the upper left Nyquist plot in which the 'instability point' (-1,0) is passed 'from the wrong side'.

As (risk of) instability is only (theoretically) expected in a few working points: potential instability will be smoothed out by the 'overall time-domain reality', in which is continuously crossing over from one to another working point (stochastic excitation of non linear system). This smoothing effect is confirmed by time domain simulation in chapter 4.

Rotor speed setpoint adaptation: Basically, the rotor speed setpoint $\Omega_{\rm r}^*$, is set to its rated value $\Omega_{\rm r}^{\rm rat}$ for generation of rated electric power. In the higher wind speed regions, the pitch angle will be feathered and far away from its 'working position'. In case of sudden falling wind gusts, each rotor speed decrease will then cause loss of electric power, in spite of above rated wind speed.

To prevent this loss of production, in the higher wind speed region the rotor speed setpoint can

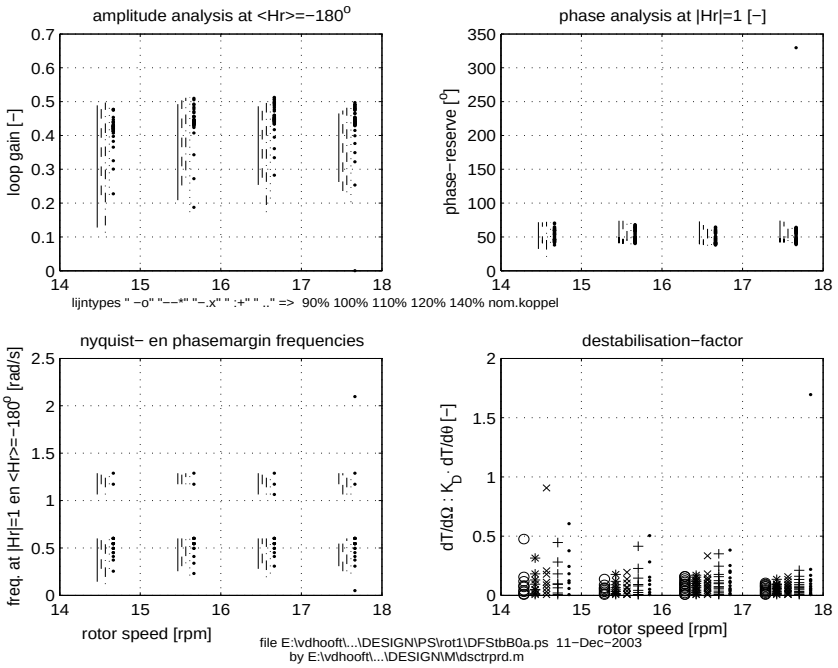

Figure 3.11: *Stability margins for the wind turbine with scheduled PD-feedback and low-pass 3p filter; aerodynamic torque levels between 90% and 140% of the rated value; wind speed range [11.25m/s - 26m/s]; rotor speed range [14.6rpm - 17.6 rpm]*

be raised slightly by 'a few rpm's', dependent on the pitch angle. The mechanism of 'kinetic buffering' (flywheel) is able to maintain rated power until the rotor speed will fall below its rated value.

To realise a smooth reference value towards the rotor speed controller, the setpoint offset $\Omega_{\mathrm{r}}^{\mathrm{off}}$ is only implemented between the lower limit $\theta_{\Omega_{\mathrm{r}}^{\mathrm{off}}}^{\mathrm{LL}}$ and the upper limit $\theta_{\Omega_{\mathrm{r}}^{\mathrm{off}}}^{\mathrm{UL}}$ in a linear way, using a first order filter with large time constant $\tau^{\Omega_{\mathrm{r}}^{\mathrm{off}}}$. Setting $\Omega_{\mathrm{r}}^{\mathrm{off}}$ to a value of 0.5-1 rpm,

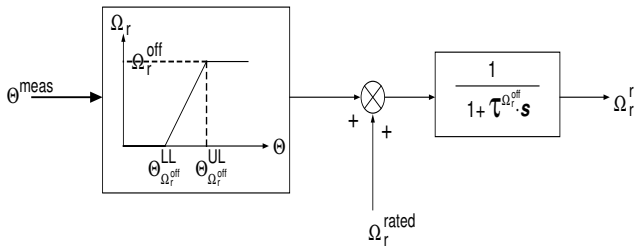

Figure 3.12: *Principle of rotor speed setpoint adaptation*

and $\theta_{\Omega_{\mathrm{r}}^{\mathrm{off}}}^{\mathrm{LL}}$, $\theta_{\Omega_{\mathrm{r}}^{\mathrm{off}}}^{\mathrm{UL}}$, to a value of 5 $^{\mathrm{o}}$ and 12 $^{\mathrm{o}}$, respectively, appears to be sufficient to avoid power loss due to sudden falling wind gusts during time domain simulations. This value is sufficient below the activation of forced rotor speed limitation (see subsection 3.2.4).

In case of power optimisation as proposed in subsection 3.4.2, this feature can be reduced considerably or even omitted by setting Ω_{r}^{*} to $\Omega_{\mathrm{r}}^{\mathrm{rat}}$.

3.2.2 Dynamic inflow compensation

As concluded in subsection 2.2.1, the dynamic effects of the wake (dynamic inflow) can not easily be neglected, specifically not for the low wind speed region. Therefore, a control structure, which compensates for the exaggerating effects of aerodynamic torque T_{a} has been designed and dimensioned. The structure of the compensator, eq.(3.15) in s-domain, is a reciprocal implementation of the 'assumed' wake behaviour as (linear) described in eq.(2.7).

$$H_{\mathrm{DI}}^{\mathrm{c}}(s) = \frac{\dot{\theta}_{\mathrm{DI}}^{*}(s)}{\dot{\theta}_{\Omega_{\mathrm{r}}}^{*}(s)} = \frac{(1+\tau_{\mathrm{I}}^{\mathrm{DI}}\cdot s)}{(1+\tau_{\mathrm{D}}^{\mathrm{DI}}\cdot s)} \tag{3.15}$$

The compensation structure is a cascade extension to the rotor speed PD controller. To deal with the non linear nature, the wind speed dependancy of the dimensioning time constants $\tau_{\mathrm{ld,T_a}}^{\mathrm{DI}}$ and $\tau_{\mathrm{lg}}^{\mathrm{DI}}$ are transferred to measurable pitch angle dependancies and assigned to respectively the dimensioning parameters $\tau_{\mathrm{I}}^{\mathrm{DI}}$ and $\tau_{\mathrm{D}}^{\mathrm{DI}}$ of the dynamic inflow compensator. The pitch angle dependancy of $\tau_{\mathrm{I}}^{\mathrm{DI}}$ and $\tau_{\mathrm{D}}^{\mathrm{DI}}$ is shown in fig.(3.13).

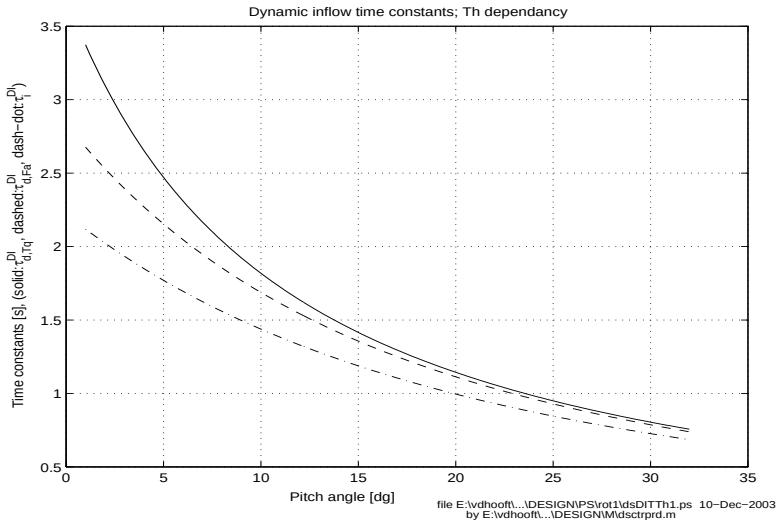

Figure 3.13: *Non linear dependancy of the lead-lag compensator time constants to the pitch angle, solid line:* $\tau_{\mathrm{ld,T_a}}^{\mathrm{DI}} = \tau_{\mathrm{D}}^{\mathrm{DI}}$ *; dotted line:* $\tau_{\mathrm{lg}}^{\mathrm{DI}} = \tau_{\mathrm{I}}^{\mathrm{DI}}$

3.2.3 Inactivity zone and limitation

Small pitch actions of the pitch actuation system are undesired because they will cause considerably mechanical loads for the actuation system. In particular if small pitch actions are due to remaining noise, despite of rotor speed filtering (subsection 3.2.1). Therefore, an inactivity zone is introduced which realises the following operations before the pitching setpoint $\dot{\theta}^{*}$ will be effectuated by the pitch actuators:

- ignoring of small pitching actions (inactivity zone);
- undisturbed passing of effective pitching actions (passing zone);
- avoiding to many transitions around the inactivity zone (hysteresis);
- enforced pitching when leaving the inactivity zone for compensation of temporal inactivity (catch up);
- limiting of the pitch speed to its maximum values (pitch speed limitation);

- ignoring pitching actions if maximum of minimum blade position is already reached (pitch angle limitation).

All above mentioned functions aim to reduce mechanical loads of the pitch actuation system without loss of control performance as intended by the pitch control algorithm. To ensure equal inactivity from rated wind speed to maximum wind speed level, the inactivity zone should be scheduled additionally. The scheduling of the inactivity zone is related to the 'PD scheduling factor $\mu_{\rm PD}$ as defined in eq.(3.12), via a weakening factor $\eta_{\rm IZ}$.

$$\begin{aligned}
\frac{\dot{\theta}^*\Big|_{(V_{\rm w}=V_{\rm w}^{\rm rat})}}{\dot{\theta}^*\Big|_{(V_{\rm w}=V_{\rm w}^{\rm co})}} &= \frac{\Big((T_{\rm a})'_{\theta}\cdot(T_{\rm a})'_{\rm V_w}\cdot\sigma_{\rm l}\Big)\Big|_{V_{\rm w}=V_{\rm w}^{\rm rat}}}{\Big((T_{\rm a})'_{\theta}\cdot(T_{\rm a})'_{\rm V_w}\cdot\sigma_{\rm l}\Big)\Big|_{V_{\rm w}=V_{\rm w}^{\rm co}}} \\
&= \mu_{\rm PD}\cdot\left[\frac{(T_{\rm a})'_{\rm V_w}\Big|_{V_{\rm w}=V_{\rm w}^{\rm rat}}}{(T_{\rm a})'_{\rm V_w}\Big|_{V_{\rm w}=V_{\rm w}^{\rm co}}}\cdot\frac{(15+a\cdot V_{\rm w}^{\rm rat})}{(15+a\cdot V_{\rm w}^{\rm co})}\right] \\
&= \mu_{\rm PD}\cdot\eta_{\rm IZ} \qquad (3.16)
\end{aligned}$$

This weakening factor caters for the higher turbulence at higher wind speeds. In eq.(3.16) the standard deviation of the longitudinal wind speed $\sigma_{\rm l}$ has been approximated by eq.(3.17) as defined in [1].

$$\sigma_{\rm l} = I_{15}\cdot(15[{\rm m/s}]+a\cdot V_{\rm w})\,/\,(a+1) \qquad (3.17)$$

Assuming that $(T_{\rm a})'_{\rm V_w}$ is equal between rated wind speed ($V_{\rm w}^{\rm rat}$ =12.3 m/s) and cut-out wind speed ($V_{\rm w}^{\rm co}$ =25 m/s) [4] and a=2, a schedule weakening factor $\eta_{\rm IZ}$value of 0.56 was determined. In fig.(3.14) the scheduled inactivity zone is visualised for different pitch angles during full load operation. At partial load operation specific values of the inactivity zone were used, see section 3.3.

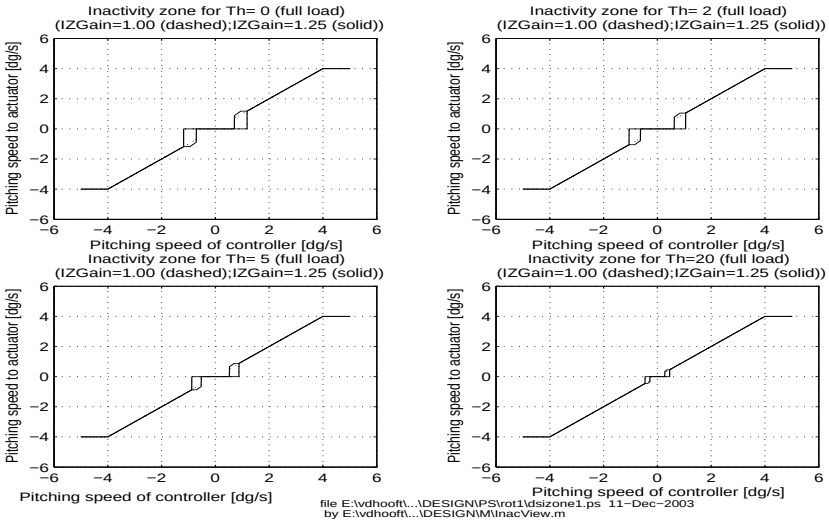

Figure 3.14: *Visualisation of scheduled inactivity zone for pitch angles 0, 2, 5, 20* $^{\rm o}$

It can be easily seen, that both the inactivity zone and accompanying hysteresis differs considerably depending on the pitch angle. Within the inactivity zone no pitch activity is effectuated, while the passing zone (unity gain) is limited by the maximum pitching speed values ($|\dot{\theta}_{\rm full}^{\rm max}|$= 4 $^{\rm o}/{\rm s}$). The base value of the inactivity zone, $\dot{\theta}_{\rm IZ,base}^{\rm full}$, is defined *from the origin to the hystereses centre without scheduling* and set to 0.30 $^{\rm o}/{\rm s}$; this means that for the shown pitch angles

[4] this is a conservative assumption, a typical practical value for $(T_{\rm a})'_{\rm V_w}\Big|_{V_{\rm w}=V_{\rm w}^{\rm rat}}$ / $(T_{\rm a})'_{\rm V_w}\Big|_{V_{\rm w}=V_{\rm w}^{\rm co}}$ is 0.6, taking this quotient into account results in $\eta_{\rm IZ}$= 0.34, which implies more activity in the low wind speed region

(0,2,5,20 ^{o}) an activity zone is applied of respectively 0.94, 0.84, 0.70 and 0.36 $^{o}/s$. The width of the hysteresis (defined as the distance between a transtion point and its centre), is related to the base value of the inactivity zone by a factor $\dot{\theta}^{\rm full}_{\rm hys,base}$ and set to 0.5; this means that a hysteresis is applied of half the activity zone. The amount of pitching speed compensation for having stayed in the inactivity zone is clearly visible in the first upper left plot, the solid line shows an additional control gain (multiplier of 1.25).

Another feature, although not visualised in fig.(3.14), is a mechanism that excludes pitching actions if the maximum of minimum blade position ($\theta^{\rm max}$=90 ^{o}, $\theta^{\rm min}$= 1 ^{o}) has already been reached. Detection is based on both the direction (sign) of the pitching speed setpoint and the actual pitch angle, if the upper or lower limit of the pitch angle should be exceeded, no pitch actuation is allowed by overruling the pitching speed to a zero value. At partial load operation specific values of the upper and lower limits can be used, see section 3.3.

3.2.4 Forced rotor speed limitation

A maximum rotor speed is guaranteed in order to limit wind turbine loading and to minimize the variable speed range of the generator and converter. Commonly, exceeding the rotor speed alarm value will lead to intervention of the turbine supervisory control system and probably result in turbine shut down. In order to prevent this type of shut-down, the pitch control algorithm contains a so called 'forced rotor speed limitation', a mechanism that ensures limitation of the rotor speed by forcing the rotor blades towards feathering direction. The principle of forced rotor speed limitation is shown in fig.(3.15). As soon as the 'switch' condition is valid

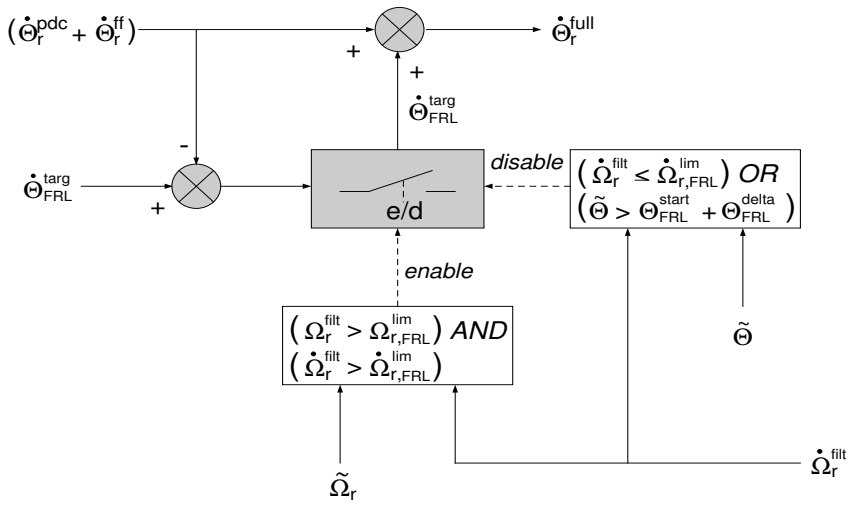

Figure 3.15: *Principle of forced rotor speed limitation by forcing the rotor blades in feathering direction*

(enable), the pitching speed setpoint is forced to the target value, $\dot{\theta}^{\rm targ}_{\rm frl}$ (3-4 $^{o}/s$). To avoid switching transients at *disabling*, the target value is effectuated by adding the deficit to the calculated pitch speed setpoint $\dot{\theta}^{*}_{\Omega_r}$ feedback and wind speed feed forward value. *Enabling* occurs as soon as the measured rotor speed value exceeds the forced rotor speed limit value, $\Omega^{\rm lim}_{\rm r,frl}$ = $\Omega^{\rm max}_{\rm r}$ - [1 .. 1.5 rpm] (17rpm), and the rotor speed is still increasing ($\dot{\Omega}^{\rm filt}_{\rm r}$>0). To minimise loss of energy yield, disabling of the forced rotor speed limitation takes place as soon as the rotor speed decreases ($\dot{\Omega}^{\rm filt}_{\rm r}$<0) or the pitch angle has been increased for $\theta^{\rm off}_{\rm frl}$ degrees (3 ^{o}) since the intervention was started. The forced pitching speed $\dot{\theta}^{\rm targ}_{\rm frl}$ is not affected by the dynamic inflow compensator, the inactivity zone or pitching speed limitation.

3.2.5 Estimated wind speed feed forward

The principle of wind speed feed forward control is based on a rotor effective wind speed estimation from the aerodynamic torque for pitch actuation that is mathed to the rated power. Strictly, it should be named as 'pseudo' feed forward control, because the wind speed is not directly fed in as a measured value, but is reconstructed from measurements and 'a-priori' knowledge of rotor behaviour ('feed back loop'):

- low pass filtered measurements of rotorspeed ($\tilde{\Omega}_{\rm r}^{\rm f}$), pitch angle ($\tilde{\theta}^{\rm f}$) and electric power ($\tilde{P}_{\rm e}^{\rm f}$);
- aerodynamic and mechanical behaviour: loss parameters ($\hat{C}_{\rm c}$ and $\hat{C}_{\Omega_{\rm r}}$), rotor torque coefficients ($\hat{C}_{\rm q}(\lambda,\theta)$), air density $\hat{\rho}_{\rm air}$;
- rotor parameters: rotordiameter ($\hat{R}_{\rm b}$), total inertia ($\hat{J}_{\rm t}$).

The low pass filtered rotor acceleration $\dot{\tilde{\Omega}}_{\rm r}^{\rm f}$ is derived numerically from $\tilde{\Omega}_{\rm r}$ and filtered afterwards. Mechanic losses are incorporated by estimation of torque losses, eq.(3.18)

$$\hat{T}_{\rm l} = \hat{C}_{\rm c} + \hat{C}_{\Omega_{\rm r}} \cdot \tilde{\Omega}_{\rm r} \tag{3.18}$$

The estimated wind speed feed forward structure consists of three sequential steps which should be executed on-line:

- reconstruction of aerodynamic torque, $\hat{T}_{\rm a}$;
- wind speed estimation, $\hat{V}_{\rm w}$;
- pitch speed setting, $\dot{\theta}^{*}_{\hat{V}_{\rm w}}$.

These steps will be discussed below in detail.

Reconstruction of aerodynamic torque The aerodynamic torque ($\tilde{T}_{\rm a}$) is reconstructed from the (low frequency) power balance

$$\tilde{T}_{\rm a} = \hat{J}_{\rm t} \cdot \dot{\tilde{\Omega}}_{\rm r}^{\rm f} + \left(\tilde{P}_{\rm e}^{\rm f}/\tilde{\Omega}_{\rm r}^{\rm f}\right) + \hat{T}_{\rm l} \tag{3.19}$$

in which $\hat{J}_{\rm t}$ is taken equal to $J_{\rm t}$in eq.(2.16). If the dynamic behaviour of the electric torque actuator (generator including converter) is negligible (bandwidth 5-10 times bandwidth low pass filtering), the power measurement can be avoided by replacing the second term of eq.(3.19) with the power production setpoint $T_{\rm e}^{*}(\Omega_{\rm r})$. Thus an explicit relation exists between $\tilde{\Omega}_{\rm r}^{\rm f}$ and $\hat{T}_{\rm a}$.

Wind speed estimation Due to the low pass rotor speed filtering, the estimated wind speed value $\hat{V}_{\rm w}$ will be a (delayed) approximation of the fictive rotor uniform wind speed, $V_{\rm w}^{\rm unif}$. The relationship between $\hat{T}_{\rm a}$ and $\hat{V}_{\rm w}$ is described in accordance with eq.(2.1):

$$\hat{C}_{\rm q}(\tilde{\theta}^{\rm f},\hat{\lambda}) \cdot \tfrac{1}{2}\hat{\rho}_{\rm air}\pi\hat{R}_{\rm b}^{3} \cdot (\hat{V}_{\rm w})^2 = \hat{T}_{\rm a}(\dot{\tilde{\Omega}}_{\rm r}^{\rm f}, \tilde{\Omega}_{\rm r}^{\rm f}) \tag{3.20}$$

In eq.(3.20), fore-aft tower displacements, $\dot{x}_{\rm nd}$ are not taken into account. However, $\hat{V}_{\rm w}$ can be compensated for these fore-aft movements afterwards, if the tower top acceleration $\ddot{x}_{\rm nd}$ is measured. The dependency of $\hat{C}_{\rm q}$ from the tip speed ratio $\hat{\lambda}$:

$$\hat{\lambda} = \frac{\tilde{\Omega}_{\rm r}^{\rm f} \cdot \hat{R}_{\rm b}}{\hat{V}_{\rm w}} \tag{3.21}$$

results in an implicit relationship between $\hat{T}_\mathrm{a}$ and $\hat{V}_\mathrm{w}$.
In the operation range of the turbine, the relation T_a= f(V_w) is not always a function in mathematical sense. In other words, there's may exist two valid solutions for $\hat{V}_\mathrm{w}$ in an operation point determined by $\hat{T}_\mathrm{a}$, $\tilde{\Omega}_\mathrm{r}$ and $\tilde{\theta}$. This happens specifically for rotor speeds at small pitch angles (see fig.(3.16)). The physical meaning of two solutions is found in the nature of air

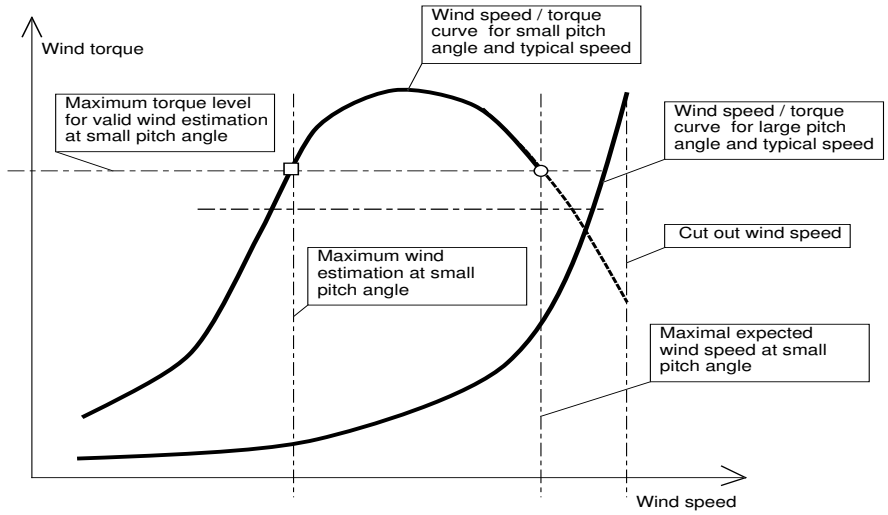

Figure 3.16: *Relationship between wind torque and wind speed for estimation procedure for certain values of pitch angle, wind torque and rotor speed*

flow, the 'low wind speed solution' implies attached flow, while the 'high wind speed solution' implies stalled or turbulent flow. Stall solutions are left out of consideration, by introducing a maximum allowable aerodynamic torque level for wind speed estimation, $T^{\max}_{\hat{\mathrm{V}}_\mathrm{w}}(\tilde{\theta},\tilde{\Omega}_\mathrm{r})$, which should be set such that stall solutions are avoided, but the estimation range still covers the turbine operation range. As a consequence, the special cases of stall conditions for a 'pitch to vane turbine' are excluded and will yield a 'no valid solution' for the estimated wind speed.

Then $\hat{T}_\mathrm{a}$ = f($\hat{V}_\mathrm{w}$) shows monotonious behaviour for all relevant values of $\tilde{\theta}$ and $\tilde{\Omega}_\mathrm{r}$. A unique solution for $\hat{V}_\mathrm{w}$ can be obtained from eq.(3.19) and eq.(3.20) via a quick converging numeric iterative method like Newton Raphson ('gradient method'):

$$\hat{V}_\mathrm{w}^{(\mathrm{k})} = \hat{V}_\mathrm{w}^{(\mathrm{k}-1)} - \frac{\left(\tilde{T}_\mathrm{a} - \hat{T}_\mathrm{a}^{(\mathrm{k}-1)}\right)}{\left(\frac{\mathrm{d}\hat{T}_\mathrm{a}}{\mathrm{d}\hat{V}_\mathrm{w}}\right)_{\hat{V}_\mathrm{w}^{(\mathrm{k}-1)}}} \tag{3.22}$$

The superscript (k) and (k-1) in eq.(3.22), represents time-discrete instances for the actual and old values, respectively. Usually, the iteration loop will be interrupted after 2 or 3 steps because of sufficient accuracy regarding $|\tilde{T}_\mathrm{a} - \hat{T}_\mathrm{a}|$ and $|\hat{V}_\mathrm{w}^{(\mathrm{k})} - \hat{V}_\mathrm{w}^{(\mathrm{k}-1)}|$.
The aerodynamic torque coefficients in eq.(3.20) are off-line fitted to a 2D-polynomial function:

$$\hat{C}_\mathrm{q}(\tilde{\theta}^\mathrm{f}, \hat{\lambda}^{-1}) = \sum_{\mathrm{i}=1}^{\mathrm{N}_\theta+1} \sum_{\mathrm{j}=1}^{\mathrm{N}_{\Omega_\mathrm{r}}+1} C_{\mathrm{C_q}}(i,j) \cdot \theta^{(j-1)} \cdot \lambda^{-(i-1)} \tag{3.23}$$

The maximum allowable aerodynamic torque levels $T^{\max}_{\hat{\mathrm{V}}_\mathrm{w}}(\tilde{\theta},\tilde{\Omega}_\mathrm{r})$ for wind speed estimation, which checks on 'stall' solutions, are also fitted off-line to a 2D-polynomial function:

$$T^{\max}_{\hat{\mathrm{V}}_\mathrm{w}}(\tilde{\theta},\tilde{\Omega}_\mathrm{r}) = \sum_{\mathrm{i}=1}^{\mathrm{N}_{\Omega_\mathrm{r}}+1} \sum_{\mathrm{j}=1}^{\mathrm{N}_\theta+1} C_{\mathrm{T}^{\max}_{\hat{\mathrm{V}}_\mathrm{w}}}(i,j) \cdot \theta^{(j-1)} \cdot \Omega_\mathrm{r}^{(i-1)} \tag{3.24}$$

To avoid to many transitions between the valid/invalid states, the actual aerodynamic torque limit for wind speed estimation is low pass filtered (10s) and switch hysteresis (+/- 5%) is applied.

To ensure numeric convergence (start-up, invalid solution), a favourable initial wind speed estimation ($\hat{V}_{\mathrm{w}}^{\mathrm{ini}}$) is calculated from a specific 2D-polynomial function,

$$\hat{V}_{\mathrm{w}}^{\mathrm{ini}}(\tilde{\theta}, \tilde{\Omega}_{\mathrm{r}}) = \sum_{\mathrm{i}=1}^{\mathrm{N}_{\Omega_{\mathrm{r}}}+1} \sum_{\mathrm{j}=1}^{\mathrm{N}_{\theta}+1} C_{\hat{\mathrm{V}}_{\mathrm{w}}^{\mathrm{ini}}}(i,j) \cdot \theta^{(j-1)} \cdot \Omega_{\mathrm{r}}^{(i-1)} \tag{3.25}$$

This polynomial is also calculated off-line and is based on sufficient torque to wind speed sensitivity for all relevant operation points.

Finally, fig.(3.17) shows for typical values of pitch angles and rotor speed within the operation range the theoretical (lines) and polynomial fits (dots) of wind speed estimation for the allowed aerodynamic torque range. The 'asterisk' markers emphasise the initial operation points, from which convergence is guaranteed if wind speed estimation should start-up from scratch.

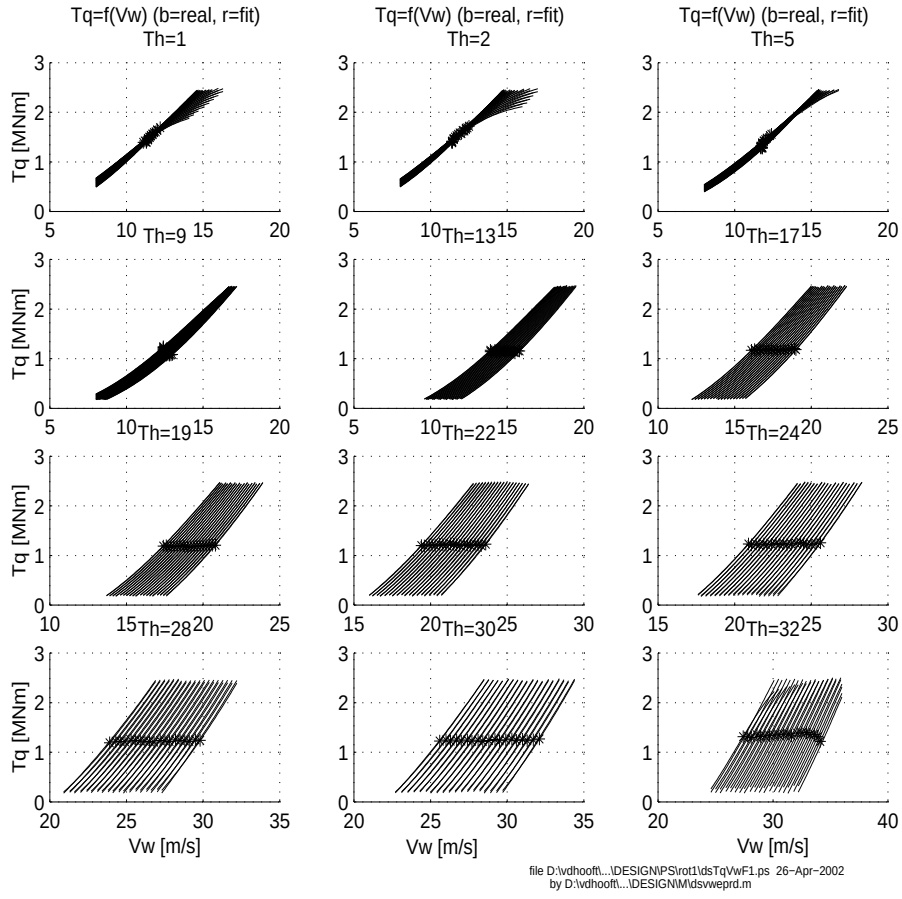

Figure 3.17: *Theoretical and fitted results of wind speed estimation from aerodynamic torque for the wind turbine operation range*

Pitch speed setting The estimated wind speed will be used to realise an additional pitch control action, which optimises the turbine power production and improves its behaviour at sudden wind gusts. A target pitch angle value $\theta^*_{\hat{\mathrm{V}}_{\mathrm{w}}}$ is determined from the desired condition to maintain stationary rated power production, and is related to the estimated wind speed, $\hat{V}_{\mathrm{w}}$,

and the measured rotor speed $\tilde{\Omega}_{\rm r}^{\rm f}$ by eq.(3.26)

$$\hat{C}_{\rm p}(\theta^*_{\hat{\rm V}_{\rm w}},\hat{\lambda})\cdot\tfrac{1}{2}\hat{\rho}_{\rm air}\pi\hat{R}_{\rm b}^2\cdot(\hat{V}_{\rm w})^3 = P_{\rm a}^{\rm rat} \tag{3.26}$$

Determination of $\theta^*_{\hat{\rm V}_{\rm w}}$ from eq.(3.26) is complicated because of the implicit relationship with $\hat{V}_{\rm w}$. However, this can be solved off-line numerically, which results in a 2D-polynomial function (eq.(3.27), $V_{\rm w}^{-1}$ dependancy)

$$\theta^*_{\hat{\rm V}_{\rm w}}(\hat{V}_{\rm w},\tilde{\Omega}_{\rm r}) = \sum_{\rm i=1}^{{\rm N_{V_w}}+1{\rm N}_{\Omega_{\rm r}}+1}\sum_{\rm j=1} C_{\theta^*_{\hat{\rm V}_{\rm w}^{-1}}}(i,j)\cdot\Omega^{(j-1)}\cdot V_{\rm w}^{-(i-1)} \tag{3.27}$$

The pitch speed setpoint, $\dot{\theta}^*_{\hat{\rm V}_{\rm w}}$ for wind speed changes is determined from

$$\dot{\theta}^*_{\hat{\rm V}_{\rm w}} = (\theta^*_{\hat{\rm V}_{\rm w}})'_{\hat{\rm V}_{\rm w}}\cdot\dot{\hat{V}}_{\rm w} \tag{3.28}$$

in which $(\theta^*_{\hat{\rm V}_{\rm w}})'_{\hat{\rm V}_{\rm w}}$ can be found from eq.(3.27)

$$(\theta^*_{\hat{\rm V}_{\rm w}})'_{\hat{\rm V}_{\rm w}}(\hat{V}_{\rm w},\tilde{\Omega}_{\rm r}) = \sum_{\rm i=1}^{{\rm N_{V_w}}+1{\rm N}_{\Omega_{\rm r}}+1}\sum_{\rm j=1} -(i-1)\cdot C_{\theta^*_{\hat{\rm V}_{\rm w}^{-1}}}(i,j)\cdot\Omega^{(j-1)}\cdot V_{\rm w}^{-i} \tag{3.29}$$

From control viewpoint, eq.(3.28) implies a D-action from the estimated wind speed to the pitch speed including a non linear gain to maintain rated power. To comply with stability and numerical noise restrictions, a scale factor $K_{\rm D}^{\hat{\rm V}_{\rm w}}$ and moderate differentiation time constant $\tau_{\rm D}^{\hat{\rm V}_{\rm w}}$ is introduced (in Laplace domain):

$$H^{\rm c}_{\hat{\rm V}_{\rm w}}(s) = \frac{\dot{\theta}^*_{\hat{\rm V}_{\rm w}}(s)}{\hat{V}_{\rm w}(s)} = (\theta^*_{\hat{\rm V}_{\rm w}})'_{\hat{\rm V}_{\rm w}}\cdot K_{\rm D}^{\hat{\rm V}_{\rm w}}\cdot\frac{\tau_{\rm D}^{\hat{\rm V}_{\rm w}}\cdot s}{1+\tau_{\rm D}^{\hat{\rm V}_{\rm w}}\cdot s} \tag{3.30}$$

Fig.(3.18) shows the sensitivity of the pitch speed to the rate of change in the wind speed. (eq.(3.29)) Due to the high sensitivity to the wind acceleration, the maximum value is usually limited to 4 $^{\rm o}/{\rm s}$ to avoid nervous pitch control actions. In frequency domain the moderate D-action acts as a first order high pass filter with gain $K_{\rm D}^{\hat{\rm V}_{\rm w}}$ and cut-off frequency at $1/\tau_{\rm D}^{\hat{\rm V}_{\rm w}}$. In combination with the low-pass filtered rotor speed and acceleration the serial behaviour results in a bandpass characteristic. Therefore, the value of $1/\tau_{\rm D}^{\hat{\rm V}_{\rm w}}$ should be set to a value lower than $\omega_0^{\rm 3p}$ (and $\omega_0^{\rm col}$), creating sufficient passing bandwidth and not affecting the very low (stationary) frequency behaviour. This results usually in a typical value of 0.5-1s. The scale factor $K_{\rm D}^{\hat{\rm V}_{\rm w}}$ is more arbitrary, but a value greater than unity is not allowed (0.5 - 0.8).

Two conditional rules are added to optimise the co-operation between estimated wind speed feed forward control and rotor speed control; pitch speed contributions

- in vane direction are only effectuated if $\tilde{\Omega}_{\rm r}^{\rm f} > \Omega^{\rm max}_{\rm r,\hat{V}_w}$;
- in work direction are only effectuated if $\tilde{\Omega}_{\rm r}^{\rm f} < \Omega^{\rm min}_{\rm r,\hat{V}_w}$;

Typical values for $\Omega^{\rm max}_{\rm r,\hat{V}_w}$ and $\Omega^{\rm min}_{\rm r,\hat{V}_w}$ are ($\Omega_{\rm r}^{\rm rat}$ +1 rpm) and $\Omega_{\rm r}^{\rm rat}$.

From the viewpoint of control theory ‘estimated wind speed feed forward control’ adds an additional DD-control action to rotor speed feedback (‘jerk control’).

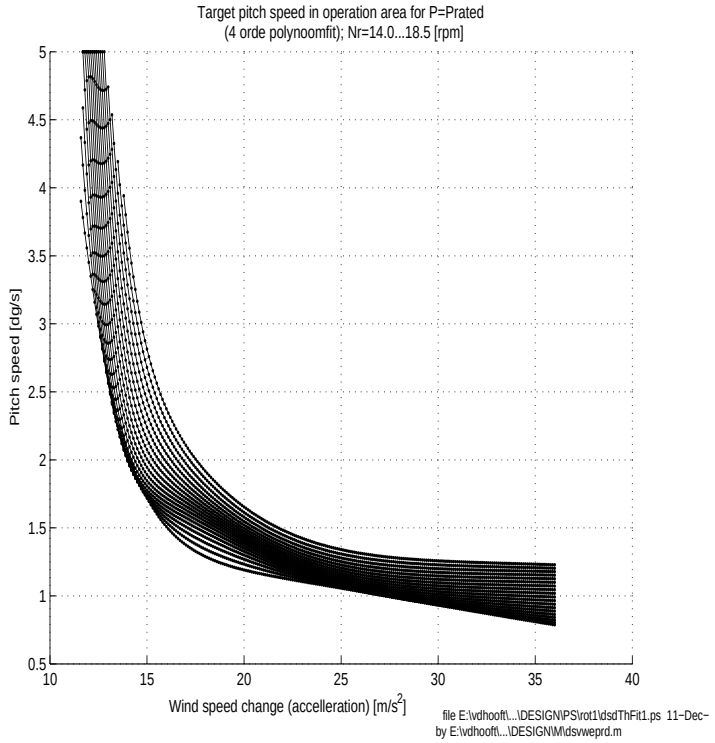

Figure 3.18: *Pitch speed target values for wind speed variations (acceleration) within the wind turbine operation range*

Evaluation: In fig.(3.19), both the estimated and (forced) uniform wind speed are shown. It is concluded that the estimated wind speed in the lower window is very similar to the uniform wind speed in the upper window, except a phase lag due to the use of filtered measurements for pitch angle and rotor speed.

The behaviour of the estimated wind speed feed forward control is shown in fig.(3.20). The simulation is calculated at a mean wind speed level just above rated wind speed (120%) and the control performance without and with feed forward are shown in the upper and lower four windows, respectively. Due to the estimated wind speed feed forward, the power production increases from 92% to 97.2%. The standard deviation of the rotor speed (as a measure for fluctuation) decreases from 0.462 rpm to 0.401 rpm. This is due to more adequate pitch control to wind speed changes, either to working position as to feathering position.

Further evaluation at different wind speed levels and taking a representative Weibull distribution function into account (remote offshore at North sea) results in 0.9% improvement of overall energy yield (with respect to de-activation of the feed forward and without the optimisation as will be discussed in subsection 3.4.2).

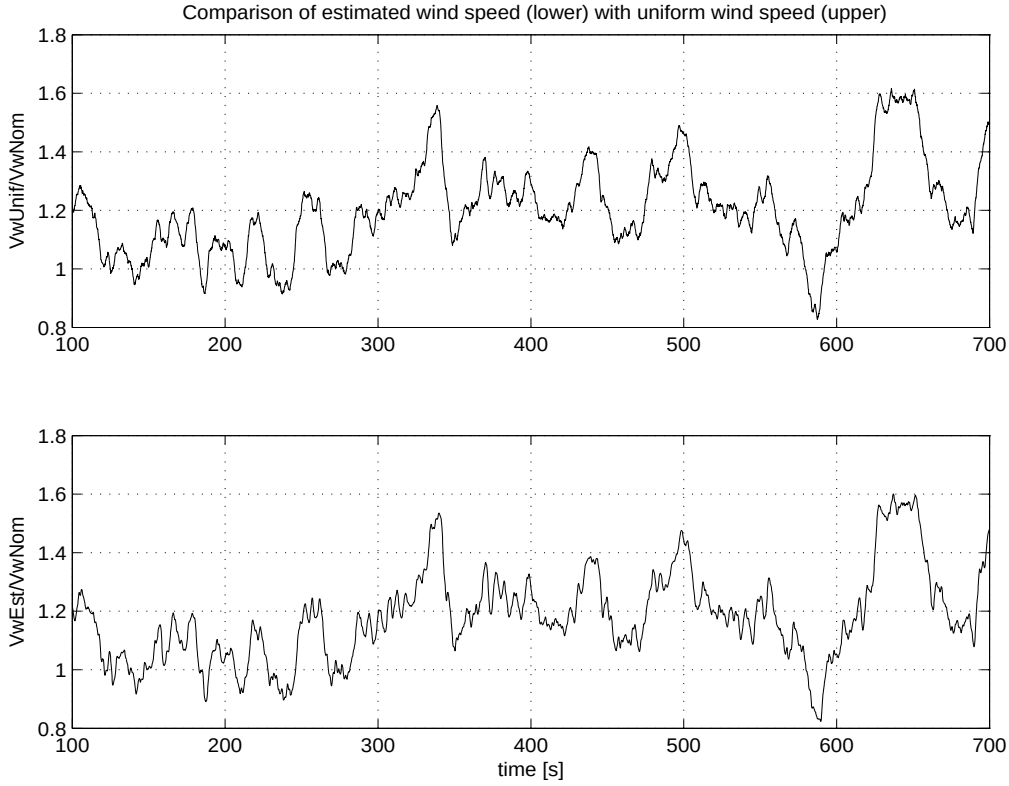

Figure 3.19: *Comparison of uniform wind speed (upper window) and estimated wind speed (lower window) at 120% of its rated level*

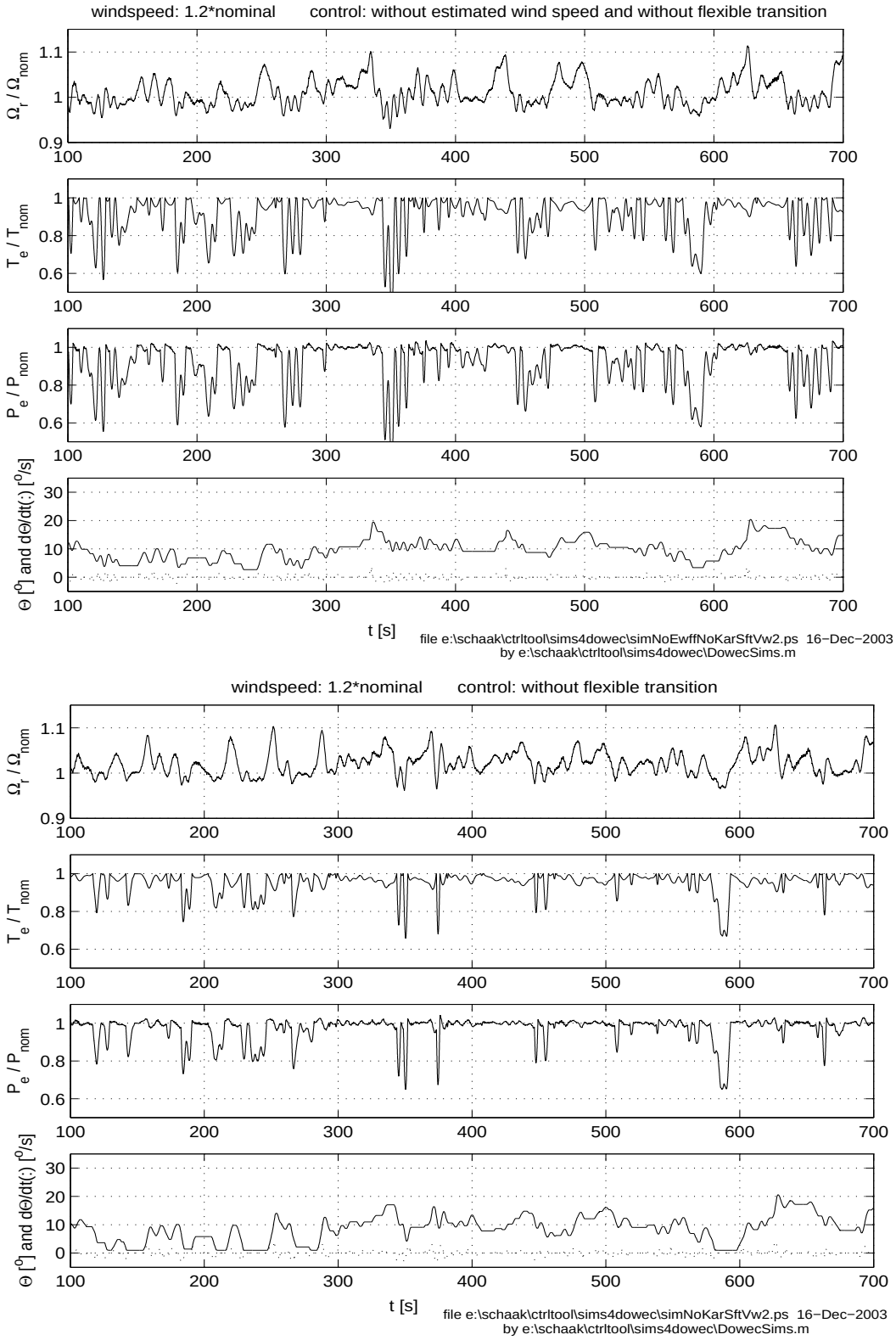

Figure 3.20: *Comparison between control without (upper windows) and with (lower windows) the use of estimated wind speed feed forward*

3.3 Pitch control algorithm at partial load operation

For partial load operation the blade pitch angle is set to a 'rotor speed dependent' setpoint value using a simple servo controller. The pitch angle setpoint values are stored in a user defineable table (Ω_r, θ^*_part) and set to values which represent maximum power coefficient operation or lower noise production. Pitch angles that represent maximum power at optimum lambda conditions are determined from the power coefficient curves of the rotor as shown in fig.(2.2). Linear interpolation is used to achieve an accurate pitch angle setpoint θ^*_part for the filtered rotor speed $\Omega^\mathrm{f}_\mathrm{r}$.

A simple proportional feedback structure eliminates any deviation (for step shaped changes) between the measured pitch angle $\tilde{\theta}^\mathrm{f}$ and the pitch angle setpoints θ^*_part , by setting the partial load pitching speed $\dot{\theta}^*_\mathrm{part}$ (see fig.(3.21)). The proportional gain K^θ_P is dimensioned on a linear

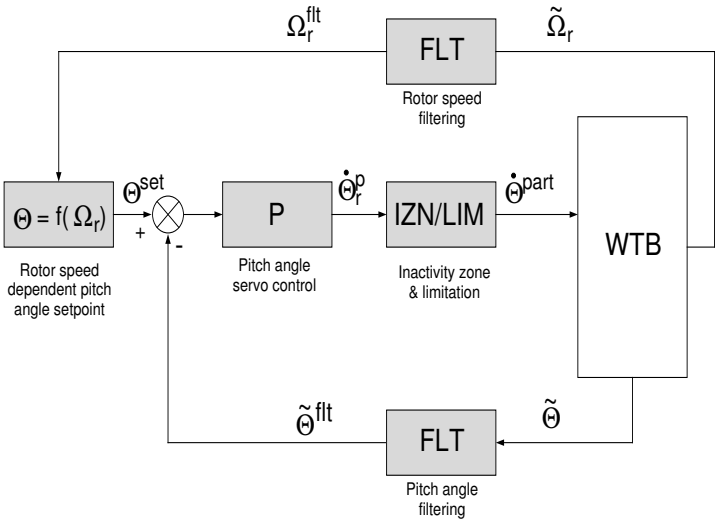

Figure 3.21: *Pitch angle servo control at partial load conditions*

model that is build up by a delayed integrator. The delay time equals $T^{\Omega_\mathrm{r}}_\mathrm{d}$ in eq.(3.7). Stability is ensured if

$$K^\theta_\mathrm{P} \leq \frac{\pi}{4 \cdot (T^\theta_\mathrm{d})}. \tag{3.31}$$

Pitch control for partial load operation does not make use of dynamic inflow compensation, because of the relative small changes of the pitch angle and pitch speed. The structure of the inactivity zone and limitation is equal to the structure at full load operation (subsection 3.2.3), although specific parameters are used to achieve suitable behaviour in this operation region.

Because of the interaction between pitch control and generator control, the transition between partial load and is discussed in subsection 3.4.2.

3.4 Torque setpoint control

Electric torque control will primarily be used for power regulation during partial and full load operation (subsection 3.4.1). Additionally, it is a valuable controlled input to optimise the transition zone around rated conditions between partial and full load control (subsection 3.4.2) and to reduce extreme rotor speed values (subsection 3.4.3). In order to reduce turbine loading, more high-frequency variations can be used to reduce torsional drive train and sideward tower vibrations (chapter 5).

3.4.1 Stationary power production curve

The stationary relation for power production is determined in accordance with the design values of $\Omega_{\rm r}^{\rm rat}$, $\Omega_{\rm r}^{\rm min}$, $\Omega_{\rm r}^{\rm max}$ and $P_{\rm e}^{\rm rat}$ as defined in table(2.1).

Fig.(3.22) shows the generator curves in which five operation regions, or 'generator states', are distinguished between typical rotor speed levels.

$$
\begin{array}{lll}
1. \text{ no power production} & : & (\tilde{\Omega}_{\rm r}^{\rm f} < \Omega_{\rm r}^{\rm ci}) \ \text{OR} \ (\tilde{\Omega}_{\rm r}^{\rm f} \geq \Omega_{\rm r}^{\rm co}); \\
2. \text{ start-up} & : & \Omega_{\rm r}^{\rm ci} \leq \tilde{\Omega}_{\rm r}^{\rm f} < \Omega_{\rm r}^{\lambda_{\rm opt}^{\rm in}}; \\
3. \text{ optimum tip speed ratio} & : & \Omega_{\rm r}^{\lambda_{\rm opt}^{\rm in}} \leq \tilde{\Omega}_{\rm r}^{\rm f} < \Omega_{\rm r}^{\lambda_{\rm opt}^{\rm out}}; \\
4. \text{ transition} & : & \Omega_{\rm r}^{\lambda_{\rm opt}^{\rm out}} \leq \tilde{\Omega}_{\rm r}^{\rm f} < \Omega_{\rm r}^{\rm rat}; \\
5. \text{ full power} & : & \Omega_{\rm r}^{\rm rat} \leq \tilde{\Omega}_{\rm r}^{\rm f} < \Omega_{\rm r}^{\rm co}.
\end{array}
\tag{3.32}
$$

Due to the variable speed concept, the electric torque of the generator will be controlled

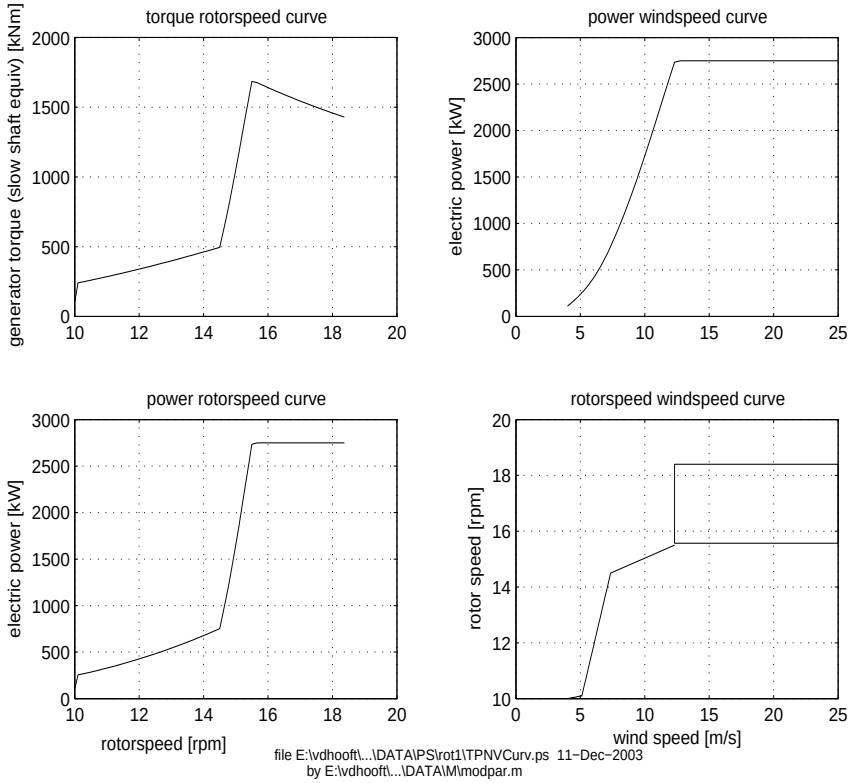

Figure 3.22: *Steady state figures of generator torque, -power and -speed*

directly by the converter; therefore the electric torque to rotor speed relationship shall be determinative for turbine behaviour and performance.

Due to the turbine design limits, no power will be produced outside the wind speed design range below the cut-in wind speed $V_{\rm w}^{\rm ci}$ and above the cut-out wind speed $V_{\rm w}^{\rm co}$, therefore $T_{\rm e}^{\rm cv}$=0 within this range.
The start-up region is usually small but necessary to (over)compensate the turbine's own losses. The torque setpoint is simply realised by a linear transition between the rotor speed that corresponds with cut-in wind speed $\Omega_{\rm r}^{\rm ci}$ and lowest rotor speed $\Omega_{\rm r}^{\lambda_{\rm opt}^{\rm in}}$ for which optimal lambda operation is pursued:

$$
T_{\rm e\,,startup}^{*} = \left(\frac{\tilde{\Omega}_{\rm r}^{\rm f} - \Omega_{\rm r}^{\rm ci}}{\Omega_{\rm r}^{\lambda_{\rm opt}^{\rm in}} - \Omega_{\rm r}^{\rm ci}} \right) \cdot T_{\rm e}^{\lambda_{\rm opt}}(\Omega_{\rm r}^{\lambda_{\rm opt}^{\rm in}}) \tag{3.33}
$$

In region 3 (below rated wind speed) the rotor speed is adjusted proportional to the (below rated) wind speed by electric torque control, in such a way that the aerodynamic power extracted by the rotor is maximised. This implies a constant value of the tip speed ratio, at which the power coefficient is maximal: $\lambda_{\rm opt}$. The torque setpoint in the optimum tip speed region ($\Omega_{\rm r}^{\lambda_{\rm opt}^{\rm in}}$ - $\Omega_{\rm r}^{\lambda_{\rm opt}^{\rm out}}$) is easy to describe by a low order polynomial approximation:

$$T_{\rm e\,,\lambda_{\rm opt}}^{*} = \sum_{\rm i=1}^{{\rm N}_{\lambda_{\rm opt}}+1} C_{T_{\rm e}^{\lambda_{\rm opt}}}(i) \cdot (\tilde{\Omega}_{\rm r}^{\rm f})^{i-1} \tag{3.34}$$

From the viewpoint of efficiency, a steep transition (region 4) from region 3 to constant power control (region 5) is desired, although this is restricted by maximum allowable torque steepness of the generator curve. The transition region is realised by a linear torque transition between $\Omega_{\rm r}^{\lambda_{\rm opt}^{\rm out}}$ and the rated rotor speed $\Omega_{\rm r}^{\rm rat}$

$$T_{\rm e\,,trans}^{*} = T_{\rm e}^{\lambda_{\rm opt}}(\Omega_{\rm r}^{\lambda_{\rm opt}^{\rm out}}) + \left(\frac{\tilde{\Omega}_{\rm r}^{\rm f} - \Omega_{\rm r}^{\lambda_{\rm opt}^{\rm out}}}{\Omega_{\rm r}^{\rm rat} - \Omega_{\rm r}^{\lambda_{\rm opt}^{\rm out}}}\right) \cdot \left(\frac{P_{\rm e}^{\rm rat}}{\Omega_{\rm r}^{\rm rat}} - T_{\rm e}^{\lambda_{\rm opt}}(\Omega_{\rm r}^{\lambda_{\rm opt}^{\rm out}})\right) \tag{3.35}$$

The region above rated conditions (region 5) is destinated to produce constant rated electric power to the grid:

$$T_{\rm e\,,full}^{*} = \frac{P_{\rm e}^{\rm rat}}{\tilde{\Omega}_{\rm r}^{\rm f}} \tag{3.36}$$

Most of the turbine production time will take place around rated conditions. Therefore it will be valuable to optimise the transition around rated conditions both for generator control as well as for pitch control and their interactions. This will be subject of subsection 3.4.2.

To avoid injection of rotor speed disturbances (3p, blade lead-lag, tower), in the transition between full and partial load control, the electric torque setpoint for power production is determined by the low-pass filtered rotor speed $\tilde{\Omega}_{\rm r}^{\rm f}$.

The generator operation states are determined unambigiously ('state machine') from the previous generator state and a comparison of the actual filtered rotor speed $\tilde{\Omega}_{\rm r}^{\rm f}$ with the typical separation levels of the generator states as defined in eq.(3.32):

3.4.2 Power optimisation around rated wind speed

Especially around rated conditions, production loss wil occur if the stationary generator curves for power production will be used as discussed in subsection 3.4.1. This is a consequence of relative slow pitch actuation of the rotor blades to control the rotor speed, despite of gain scheduling (subsection 3.2.1) and estimated wind speed feed forward (subsection 3.2.5). Due to wind gusts, rotor speed will then decrease below rated level (see fig.(3.20) e.g at 340s), while the pitch angle is still moving towards working position and the aerodynamic torque is only temporarily below rated level.

Optimisation approach: An effective approach has been found by optimisation of the interaction between pitch control and generator torque setpoint control around rated conditions [6]. Requirements and restrictions are determined by turbine design dimensions:

- mean electric power production at rated level, $P_{\rm e}^{\rm rat}$;
- maximum allowable electric power, $P_{\rm e}^{\rm h}$;
- maximum allowable electric torque $T_{\rm e}^{\rm h}$;
- limited rotor speed operation region (between $\Omega_{\rm r}^{{\rm P_e^{rat}},{\rm T_e^h}}$ and $\Omega_{\rm r}^{{\rm P_e^h},{\rm T_e^{rat}}}$) around rated rotor speed, $\Omega_{\rm r}^{\rm rat}$.

The optimized full load curve is situated in the hatched area as shown in fig.(3.23), while it crosses the rated operation point determined by $\Omega_{\rm r}^{\rm rat}$ and $T_{\rm e}^{\rm rat}$. The hatched area is enclosed

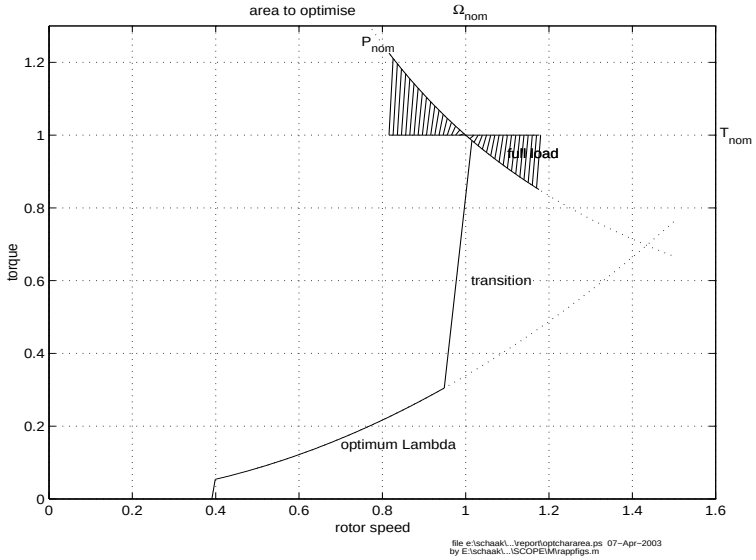

Figure 3.23: *Optimisation area around rated conditions*

by continuation of the lines of constant rated power, $P_{\rm e}^{\rm rat}$, and torque, $T_{\rm e}^{\rm rat}$ and imply above rated torque levels at the left side and above rated power levels at the right side.

The optimisation principle is based on maintaining nominal production below rated rotor speed (by increase of electric torque) during full load pitch operation. In the meantime the pitch control regulates the rotor speed towards rated level.

Full load curves: Fig.(3.24) shows typical candidates of full load curves, which comply with the hatched area of fig.(3.23):

1. constant rated power,

$$\begin{cases} T_{\rm e}^{\rm cv} = \frac{P_{\rm e}^{\rm rat}}{\tilde{\Omega}_{\rm r}^{\rm f}}, & \text{if } (\tilde{\Omega}_{\rm r}^{\rm f} \geq \Omega_{\rm r}^{\rm P_e^{rat},T_e^h}) \\ T_{\rm e}^{\rm cv} = T_{\rm e}^{\rm h}, & \text{if } (\tilde{\Omega}_{\rm r}^{\rm f} < \Omega_{\rm r}^{\rm P_e^{rat},T_e^h}) \end{cases} \tag{3.37}$$

2. constant rated torque,

$$\begin{cases} T_{\rm e}^{\rm cv} = T_{\rm e}^{\rm rat}, & \text{if } (\tilde{\Omega}_{\rm r}^{\rm f} \leq \Omega_{\rm r}^{\rm P_e^{h},T_e^{rat}}) \\ T_{\rm e}^{\rm cv} = P_{\rm e}^{\rm h}, & \text{if } (\tilde{\Omega}_{\rm r}^{\rm f} > \Omega_{\rm r}^{\rm P_e^{h},T_e^{rat}}) \end{cases} \tag{3.38}$$

3. mixed version,

$$\begin{cases} T_{\rm e}^{\rm cv} = T_{\rm e}^{\rm m}, & \text{if } (\tilde{\Omega}_{\rm r}^{\rm f} \leq \Omega_{\rm r}^{\rm P_e^{l},T_e^{m}}) \\ T_{\rm e}^{\rm cv} = T_{\rm e}^{\rm m,trans}, & \text{if } (\Omega_{\rm r}^{\rm P_e^{l},T_e^{m}} < \tilde{\Omega}_{\rm r}^{\rm f} < \Omega_{\rm r}^{\rm P_e^{m},T_e^{l}}) \\ T_{\rm e}^{\rm cv} = \frac{P_{\rm e}^{\rm m}}{\tilde{\Omega}_{\rm r}^{\rm f}}, & \text{if } (\tilde{\Omega}_{\rm r}^{\rm f} \geq \Omega_{\rm r}^{\rm P_e^{m},T_e^{l}}) \end{cases} \tag{3.39}$$

In fig.(3.24), four increasing constant torque levels ($T_{\rm e}^{\rm l}$, $T_{\rm e}^{\rm rat}$, $T_{\rm e}^{\rm m}$ and $T_{\rm e}^{\rm h}$) and four constant power curves ($P_{\rm e}^{\rm l}$, $P_{\rm e}^{\rm rat}$, $P_{\rm e}^{\rm m}$ and $P_{\rm e}^{\rm h}$) are drawn. The typical rotor speed levels in eq.(3.37) - 3.39 are then defined by using the crossing torque and power levels as superscripts.

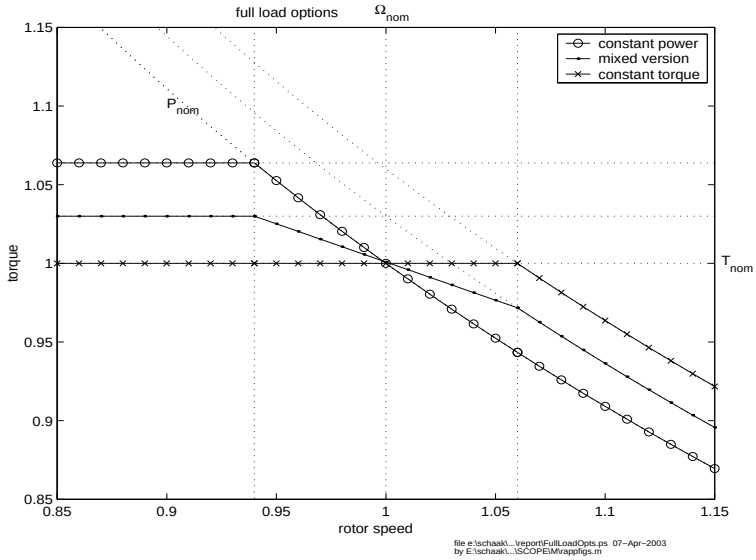

Figure 3.24: *Optimisation area around rated conditions*

The connection area, $T_{\rm e}^{\rm m,trans}$ in eq.(3.39), between the constant torque and constant power area is given by eq.(3.40), which describes a smooth (non-linear) transition by linear fractions of two allowable constant electric power curves, $P_{\rm e}^{\rm m}$, $P_{\rm e}^{\rm l}$.

$$T_{\rm e}^{\rm m,trans} = \left(\frac{\tilde{\Omega}_{\rm r}^{\rm f} - \Omega_{\rm r}^{{\rm P_e^l},{\rm T_e^h}}}{\Omega_{\rm r}^{{\rm P_e^m},{\rm T_e^l}} - \Omega_{\rm r}^{{\rm P_e^l},{\rm T_e^h}}} \right) \cdot \frac{P_{\rm e}^{\rm m}}{\tilde{\Omega}_{\rm r}^{\rm f}} + \left(\frac{\Omega_{\rm r}^{{\rm P_e^m},{\rm T_e^l}} - \tilde{\Omega}_{\rm r}^{\rm f}}{\Omega_{\rm r}^{{\rm P_e^m},{\rm T_e^l}} - \Omega_{\rm r}^{{\rm P_e^l},{\rm T_e^h}}} \right) \cdot \frac{P_{\rm e}^{\rm l}}{\tilde{\Omega}_{\rm r}^{\rm f}} \tag{3.40}$$

The 'constant torque option' will really achieve constant torque, because torque is nearly a direct controlled quantity of the converter. The 'constant power option', will result in power fluctuations around its setpoint level due to the product of the varying rotor speed and the controlled electric torque.

Pitch and generator mode control: In case of insufficient wind capture, rated power can not be maintained any longer and transition to the optimum lambda curve is desired to improve aerodynamic efficiency. Reversely, as soon there's wind capture excess during optimum lambda operation, transition to constant rated power production operation is prefered.

Due to the proposed overlap between the optimum lambda and full load torque curves, transitions will happen dynamically by 'horizontal shifting' of the stationary transition curves. The actual transition curve is then determined by the actual rotor speed and crosses the optimum lambda curve at $\tilde{\Omega}_{\rm r}^{\lambda_{\rm opt}^{\rm out}}$ and the full power curve at $\tilde{\Omega}_{\rm r}^{\rm rat}$. These points differ from the previous stationary points, $\Omega_{\rm r}^{\lambda_{\rm opt}^{\rm out}}$ and $\Omega_{\rm r}^{\rm rat}$, as defined before in subsection 3.4.1, by a decrement $\Omega_{\rm r}^{\rm dec}$.

Transition from *full load to partial load operation* is rather complicated. Determinative will be that generator torque control will enter the transition region only if pitch control has already switched to partial load control (section 3.3). This will happen if the condition as given in eq.(3.41) satifies,

$$\left(\tilde{\theta} < (\theta_{\rm part}^{*} + \theta^{\rm F2P})\right) \;\; \text{AND} \;\; \left((\dot{\theta}^{*} < 0) \;\; \text{OR} \;\; (\tilde{\Omega}_{\rm r}^{\rm f} < \Omega_{\rm r}^{\rm rat})\right) \tag{3.41}$$

The actual rotor speed decrement at full load pitch control is determined by the difference between the actual rotor speed value and its (stationary) rated value:

$$\Omega_{\rm r}^{\rm dec} = \Omega_{\rm r}^{\rm rat} - \tilde{\Omega}_{\rm r}^{\rm f} \tag{3.42}$$

The decrement is limited to 'an empirical maximum allowable shift value' of $\Omega_{\mathrm{r,max}}^{\mathrm{dec}}$ and 'a minimum shift' of ($\Omega_{\mathrm{r}}^{\mathrm{rat}}$ - $\Omega_{\mathrm{r}}^{\mathrm{P2F}}$), where pitch control will switch to full load operation.
As long as full load pitch control is active, generator full load control will be active as well.

Transition from *partial load to full load operation* happens as soon as $\tilde{\Omega}_{\mathrm{r}}^{\mathrm{f}} > \Omega_{\mathrm{r}}^{\mathrm{P2F}}$. To avoid excessive transitions, a practice value of $\Omega_{\mathrm{r}}^{\mathrm{P2F}}$ will be $\Omega_{\mathrm{r}}^{\mathrm{rat}}$ + [1 rpm]. The rotor speed decrement at partial load pitch control is based on linear shifting ($\dot{\Omega}_{\mathrm{r}}^{\mathrm{shf}}$ = 0.1 rpm/s) of the transition value back from its actual position towards the origin, where a switch to full load operation will take place.

With respect to the generator state determination as described in eq.(3.32), the typical points $\Omega_{\mathrm{r}}^{\lambda_{\mathrm{opt}}^{\mathrm{out}}}$ and $\Omega_{\mathrm{r}}^{\mathrm{rat}}$ should be replaced by their decremented quantities:

$$\begin{aligned} \tilde{\Omega}_{\mathrm{r}}^{\lambda_{\mathrm{opt}}^{\mathrm{out}}} &= \Omega_{\mathrm{r}}^{\lambda_{\mathrm{opt}}^{\mathrm{out}}} - \Omega_{\mathrm{r}}^{\mathrm{dec}} \\ \tilde{\Omega}_{\mathrm{r}}^{\mathrm{rat}} &= \Omega_{\mathrm{r}}^{\mathrm{rat}} - \Omega_{\mathrm{r}}^{\mathrm{dec}}. \end{aligned} \tag{3.43}$$

Torque setpoint determination: In case of rated power production (region 5), the torque setpoint is described by eq.(3.37) - (3.39). The relationship between electric torque, electric power and rotor speed, implies that the rotor speed setpoint (pitch control), Ω_{r}^{*} , and the torque setpoint T_{e}^{*} (generator control) may deviate form their rated values to achieve rated power production, $P_{\mathrm{e}}^{\mathrm{rat}}$ (except for the 'constant power option'). This is solved, by a corrective multiplier to the torque setpoint, which is based on continuous comparison between the (moving) averaged value of the proposed power setpoint with respect to the desired rated power level, $P_{\mathrm{e}}^{\mathrm{rat}}$:

$$T_{\mathrm{e}\,,\mathrm{full}}^{*} = \frac{P_{\mathrm{e}}^{\mathrm{rat}}}{\overline{(T_{\mathrm{e}}^{*} \cdot \tilde{\Omega}_{\mathrm{r}})}} \cdot T_{\mathrm{e}}^{\mathrm{cv}} \tag{3.44}$$

This correction will guarantee rated power production for above rated conditions.

In case of transition (region 4), the 'shifting' torque setpoint is determined by linear interpolation along the actual transition curve at the actual rotor speed $\tilde{\Omega}_{\mathrm{r}}^{\mathrm{f}}$:

$$T_{\mathrm{e}\,,\mathrm{trans}}^{*} = T_{\mathrm{e}}^{\lambda_{\mathrm{opt}}}(\tilde{\Omega}_{\mathrm{r}}^{\mathrm{f}}) + \left(T_{\mathrm{e}}^{\mathrm{h}} - T_{\mathrm{e}}^{\lambda_{\mathrm{opt}}}(\tilde{\Omega}_{\mathrm{r}}^{\mathrm{f}})\right) \cdot \left(\frac{\tilde{\Omega}_{\mathrm{r}}^{\mathrm{f}} - \tilde{\Omega}_{\mathrm{r}}^{\lambda_{\mathrm{opt}}^{\mathrm{out}}}}{\tilde{\Omega}_{\mathrm{r}}^{\mathrm{rat}} - \tilde{\Omega}_{\mathrm{r}}^{\lambda_{\mathrm{opt}}^{\mathrm{out}}}}\right) \tag{3.45}$$

where $\tilde{\Omega}_{\mathrm{r}}^{\lambda_{\mathrm{opt}}^{\mathrm{out}}}$ and $\tilde{\Omega}_{\mathrm{r}}^{\mathrm{rat}}$ as defined in eq.(3.43) and $T_{\mathrm{e}}^{\lambda_{\mathrm{opt}}}(\tilde{\Omega}_{\mathrm{r}}^{\mathrm{f}})$ is the torque value of the optimum tip speed ratio curve at $\tilde{\Omega}_{\mathrm{r}}^{\mathrm{f}}$. The torque setpoint $T_{\mathrm{e}\,,\mathrm{trans}}^{*}$ is limited at a maximum torque value of $T_{\mathrm{e}}^{\mathrm{h}}$ or $P_{\mathrm{e}}^{\mathrm{h}}/\tilde{\Omega}_{\mathrm{r}}^{\mathrm{f}}$ (maximum power).

Start-up and optimum lambda operation will be similar as decribed in eq.(3.33) and eq.(3.34), respectively.

The final torque setpoint to the converter, T_{e}^{*} , is determined after limitation of torque setpoints of the concerning operation region to maximum allowable torque changes.

Evaluation: In this paragraph, the proposed optimisations have been evaluated briefly by time domain simulations. More detailed evaluation and further research on this issue can be found in [6]. A comparison of three candidate full load curves is shown in fig.(3.25): constant power eq.(3.37), constant torque eq.(3.38) and mixed version eq.(3.39). Four normalised windows show time domain simulations for rotor speed Ω_{r} , electric torque T_{e} , electric power P_{e} and pitch angle θ ,respectively. For sake of convienience, a negative and positive shift (10% or 10 $^{\mathrm{o}}$) was used for the plots of the constant power (lower) and constant torque (upper) versions, respectively. The mixed version (middle) was plotted without offset. The simulations were calculated at a mean wind speed of 1.6 times rated wind speed for a different but similar turbine as described in chapter 2 .

From fig.(3.25) it has been concluded that the mixed version is preferable for two reasons:

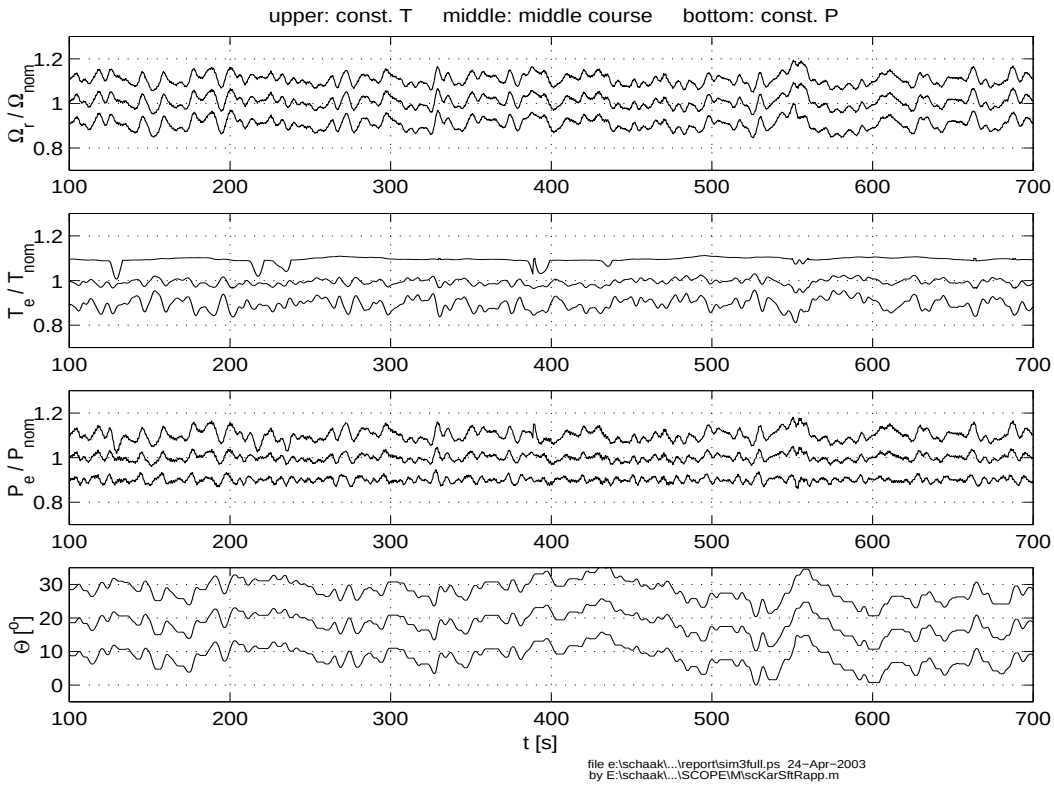

Figure 3.25: *Evaluation of proposed optimisation curves: constant torque (upper), constant power (lower) and mixed version (middle); source: [6]*

- with respect to the 'constant power' version, it shows similar power fluctuations, but half the amount of torque fluctuations;
- additional torque fluctuations are introduced with respect to the 'constant torque' version, but power fluctuations are reduced to a half.

Moderate torque fluctuations are valuable in case of additional control actions through the electric torque, like drive train damping (section 5.1), sideward tower damping (section 5.3) or rotor speed limitation (subsection 3.4.3). To show the advantages of the proposed control, two time domain simulations are illustrative:

- at rated wind speed level (fig.(3.26));
- at 1.6 times rated wind speed level (fig.(3.27)).

For the sake of comparison, conventional operation (as described in subsection 3.4.1) is shown in the upper four windows, while proposed operation (eq.(3.39)) is shown in the lower four windows.

Fig.(3.26) shows turbine operation around rated conditions. The continuation of the constant power curve below rated rotor speed, results in rated power production as long as the pitch angle is not at working position ($1\ ^{o}$). The postponed transitions towards the constant lambda curve, as soon as the pitch control switches to partial load, are stronger. About 70% of the achieved power increase (0.53%) in this simulation. This is achieved by connecting the transition curve to the constant power curve at the above rated rotor speed; close to optimum lambda operation results in more aerodynamic efficiency). Only small differences in torque-, power- and rotor speed variations were observed.

Fig.(3.27) shows operation behaviour far above rated conditions. Obviously, the most important benefit of the proposed optimisation is that all power dips are eliminated, which causes more quiet behaviour and increase of power capture. In this simulation the standard deviations

of electric power and electric torque were reduced by 3.4% and 2.8%, respectively, while that of rotor speed remains equal. The mean power production in this simulation has been increased by 1.5%, while the mean rotor speed level was lowered by 2%.

Further evaluation in performed in [6] and taking a representative Weibull distribution function into account (remote offshore at North sea) results in 0.8% improvement of power capture. Half this increase can be attributed to elimination of power dips, and half as a consequence of shifting the transition.

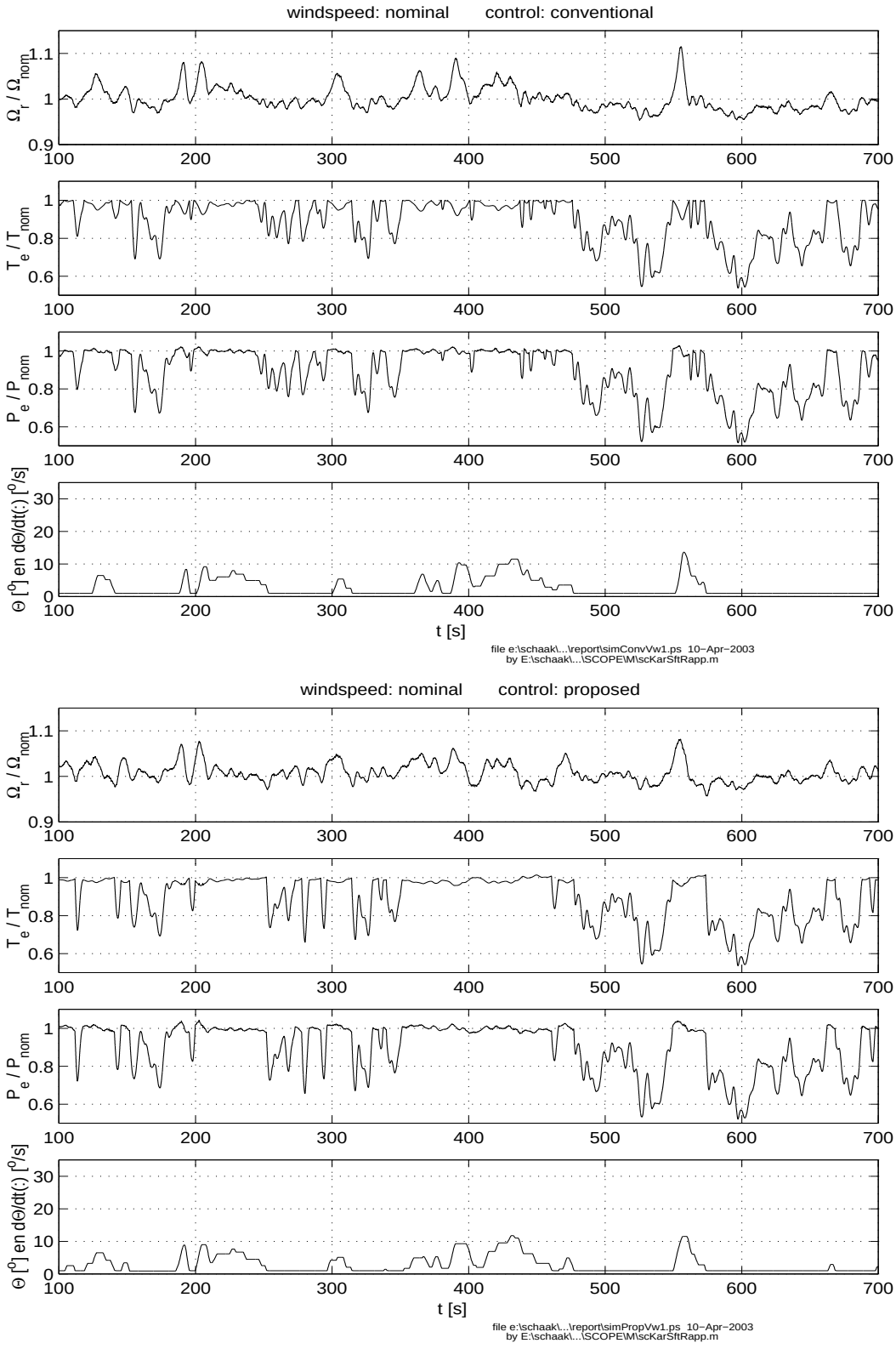

Figure 3.26: *Comparison between conventional operation (upper windows) and proposed operation (lower windows) at rated wind speed level*

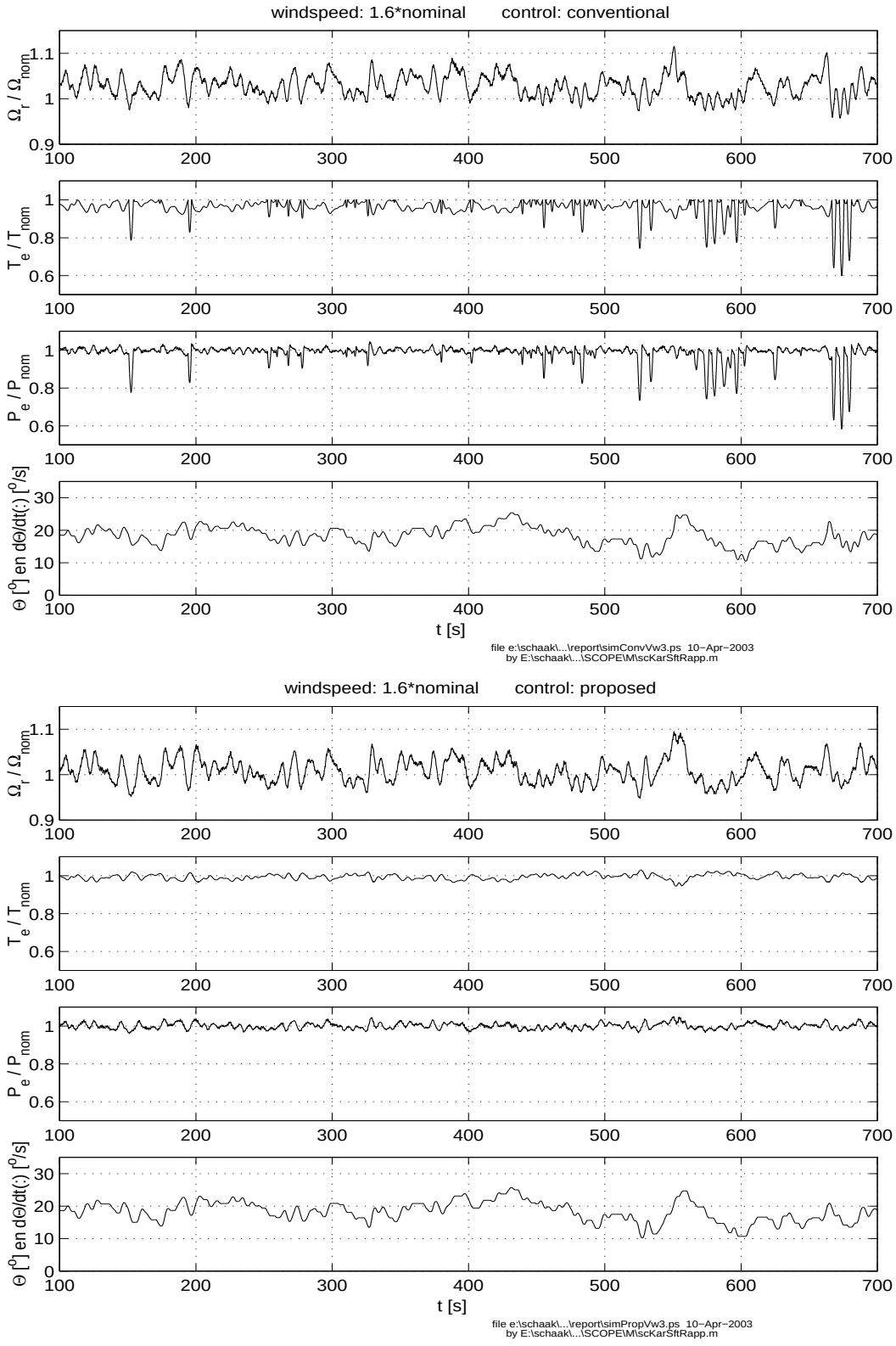

Figure 3.27: *Comparison between conventional operation (upper windows) and proposed operation (lower windows) at 1.6 times rated wind speed level*

3.4.3 Dynamic rotor speed limitation

In case of a doubly fed asynchronous generator with rotor control (subsection 2.2.4), reduction of rotor speed variations is an important issue to limit the electrical dimensions of the converter.

With the knowledge that both converter and generator are able to stand overloading as long as their thermal limitations are not exceeded, the electrical system can be used to react quickly on rotor speed variations, during full load operation. This in contradiction with bandwidth limited pitch control (pitch actuation, mechanical friction).

Design of feedback structure: A feedback mechanism that dynamically realises a smooth electric torque increase in case of rotor acceleration and vice versa is shown in fig.(3.28). Frequency separation of the rotor acceleration is achieved by high pass filtering of the measured

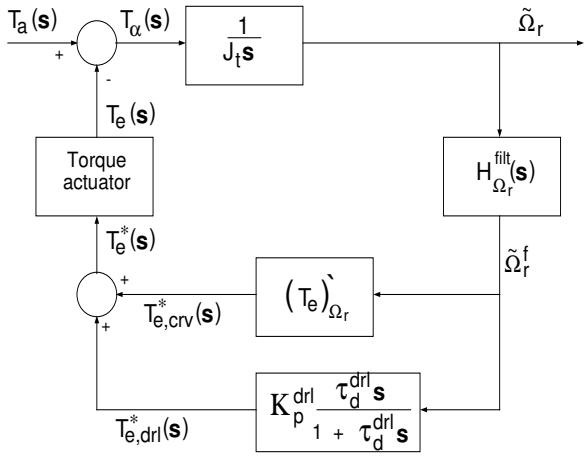

Figure 3.28: *Feedback structure of dynamic rotor speed limitation*

and low pass filtered rotor speed, $\tilde{\Omega}_{\mathrm{r}}^{\mathrm{f}}$, which results in a bandpass filtered rotor acceleration $\dot{\tilde{\Omega}}_{\mathrm{r}}^{\mathrm{f}}$. The transfer function of the feedback control loop for dynamic rotor speed limitation becomes in Laplace domain:

$$\begin{aligned} H_{\mathrm{T_e^*}\tilde{\Omega}_{\mathrm{r}}^{\mathrm{f}}}^{\mathrm{DRL}}(s) = \frac{T_{\mathrm{e,drl}}^*(s)}{\tilde{\Omega}_{\mathrm{r}}^{\mathrm{f}}(s)} &= H_{\mathrm{DRL}}^{\mathrm{c}}(s) \cdot H_{\Omega_{\mathrm{r}}}^{\mathrm{filt}}(s) \\ &= K_{\mathrm{P}}^{\mathrm{DRL}} \cdot \frac{\tau_{\mathrm{D}}^{\mathrm{DRL}} \cdot s}{1 + \tau_{\mathrm{D}}^{\mathrm{DRL}} \cdot s} \cdot H_{\Omega_{\mathrm{r}}}^{\mathrm{filt}}(s) \end{aligned} \tag{3.46}$$

in which, $H_{\Omega_{\mathrm{r}}}^{\mathrm{filt}}$(s) has already been defined in eq.(3.5).

The low cut-off frequency of the bandpass filter is determined by $1/\tau_{\mathrm{D}}^{\mathrm{DRL}}$. Because the high cut-off frequency is fixed by $H_{\Omega_{\mathrm{r}}}^{\mathrm{filt}}$, $\tau_{\mathrm{D}}^{\mathrm{DRL}}$can be determined emperically by definition of a minimum pass band and the restriction that stationary influences should be avoided. A minimum bandpass between (1 - 1.5 $\mathrm{rad/s}$) usually results in acceptable behaviour.

The feedback gain, $K_{\mathrm{P}}^{\mathrm{DRL}}$ is restricted by loop stability. To determine $K_{\mathrm{P}}^{\mathrm{DRL}}$ analytically, the amplitude and phase margin requirements of Bode are applied to a simplified open loop transfer function, which incorporates only two dominating behaviour dynamics:

- rotation of the turbine rotor: eq.(2.15);
- dynamic rotor speed limitation: eq.(3.47).

The control structure has a stabilising effect to the (de-stabilising) stationary generator feed back loop during the 'constant power region' (region 5, subsection 3.4.1). Therefore, an additional advantage is that it is allowed to raise the pitch control gains with 25%. Analysis has shown that improved stability can be achieved by changing PD-control as derived in eq.(3.8), to moderate PD control as described in Laplace domain by eq.(3.47)

$$H^{\mathrm{c}}_{\Omega_{\mathrm{r}},\mathrm{mod}}(s) = K^{\Omega_{\mathrm{r}}}_{\mathrm{P}} \cdot \left(\frac{1 + \tau^{\Omega_{\mathrm{r}}}_{\mathrm{D}} \cdot s}{1 + b\tau^{\Omega_{\mathrm{r}}}_{\mathrm{D}} \cdot s} \right) \tag{3.47}$$

The moderation factor, b, in eq.(3.47) is defined as a fraction of $\tau^{\Omega_{\mathrm{r}}}_{\mathrm{D}}$ and is empirically set to a value of that causes a high frequent weakening of differentiation above 2 rad/s.

Fig.(3.29) shows a typical analysis result of the torque loop behaviour of dynamic rotor speed limitation in a specific operation point, just above rated conditions (non dominating turbine phenomenae are here included). The value of $K^{\mathrm{DRL}}_{\mathrm{P}}$ has been determined to 47000 kNm/(rad/s)

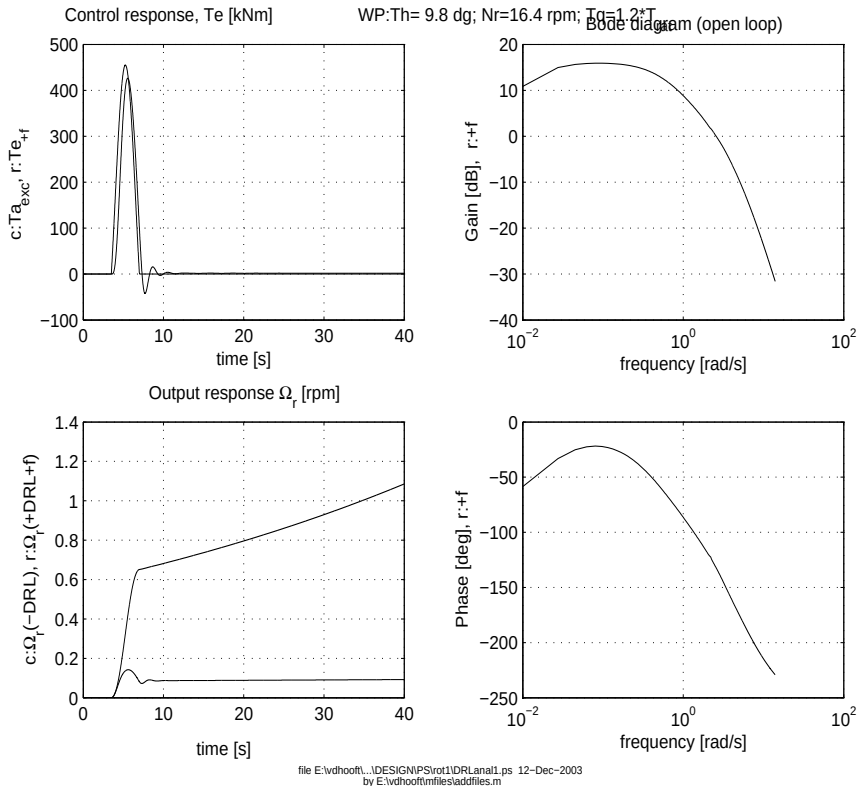

Figure 3.29: *Design result at typical operation point θ =9.8°, Ω_{r} = 16.4 rpm 1.2 T_{rat} ; EOG time response (left hand side) and bode diagram (right hand side);* ω_{nq} *= 5.4* $\mathrm{rad/s}$, ω_{ϕ} *= 2.6* $\mathrm{rad/s}$, $K^{\mathrm{DRL}}_{\mathrm{P}}$ *= 47000 kNm/(rad/s)*

The bode plots at the right hand, show the desired stability behaviour (45 $^{\mathrm{o}}$ phase margin at 0 dB gain, at least -6dB amplitude margin at -180 $^{\mathrm{o}}$). The left side plots show a electric torque response to an EOG aerodynamic torque gust [1] (upper left plot, 25% of rated amplitude). The lower right plot shows the expected unstable behaviour of the constant power controlled generator, which should be stabilised by the pitch control loop, and the stabilised behaviour due to dynamic rotor speed limitation.

To avoid excessive values for both electric power and torque, in practice the fluctuations will be (arbitrary) limited to 125% of their rated values.

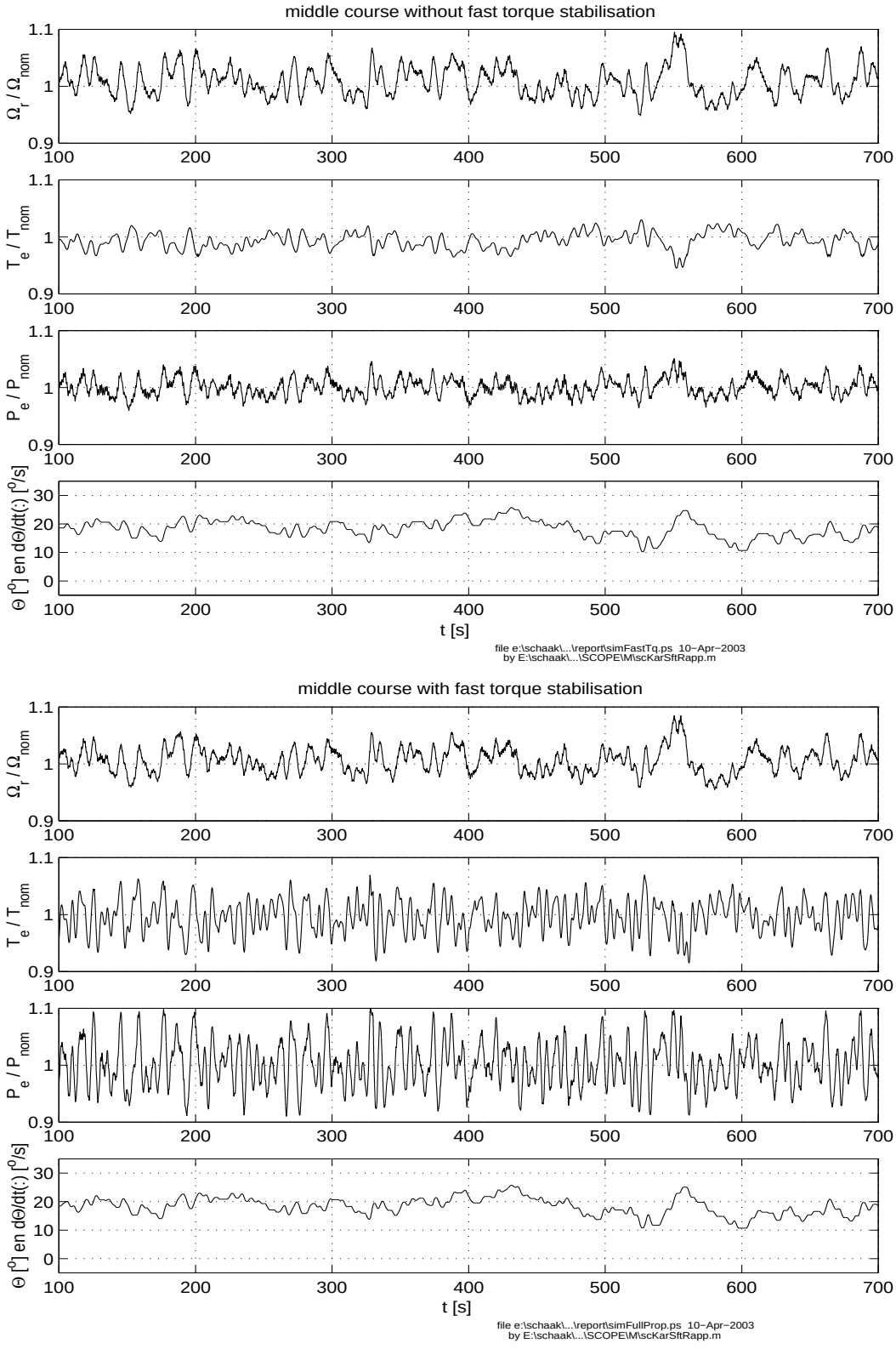

Figure 3.30: *Use of 'mixed optimised control' without (upper) and with (lower) dynamic rotor speed limitation at 1.6 times rated wind speed level*

Evaluation: It has been shown that the proposed feedback structure will be effective if the conventional generator curves as described in subsection 3.4.1 are applied. The combination with the 'mixed version' optimisation as described in subsection 3.4.2 is shown in fig.(3.30) at a mean wind speed of 1.6 times rated level. The upper four windows show results without dynamic rotor speed limitation, while the lower four windows show results when the proposed structure is included. The rotor speed variations are limited, but torque and power fluctuations are considerably increased. This will be a critical drawback, concerning drive train loading and sideward tower deformation.

4 POWER CONTROL SIMULATION RESULTS

In this chapter, time domain simulation verification results for different mean wind speeds are shown to illustrate the overal control behaviour and performance of the turbine power control algorithm as developed in chapter 3.

4.1 Simulation conditions

In the next sub-sections the specifications of the turbine model, the external phenomena and power control algorithm are listed as they were used during time domain simulation. Finally, the different simulation runs are explained and shortly discussed.

4.1.1 Turbine model

In section 2.2, the system for the DOWEC wind turbine has been modelled by a (quasi) linear approach. For the time domain simulations the sub-system dynamics, as listed in table(4.1), were taken into account and dimensioned:

Table 4.1: *DOWEC turbine modelling for time domain simulation and evaluation*

Modelling ref.	*Sub-system*		
Description	*Symbol*	*Value*	*Unit*
Rotor aerodynamic conversion	*eq.(2.3) ... eq.(2.6);*		
Rotor radius	R_{b}	46	m
Air density	ρ_{air}	1.225	$\mathrm{kg/m^3}$
Power coefficient curves	$C_{\mathrm{p}}(\lambda,\theta)$	fig.(2.2)	-
Thrust coefficient curves	$C_{\mathrm{t}}(\lambda,\theta)$	fig.(2.2)	-
Dynamic inflow correction	*eq.(2.7); eq.(2.8)*		
DI lagging time constant	$\tau_{\mathrm{lg}}^{\mathrm{DI}}$	fig.(2.3)	s
DI lead time constant T_{a}	$\tau_{\mathrm{ld}}^{\mathrm{Ta}}$	fig.(2.3)	s
DI lead time constant F_{a}	$\tau_{\mathrm{ld}}^{\mathrm{Fa}}$	fig.(2.3)	s
Rotating mechanical system	*eq.(2.9) ... eq.(2.14)*		
Rotor inertia	J_{r}	12.6e6 sse	$\mathrm{kgm^2}$
Generator inertia	J_{g}	239 hse	$\mathrm{kgm^2}$
Drive train resonance frequency	ω_0^{d}	14.4	$\mathrm{rad/s}$
Drive train damping rate	β_{d}	0.005	-
Gearbox ratio	i_{gb}	70.65	-
Shaft efficiency	η_{sh}	0.97	-
Tower dynamics	*eq.(2.17) ... eq.(2.19)*		
Tower resonance frequency	ω_0^{t}	2.2	$\mathrm{rad/s}$
Tower damping rate	β_{t}	0.005	-
Hub height	Z_{t}	94	m
Tower top diameter	$d_{\mathrm{tw}}^{\mathrm{top}}$	2.52	m
Tower base diameter	$d_{\mathrm{tw}}^{\mathrm{base}}$	4.2	m
Steel density	ρ_{steel}	8e3	$\mathrm{kg/m^3}$
Steel elasticity modulus	E_{steel}	210e9	$\mathrm{N/m^2}$
Nacelle mass	m_{nac}	1.2e5	kg
Electric conversion	*eq.(2.23); eq.(2.25)*		
Generator system resonance frequency	ω_0^{g}	38	$\mathrm{rad/s}$
Generator system damping rate	β_{g}	0.7	-
Pitch actuation system	*eq.(2.26)*		
Pitch actuator resonance frequency	ω_0^{pt}	80	$\mathrm{rad/s}$
Pitch actuator damping rate	β_{pt}	0.3	-
Pitch actuator delay	$T_{\mathrm{d}}^{\mathrm{ptv}}$	0.039	s
Coulomb friction delay	$T_{\mathrm{d}}^{\mathrm{ptx}}$	0.1	s

4.1.2 External phenomena

During time domain simulation, only rotor effective wind speed, subsection 2.3.1, was used as an external phenomenon. In table(4.2), the model is specified and dimensioned

Table 4.2: *Wind speed modelling for time domain simulation and evaluation*

Modelling ref.	*Sub-system*		
Description	*Symbol*	*Value*	*Unit*
Rotor effective windspeed	*eq.(2.27)*		
Rotor tilt angle	α_{tilt}	5	$^{\mathrm{o}}$
Rotor cone angle	α_{cone}	0	$^{\mathrm{o}}$
Number of blades	B	3	-
Rated rotor speed	$\Omega_{\mathrm{r}}^{\mathrm{rat}}$	15.57	rpm
Rated wind speed	$V_{\mathrm{w}}^{\mathrm{rat}}$	12.3	$\mathrm{m/s}$
Turbulence intensity	I_{15}	16	-
Wind shear coefficient	α_{sh}	0.1	-
Hub height	Z_{t}	94	m
Rotor radius	R_{b}	46	m

4.1.3 Power control algorithm

In chapter 3, the power control structure design and analysis was described. In table(4.3) and table(4.4) the analytical and empirical parameters of the used control options are listed as they were used for time domain simulation. The following control options were left out of consideration, because it has been concluded (for this turbine) that they do not improve the control behaviour:

- rotor speed setpoint adaptation, subsection 3.2.1;
- dynamic rotor speed limitation, subsection 3.4.3.

Additionally, the constant power option has been used to optimise power production around rated conditions, subsection 3.4.2.

4.1.4 Simulation runs

The control algorithm as specified in subsection 4.1.3 has been evaluated to the DOWEC turbine (subsection 4.1.1) at four different mean values of wind speed (subsection 4.1.2): [1.0, 1.2, 1.6, 2.0] $\cdot$ $V_{\mathrm{w}}^{\mathrm{rat}}$ (12.3 m/s). The results are shown and shorlty discussed in section 4.2, section 4.3, section 4.4 and section 4.5 respectively.

In section 4.6, attention is paid to verification of results by an aerodynamic code.

Each simulation shows five windows, in which wind speed, rotor speed, electric torque, electric power and pitch angle/pitch speed are respectively depicted. All quantities are normalised to their pertaining rated value.

Table 4.3: *Pitch control specification for time domain simulation and evaluation (I)*

Sub-system	*Modelling ref.*		
Description	*Symbol*	*Value*	*Unit*
Rotor speed feedback control	*eq.(3.5);eq.(3.8) eq.(3.12)*		
3p Low pass rotor speed filter	$H_{\Omega_\mathrm{r}}^{\mathrm{filt,3p}}$	table(3.1) col1	-
Collective lead lag band notch filter	$H_{\Omega_\mathrm{r}}^{\mathrm{filt,cb}}$	table(3.1) col2	-
Tower band notch filter	$H_{\Omega_\mathrm{r}}^{\mathrm{filt,tow}}$	table(3.1) col3	-
Proportional gain rotor speed control	$K_\mathrm{P}^{\Omega_\mathrm{r}}$	1.14	$(^\mathrm{o}/\mathrm{s})/(\mathrm{rad/s})$
Differential gain rotor speed control	$K_\mathrm{D}^{\Omega_\mathrm{r}}$	17.33	$(^\mathrm{o}/\mathrm{s})/(\mathrm{rad/s}^2)$
Differential time constant speed control	$\tau_\mathrm{D}^{\Omega_\mathrm{r}}$	15.19	s
Sample time rotor speed control	T_c	0.1	s
Scheduling coefficients	$C_{\mu_\mathrm{PD}}(\theta, \Omega_\mathrm{r})$	dim(2X3)	[$^\mathrm{o}$,rad/s]
Maximum value scheduling factor	$\theta_{\mu_\mathrm{PD}}^{\max}$	7	$^\mathrm{o}$
Minimum value scheduling factor	$\theta_{\mu_\mathrm{PD}}^{\min}$	1	$^\mathrm{o}$
Dynamic inflow compensation	*eq.(3.15)*		
Lead time constant compensator	$\tau_\mathrm{I}^{\mathrm{DI}}$	fig.(3.13)	-
Lag time constant compensator	$\tau_\mathrm{D}^{\mathrm{DI}}$	fig.(3.13)	-
Inactivity zone and limitation	*subsection 3.2.3; eq.(3.16)*		
Inactivity zone weakening factor	η_{IZ}	0.56	-
Max. allowable pitch speed full load	$\dot{\theta}_{\mathrm{full}}^{\max}$	4	$^\mathrm{o}/\mathrm{s}$
Max. allowable pitch speed partial load	$\dot{\theta}_{\mathrm{part}}^{\max}$	0.8	$^\mathrm{o}/\mathrm{s}$
Max. allowable pitch speed start-up	$\dot{\theta}_{\mathrm{part}}^{\max}$	0.5	$^\mathrm{o}/\mathrm{s}$
Base value inactivity zone full load	$\dot{\theta}_{\mathrm{IZ,base}}^{\mathrm{full}}$	0.30	$^\mathrm{o}/\mathrm{s}$
Base value inactivity zone partial load	$\dot{\theta}_{\mathrm{IZ,base}}^{\mathrm{part}}$	0.25	$^\mathrm{o}/\mathrm{s}$
Base value hysteresis full load	$\dot{\theta}_{\mathrm{hys,base}}^{\mathrm{full}}$	0.25	-
Base value hysteresis partial load	$\dot{\theta}_{\mathrm{hys,base}}^{\mathrm{part}}$	0.25	-
Compensation gain for leaving IZ	$\dot{\theta}_{\mathrm{IZ}}^{\mathrm{comp}}$	1.25	-
Max. allowable pitch angle full load	$\theta_{\mathrm{full}}^{\max}$	90	$^\mathrm{o}$
Min. allowable pitch angle full load	$\theta_{\mathrm{full}}^{\min}$	1	$^\mathrm{o}$
Max. allowable pitch angle partial load	$\theta_{\mathrm{part}}^{\max}$	90	$^\mathrm{o}$
Min. allowable pitch angle partial load	$\theta_{\mathrm{part}}^{\min}$	1	$^\mathrm{o}$
Forced rotor speed limitation	*fig.(3.15)*		
Rotor speed level for enable	$\Omega_{\mathrm{r,frl}}^{\mathrm{lim}}$	17	rpm
Rotor accelleration for enable/disable	$\dot{\Omega}_{\mathrm{r,frl}}^{\mathrm{lim}}$	0	rpm/s
Forced pitch speed target	$\dot{\theta}_{\mathrm{frl}}^{\mathrm{targ}}$	3	$^\mathrm{o}/\mathrm{s}$
Target pitch degrees to vane	$\theta_{\mathrm{frl}}^{\mathrm{delta}}$	3	$^\mathrm{o}$
Estimated wind speed feed forward	*eq.(3.18) ... eq.(3.30)*		
Pol. coeff. a priori torque coefficients	$\hat{C}_\mathrm{q}(\tilde{\theta}^\mathrm{f},\hat{\lambda}^{-1})$	dim(5X5)	[$^\mathrm{o}$,-]
Pol. coeff. of max. allowed aero torque	$T_{\hat{\mathrm{V}}_\mathrm{w}}^{\max}(\tilde{\theta},\tilde{\Omega}_\mathrm{r})$	dim(5X5)	[$^\mathrm{o}$,rpm]
Pol. coeff. of init. wind sp. estimations	$\hat{V}_\mathrm{w}^{\mathrm{ini}}(\tilde{\theta},\tilde{\Omega}_\mathrm{r})$	dim(5X5)	[m/s,rpm]
Pol. coeff. of EWFF scheduling	$(\theta^*_{\hat{\mathrm{V}}_\mathrm{w}})'_{\hat{\mathrm{V}}_\mathrm{w}}(\hat{V}_\mathrm{w},\tilde{\Omega}_\mathrm{r})$	dim(6X6)	[$^\mathrm{o}$,m/s]
Feed forward gain	$K_\mathrm{D}^{\hat{\mathrm{V}}_\mathrm{w}}$	0.5	-
Moderate diff time constant	$\tau_\mathrm{D}^{\hat{\mathrm{V}}_\mathrm{w}}$	0.5	s
To work pitch speed limit	$\Omega_{\mathrm{r},\hat{\mathrm{V}}_\mathrm{w}}^{\max}$	15.57	rpm
To vane pitch speed limit	$\Omega_{\mathrm{r},\hat{\mathrm{V}}_\mathrm{w}}^{\min}$	16.50	rpm
Partial load pitch angle servo	*section 3.3*		
Target pitch angles	θ^*_{part}	1	$^\mathrm{o}$
Rotor speed ref points	$\Omega^*_{\mathrm{r,part}}$	10.00:0.7957:15.57	rpm
Proportional servo gain	$K_\mathrm{P}^{\dot{\theta}}$	1.65	$(^\mathrm{o}/\mathrm{s})/(^\mathrm{o})$

Table 4.4: *Torque control specification for time domain simulation and evaluation (II)*

Sub-system	*Modelling ref.*		
Description	*Symbol*	*Value*	*Unit*
Stationary power production curve	*eq.(3.32) ... eq.(3.36)*		
Minimum allowed rotor speed	$\Omega_{\mathrm{r}}^{\mathrm{min}}$	9.909	rpm
Maximum allowed rotor speed	$\Omega_{\mathrm{r}}^{\mathrm{max}}$	18.402	rpm
Cut-in wind speed	$V_{\mathrm{w}}^{\mathrm{ci}}$	4	$\mathrm{m/s}$
Cut-out wind speed	$V_{\mathrm{w}}^{\mathrm{co}}$	25	$\mathrm{m/s}$
Opt lambda entering rotor speed	$\Omega_{\mathrm{r}}^{\lambda_{\mathrm{opt}}^{\mathrm{in}}}$	10.304	rpm
Opt lambda leaving rotor speed	$\Omega_{\mathrm{r}}^{\lambda_{\mathrm{opt}}^{\mathrm{out}}}$	14.496	rpm
Rated rotor speed	$\Omega_{\mathrm{r}}^{\mathrm{rat}}$	15.570	rpm
Pol. Coeff. Opt. lambda curve	$C_{T_{\mathrm{e}}^{\lambda_{\mathrm{opt}}}}$	$[215.171, 0.197, -0.117]$	kNm/(rad/s)
Rated electric power	$P_{\mathrm{e}}^{\mathrm{rat}}$	2750	kW
Power optimisation around rated wind speed	*eq.(3.37); eq.(3.41); eq.(3.42)*		
Constant power option			
Maximum power limit	$P_{\mathrm{e}}^{\mathrm{h}}$	2832.5	kW
Minimum power limit	$P_{\mathrm{e}}^{\mathrm{l}}$	2667.5	kW
Maximum torque limit	$T_{\mathrm{e}}^{\mathrm{h}}$	1737.21	kNm
Partial to full rotor speed	$\Omega_{\mathrm{r}}^{\mathrm{P2F}}$	15.82	rpm
Max shift speed of transition to partial	$\Omega_{\mathrm{r,max}}^{\mathrm{dec}}$	1.1	rpm
Max shift acceleration of transition to full	$\dot{\Omega}_{\mathrm{r}}^{\mathrm{shf}}$	0.1	rpm/s
Max torque rate during full load	$\dot{T}_{\mathrm{e,max}}^{\mathrm{full}}$	200	kNm/s

4.2 Control performance at rated wind speed

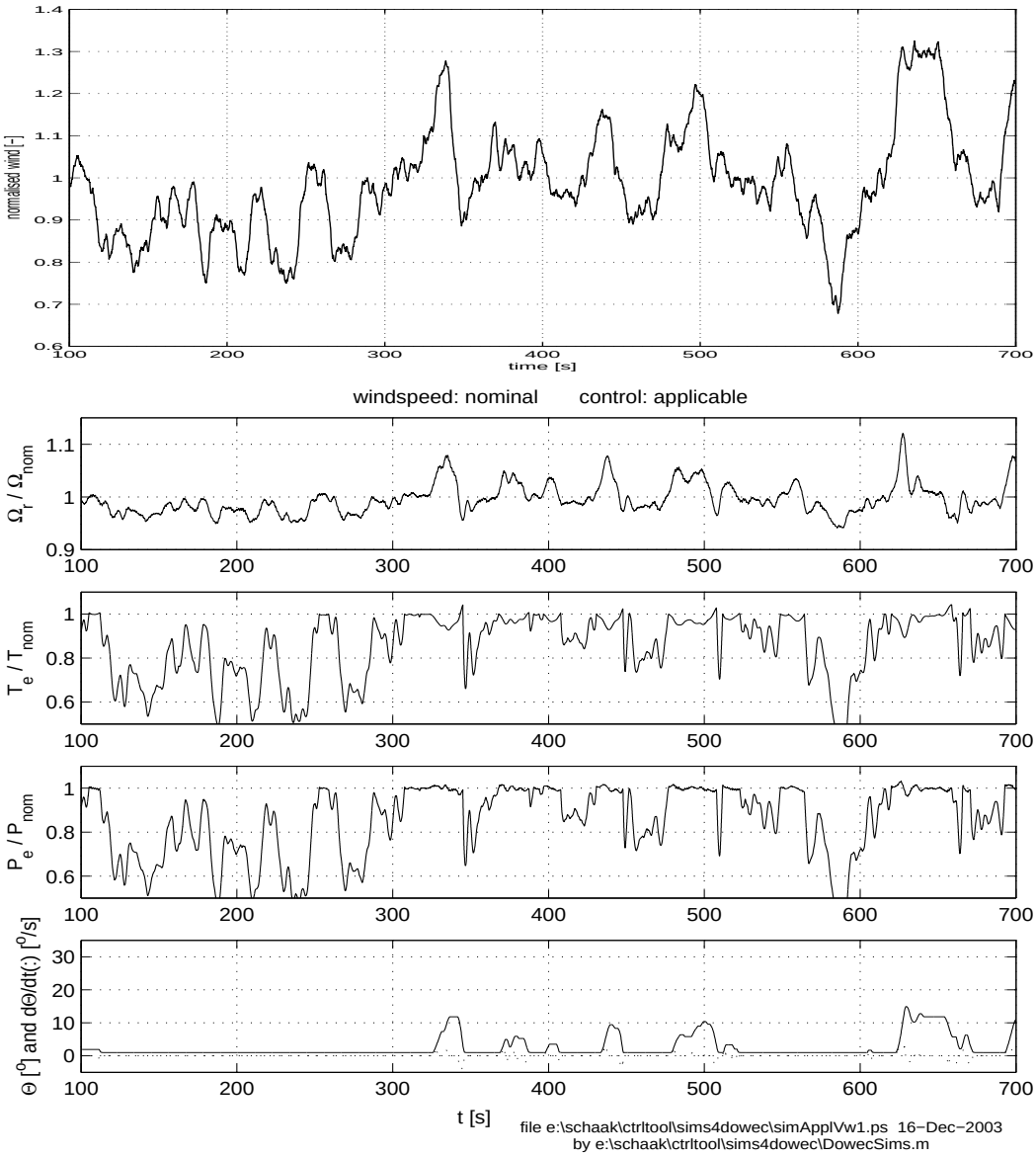

Figure 4.1: *Control performance at rated wind speed level*

The mean power production amounts to 2358kW (85.7% of nominal). Obviously, this is below rated power, because wind speed is also below rated for large periods of time. During these periods of time the pitch angle is set to working position (1 ^{o}) and electric torque control is operating at optimum lambda. As soon as wind speed increases to above rated level, constant rated power production will take place (this is clearly visible between 300s-340s. The large wind gust at 590s, from 70% to 130% of the rated wind speed level, is parried by 11% rotor speed increase and maintaining rated power production. The mean rotor speed is close to its rated value (0.995%), as a measure for fluctuation the standard deviation amounts to 0.437 rpm.

4.3 Control performance above rated wind speed

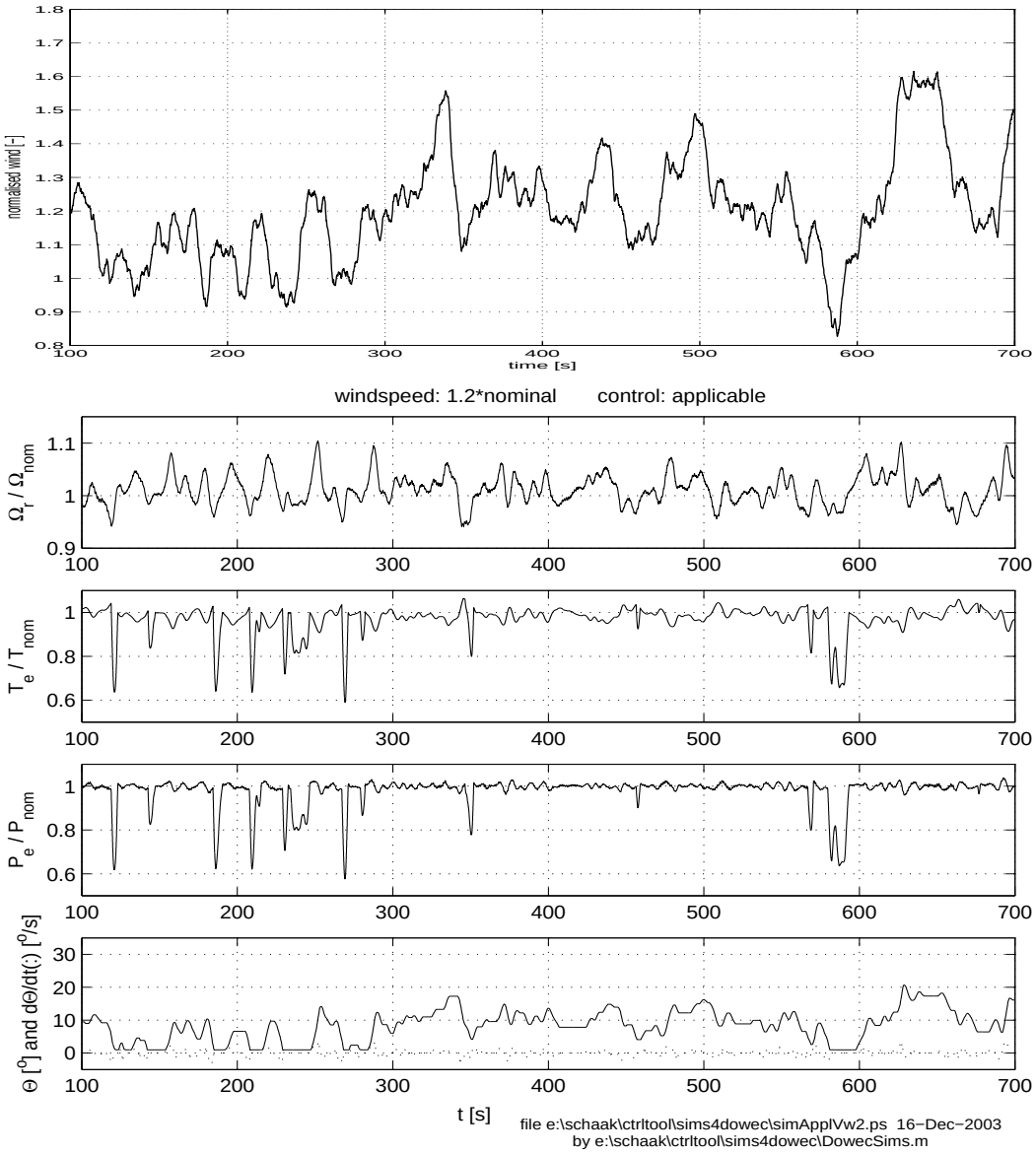

Figure 4.2: *Control performance above rated wind speed level*

The mean power production amounts to 2691kW (97.9% of nominal). The reason why rated mean power production is not achieved can be explained by a few moments of below rated wind speed level. Again, during these periods of time the pitch angle is set to working position (1 ^{o}) and electric torque control is operating at optimum lambda. During above rated wind speed periods, constant rated power production will take place, without significant fluctuations. The large wind gust at 590s, leads to 10% above rated rotor speed level while rated power production is maintained. The mean rotor speed is almost equal to its rated value (1.011%), as a measure for fluctuation the standard deviation amounts to 0.446rpm.

4.4 Control performance at high wind speed

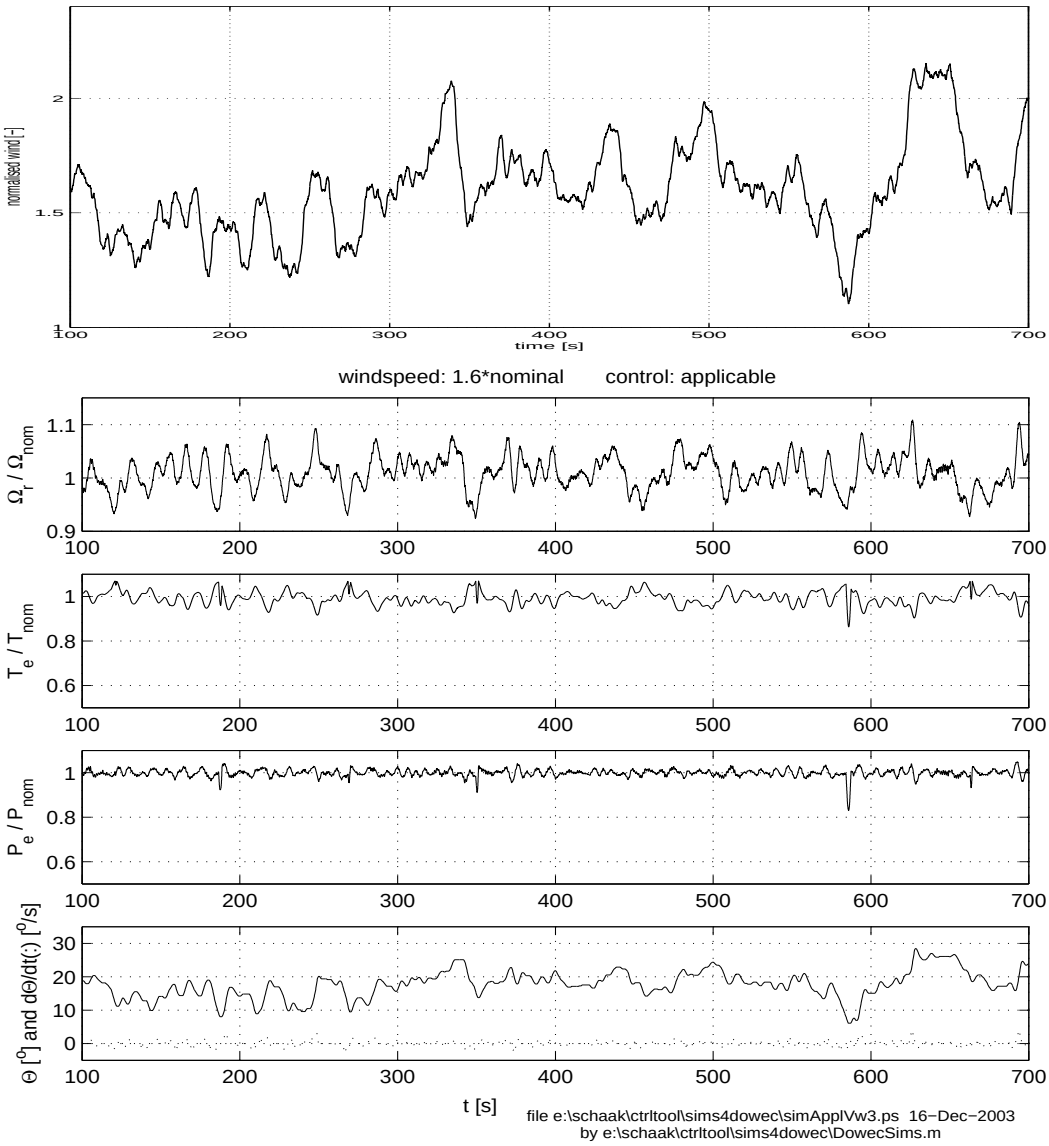

Figure 4.3: *Control performance at high wind speed level*

At this wind speed level mean power is at rated level (2747kW (99.9% of nominal). During above rated wind speed periods, constant rated power production will take place, without significant fluctuations. The electric torque fluctuations during full load operation are +/-6% (design value). The pitch angle tracks the wind speed course accurately and the large wind gust at 590s from 70% to 130% of the rated wind speed level, is parried to a rotor speed level of 110% and maintaining rated power production. The shown power drops will be removed by future developments [6], these are due to a somewhat different mechanism of interaction between pitch and electric torque control as described earlier. In contradiction to subsection 3.4.2, the electric torque increase below rated rotor speed is here pitch angle dependent, which means that for pitch angle values between 1-10 ^{o} the allowed amount of torque increases gradually. The mean rotor speed is nearly equal to its rated value (1.009%), as a measure for fluctuation the standard deviation amounts to 0.494rpm.

4.5 Control performance at very high wind speed

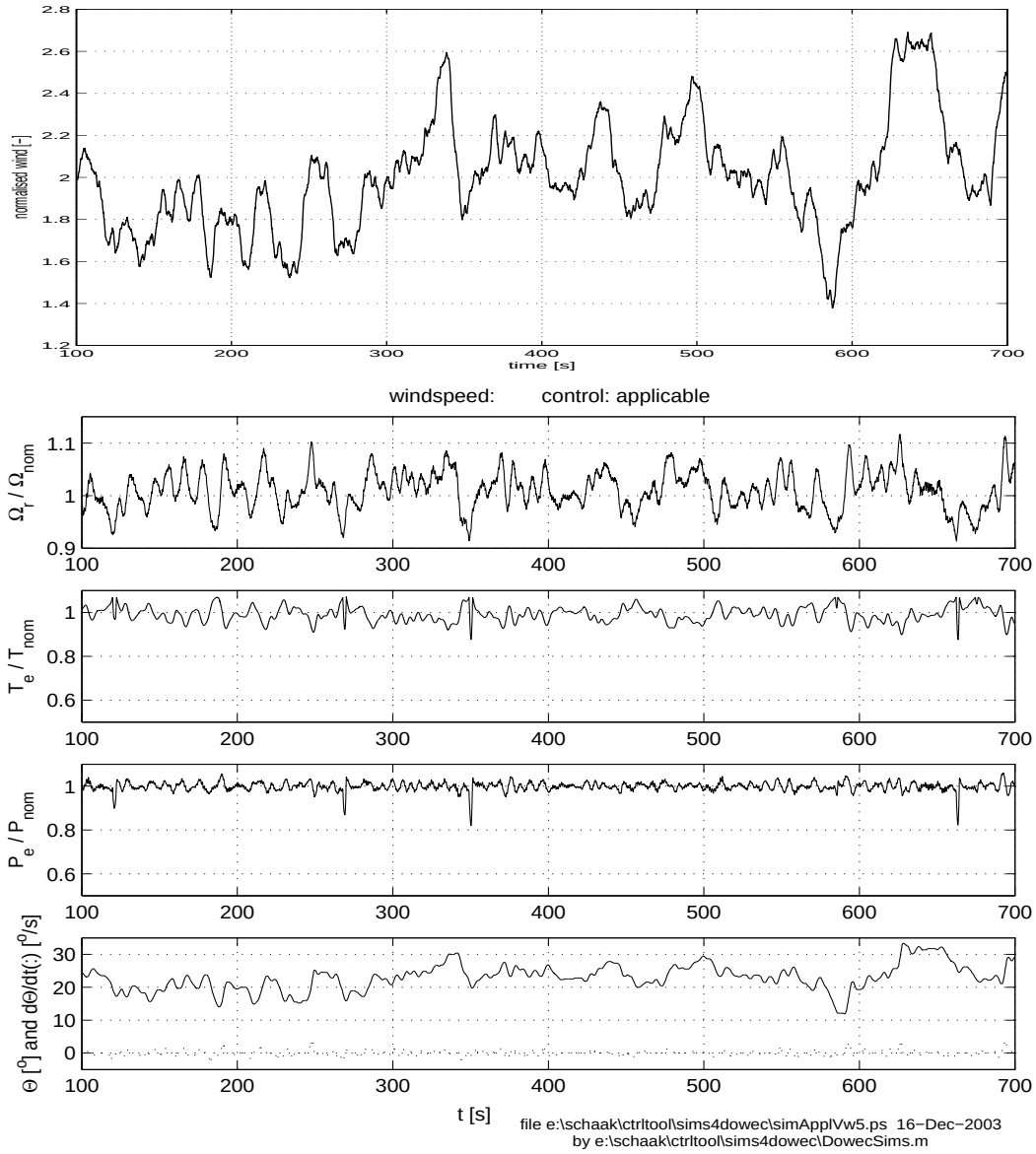

Figure 4.4: *Control performance at very high wind speed level*

This simulation shows similar behaviour as shown in section 4.4 and therefore, it proves the control performance at very high wind speeds (up to 260% of its rated value). In this operation area the turbine safety system will become active (shut-down) to protect for overloading. The simulation shows mean power production at rated level (2746kW, 99.9% of nominal), mean rotor speed level (1.010%) and a rotor speed standard deviation of 0.558 rpm. At the severe wind gust at 590s, rotor speed is increased to 11.5% above its rated value.

4.6 Verification study by aerodynamic code

The phenomenical results as simulated in the previous sections, show promising behaviour which is in compliance with the control objectives as defined in section 3.1.

Verification in more detail has been done by the DOWEC partner NEG-Micon Holland in a control comparison study using the aerodynamic code FLEX5. Due to the confidentiality of this study, only general results related to the DOWEC algorithm will be listed below:

The comparison for the DOWEC turbine with a state-of-the-art control structure has been resulted in improvements concerning:

- extreme fore-aft tower bending moment (reduction of 40%);
- fatigue fore-aft tower bottom bending equivalent moment (reduction of 50%);
- variations in blade pitch rate (standard dev. reduction of 0.65 dg/s);
- tilt moment (reduction of 10%).

The mean power production (10min) above rated wind speed was over 99% of its rated value. Opposite to the improvements it has brought about larger variations in generator speed (standard deviation increase of 0.5 rpm), increase of yaw moment (12%) and radial blade forces (14%).

Larger variations in generator speed can be taken for granted, because of the ‘variable speed’ concept: this will be a benefit for turbine loading.

In general, it is concluded that the control algorithm has considerable advantages.

5 CONTROL STRATEGIES FOR LOAD REDUCTION

In order to reduce turbine loading, more high frequent *electric torque variations* can be used to reduce drive train resonances (section 5.1) and sideward tower vibrations (section 5.3), while *pitch speed variations* enable additional damping of fore-aft tower vibrations (section 5.2). All these processes dominate in different bands of the frequency domain: power production (stationary), transition optimisation and rotor speed limitation (0.1Hz), tower resonances (0.35Hz) and drive train resonances (2.3Hz). Therefore, they can be affected by independent control loops on the condition that separation is guaranteed by (active or natural) filtering.

5.1 Drive train resonance

For variable speed turbines with a gearbox transmission, there are serious risks for severe rotor shaft vibrations. These vibrations can be reduced via the electric torque in order to reduce fatigue loads. Coupling of drive train and tower deformation modes are left out of consideration during the DOWEC project, research results can be found in [9].

5.1.1 Linear design model

Investigations to drive train resonances are based on the model as represented in fig.(5.1), which shows two representations of the drive train model. The upper scheme depicts the ideal

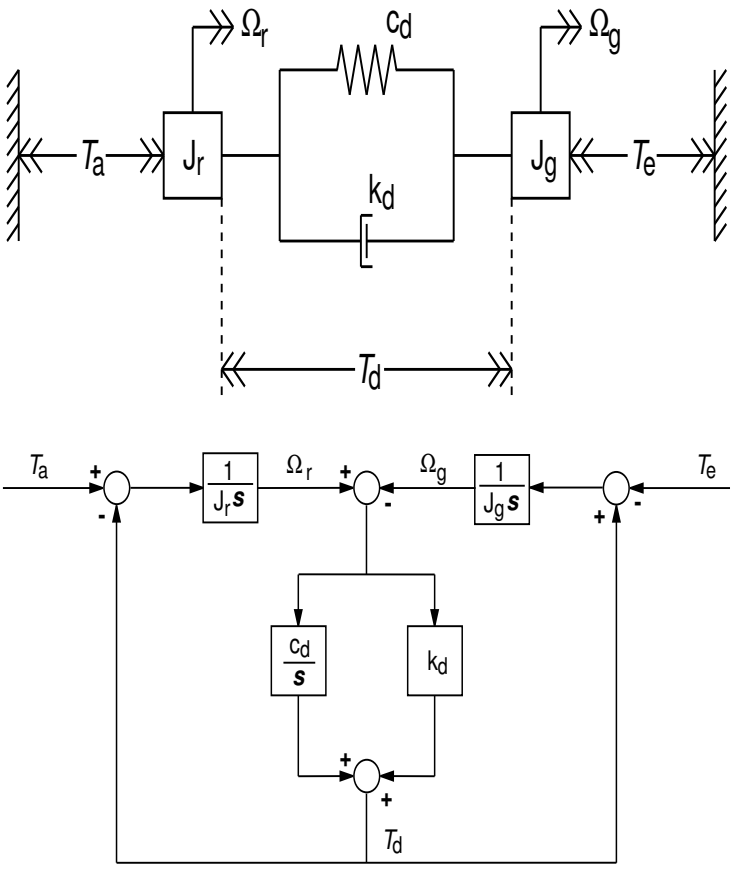

Figure 5.1: *Mechanical (upper) and transfer model (lower) of drive train*

physical model of the drive train, the lower scheme is the matching s-domain model. The drive train is characterised by the elastic coupling of the rigid assumed turbine rotor and generator rotor, with the generator properties related to the turbine shaft (i.e. the gearbox transmission

ratio, $i_{\rm gb}$, is included by scaling parameters on the torque and rotational speed at the generator side). Aerodynamic losses, higher order effects and coupled tower naying modes are supposed here to be negligible. This model is in accordance with subsection 2.2.2 and corresponds with the following equations of motion:

$$J_{\rm r} \cdot \dot{\Omega}_{\rm r} = T_{\rm a} - c_{\rm d} \cdot \gamma_{\rm sh} - k_{\rm d} \cdot \dot{\gamma}_{\rm sh} \quad (5.1)$$

$$J_{\rm g} \cdot \dot{\Omega}_{\rm g} = c_{\rm d} \cdot \gamma_{\rm sh} + k_{\rm d} \cdot \dot{\gamma}_{\rm sh} - T_{\rm e} \quad (5.2)$$

where the distorsion angle is defined as $\gamma_{\rm sh} = \int(\Omega_{\rm r} - \Omega_{\rm g}){\rm d}t$ and the distorsion speed consequently as $\dot{\gamma}_{\rm sh} = \Omega_{\rm r} - \Omega_{\rm g}$. Drive train vibrations are defined as the varying shaft torsion, which is described by the rotational speed difference.

The stiffness and damping parameter $c_{\rm d}$ and $k_{\rm d}$ can be chosen such that they model the first coupled drive-train / collective lead-lag blade vibration mode. This coupled mode appears to dominate the inplane vibration behaviour.

The linearized model for control design is depicted in fig.(5.2). Besides the drive train dynam-

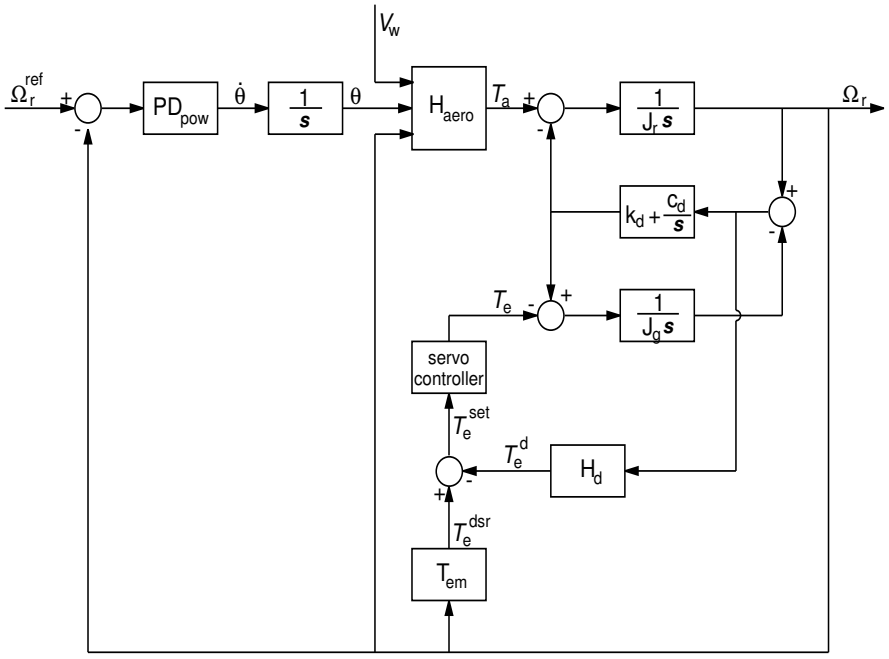

Figure 5.2: *Wind turbine model focussed on drive trian elasticity*

ics, the power control loop is shown and an additional feedback transfer $H_{\rm d}$ represents a drive train feedback structure for damping. $H_{\rm d}$ is aimed to vary the generator torque such, that it corrects the generator speed for being out of phase with the turbine rotor speed.

In accordance with eq.(3.3), analysis is done with the linear transfer function as given in eq.(5.3) , for torque variations around a specific operation point:

$$\partial T_{\rm a} = (T_{\rm a})'_{V_{\rm w}} \cdot V_{\rm w} + (T_{\rm a})'_{\theta} \cdot \theta + (T_{\rm a})'_{\Omega_{\rm r}} \cdot \Omega_{\rm r} \quad (5.3)$$

The electic torque, $T_{\rm e}$ is controlled using a simple servo controller as proposed in eq.(2.24). The setpoint to this servo controller comprises a power production setpoint and an additional control setpoint for drive train damping, $T^*_{\rm e,d}$, see eq.(2.25).

For a practical turbine, obtaining the resonance measure $\dot{\gamma}_{\rm sh}$ is no common practice. The rotational speed difference causes an additional component in both the rotor and generator speed. But because $J_{\rm r}$ is much larger than $J_{\rm g}$, it satisfies to only measure the generator shaft speed with an rotary encoder. (Remind that the model uses this component after having been scaled with the gearbox ratio, while the additional component at the modelled turbine rotor matches 1:1 with reality).

5.1.2 Feedback structures

In the design of the damping feedback transfer function H_{d} , the relationship between Ω_{g} and Ω_{r} is simplified by ignoring the influence of the feedback via the power production curve, which is very low frequent, and the influene of the *dynamics* of the torque servo behaviour, which is very high frequent.

The system transfer from Ω_{r} to Ω_{g} is given in Laplace domain by eq.(5.4):

$$\frac{\Omega_{\mathrm{g}}(s)}{\Omega_{\mathrm{r}}(s)} = \frac{\frac{k_{\mathrm{d}}-T_{\mathrm{e}}}{J_{\mathrm{g}}} \cdot s + \frac{c_{\mathrm{d}}}{J_{\mathrm{g}}} + \frac{H_{\mathrm{d}}}{J_{\mathrm{g}}} \cdot s}{s^2 + \frac{k_{\mathrm{d}}}{J_{\mathrm{g}}} \cdot s + \frac{c_{\mathrm{d}}}{J_{\mathrm{g}}} + \frac{H_{\mathrm{d}}}{J_{\mathrm{g}}} \cdot s} \tag{5.4}$$

H_{d} is aimed to achieve a unity transfer for the higher frequencies, in which shaft elasticity causes a weakening effect in transforming rotor speed fluctuations from the turbine rotor to the generator rotor. Since the term H_{d} appears equal in the numerator and denominator, this can only be achieved if the feedback predominates the transfer of eq.(5.4) in a small frequency range around the vibration frequency, ω_0^{d} .

This requirement on the ratio Ω_{r} to Ω_{g} is fullfiled if the drive train distorsion speed $\dot{\gamma}_{\mathrm{sh}}$ is fed back proportionally after band-pass filtering.

As it is a point of departure that $\dot{\gamma}_{\mathrm{sh}}$ is not available as a measurement signal, the feedback of this quantity is to be approximated. The approximation can consist in:

- either proportional feedback of the bandpass filtered measured generator speed, $\Omega_{\mathrm{g}}^{\mathrm{BPF}}$
- or proportional feedback of the bandpass filtered estimated distorsion speed, $\hat{\dot{\gamma}}_{\mathrm{sh}}$.

High pass filter: It appeared that feedback after only *high*-pass filtering did *not* inject nasty high-frequent behaviour in the drive-train. The use of a high-pass filter instead of a band-pass filter yields a much more favourable phase behaviour in the transfer function from the generator torque T_{e} to the generator speed Ω_{g} or estimated shaft distorsion speed $\hat{\dot{\gamma}}_{\mathrm{sh}}$. This allow to apply a much higher feedback gain for improvement of the damping rate β_{d} .

A second order inverse Chebychev high pass filter with 20dB reduction (cut-off frequency at 1 rad/s) has shown to be effective to avoid low frequent cross talk to the stationary power curve.

Kalman filter: The Kalman filter design is based on the drive train dynamics as decribed before in eq.(2.9) through eq.(2.13). It comprises the in-plane wind turbine dynamic behaviour under neglection of the low frequent feedback via the stationary torque/speed curve and of the torque servo dynamics. All quantities are related to rotor shaft side equivalents.

The input of the Kalman filter are the electric torque, T_{e} (system input), and the measured generator speed, $\tilde{\Omega}_{\mathrm{g}}$ (measured input). Because the electric torque is difficult to measure and therefore usually not available, an approximation of it is obtained from the electric torque setpoint signal by filtering out the high frequent contents via the servo dynamics as given in eq.(2.23).

Additionally, both inputs of the Kalman filter are filtered by a high pass filter as described in the previous paragraph: $\tilde{\Omega}_{\mathrm{g}}^{\mathrm{HPF}}$ and $T_{\mathrm{e}}^{\mathrm{HPF}}$. This is necessary to avoid low frequent content in the Kalman estimated shaft torsion speed $\hat{\dot{\gamma}}_{\mathrm{sh}}$.

Fig.(5.3) shows the 'estimator configuration for the shaft torsion speed' when using the Kalman filter; note that the estimated $\dot{\gamma}_{\mathrm{sh}}$for $t(k+1)$ is an element of the state vector prediction $\hat{x}_{k+1|k}$ for $t(k+1)$ based on information available up to $t(k)$.

It also shows the Kalman gain vector L_{drv}. These Kalman gains feed the error between the estimated generator speed $\hat{\Omega}_{\mathrm{g}}$ for $t(k)$ based on measurements up to $t(k-1)$ and the measured generator speed $\tilde{\Omega}_{\mathrm{g}}^{\mathrm{HPF}}$ on $t(k)$ into the predictor part of the estimator. The Kalman filter is

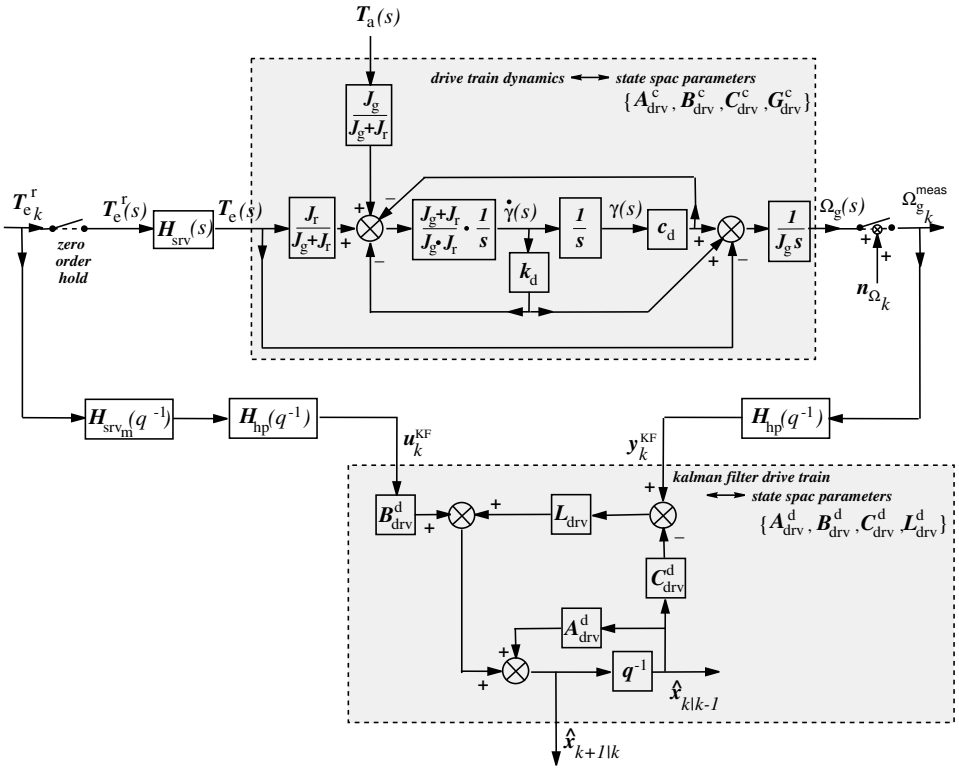

Figure 5.3: *Kalman filter design configuration for estimation of shaft torsion speed of drive train (one step prediction)*

governed by the following set of differential equations:

$$\begin{cases} \hat{\dot{\gamma}}_{\rm sh} &= \dot{\gamma}_{\rm sh} + L_{\rm drv}(1)\cdot(\tilde{\Omega}_{\rm g}^{\rm HPF} - \hat{\Omega}_{\rm g}) \\ \hat{\ddot{\gamma}}_{\rm sh} &= \frac{J_{\rm r}+J_{\rm g}}{J_{\rm r}\cdot J_{\rm g}}\cdot(-c_{\rm d}\cdot\hat{\gamma}_{\rm sh} - k_{\rm d}\cdot\hat{\dot{\gamma}}_{\rm sh}) + \frac{1}{J_{\rm g}}\cdot T_{\rm e}^{\rm HPF} + L_{\rm drv}(2)\cdot(\tilde{\Omega}_{\rm g}^{\rm HPF} - \hat{\Omega}_{\rm g}) \\ \hat{\dot{\Omega}}_{\rm g} &= \frac{1}{J_{\rm g}}\cdot(c_{\rm d}\cdot\hat{\gamma}_{\rm sh} + k_{\rm d}\cdot\hat{\dot{\gamma}}_{\rm sh} - T_{\rm e}^{\rm HPF} + L_{\rm drv}(3)\cdot(\tilde{\Omega}_{\rm g}^{\rm HPF} - \hat{\Omega}_{\rm g})) \end{cases} \tag{5.5}$$

From eq.(5.5) it appears, that besides estimation of $\hat{\dot{\gamma}}_{\rm sh}$ also the shaft torsion angle, $\hat{\gamma}_{\rm sh}$, and the generator speed $\hat{\Omega}_{\rm g}$ are results of the state estimation.

The Kalman gains $L_{\rm drv}(1)$ through $L_{\rm drv}(3)$ are obtained from the Matlab tool: Kalman(). Required inputs for this function are the state space parametrisation of the in-plane drive-train dynamics by eq.(2.9) and eq.(2.10) and the 'tuning parameters', being the expected intensity of the system noise input, $\sigma_{T_{\rm a}}$, and the expected intensity of the generator speed measurement error, $\sigma_{\tilde{\Omega}_{\rm g}}$.

The system noise variance $\sigma_{T_{\rm a}}$ is obtained from the power spectrum of the rotor effective wind speed signal (subsection 2.3.1) in frequencies above 1 Hz after multiplication with a typical value for the sensitivity of the aerodynamic torque to the wind speed: $(T_{\rm a})'_{\rm V_w}$. The measurement noise variance $\sigma_{\tilde{\Omega}_{\rm g}}$ is obtained from the properties of the applied rotary encoder for the generator speed measurement. The power spectrum of the noise in the frequency range between 1 and 20 Hz is applied. The variances $\sigma_{T_{\rm a}}$ and $\sigma_{\tilde{\Omega}_{\rm g}}$ result from integration of the respective power spectra. The sensitivity of the Kalman gains to variations in both variances is *not* that high that scheduling of the Kalman filter gains over the operating range design would be required.

Feedback of the *two*-step ahead prediction of the distorsion speed appeared to yield much better damping results than the one-step prediction by the estimator configuration in fig.(5.3).

We were triggered to do so because the overall loop delay amounts to twice the sample time. For this reason the feedback structure as depicted in fig.(5.4) has been used. The feedback gain

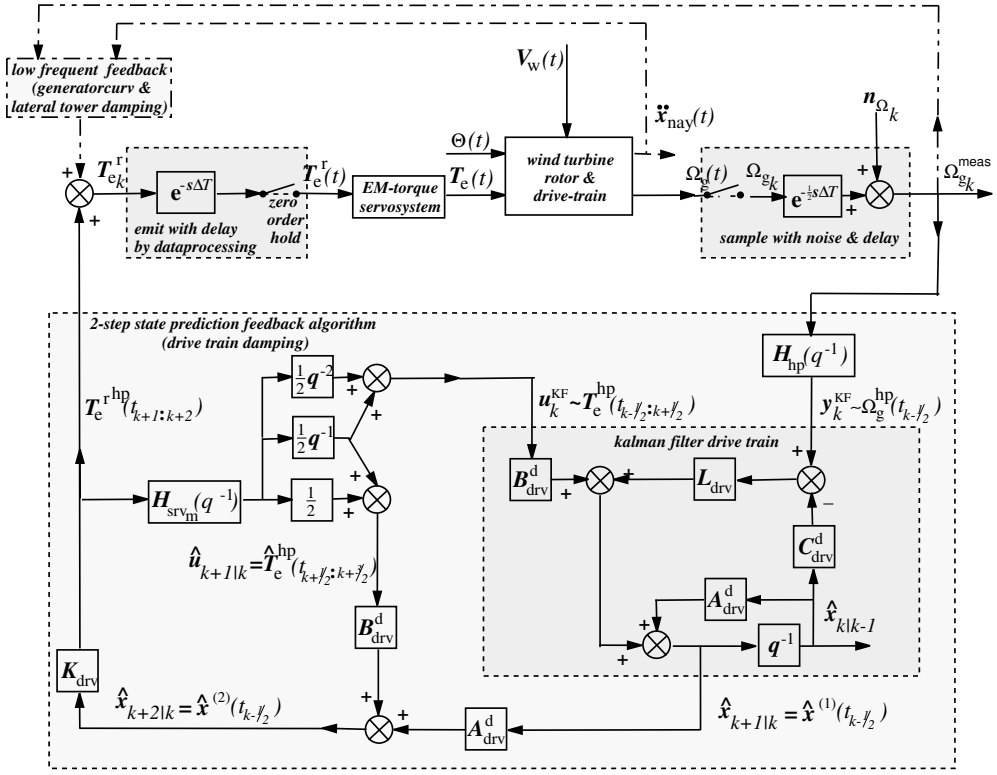

Figure 5.4: *Kalman filter algorithm implementation for estimation of shaft torsion speed of drive train (two step prediction)*

K_{drv} only has a non-zero element for the third state vector element, visually the 2-step ahead predicted value of the shaft torsion speed, $\hat{\dot{\gamma}}_{\mathrm{sh}\,k+2|k}$.

Feedback gain: The obtained distorsion speed will be fed back by a gain, K_{drv} , in order to increase the total damping ratio, $\beta_{\mathrm{d}}^{\mathrm{tot}}$ of the drive train system. The additional feedback loop results in an additional term in the drive train dynamics:

$$\frac{J_{\mathrm{r}} \cdot J_{\mathrm{g}}}{J_{\mathrm{r}} + J_{\mathrm{g}}} \cdot (\ddot{\gamma}_{\mathrm{sh}}) = -c_{\mathrm{d}} \cdot \gamma_{\mathrm{sh}} - k_{\mathrm{d}} \cdot \dot{\gamma}_{\mathrm{sh}} - \frac{J_{\mathrm{r}}}{J_{\mathrm{r}} + J_{\mathrm{g}}} \cdot K_{\mathrm{drv}} \cdot \dot{\gamma}_{\mathrm{sh}} \tag{5.6}$$

The total damping ratio $\beta_{\mathrm{d}}^{\mathrm{tot}}$ can be expressed in relation to the 'natural' damping ratio, β_{d} :

$$\beta_{\mathrm{d}}^{\mathrm{tot}} = \beta_{\mathrm{d}} \left(1 + \frac{J_{\mathrm{r}}}{J_{\mathrm{r}} + J_{\mathrm{g}}} \cdot \frac{1}{k_{\mathrm{d}}} \cdot K_{\mathrm{drv}} \right) \tag{5.7}$$

$$= \beta_{\mathrm{d}} \cdot \beta_{\mathrm{d}}^{\mathrm{F}} \tag{5.8}$$

in which β_{d} is equal to eq.(2.13) and $\beta_{\mathrm{d}}^{\mathrm{F}}$ is defined as a multiplication factor with respect to 'natural damping'. The feedback gain is determined from eq.(5.8) in the same way in both feedback options:

$$K_{\mathrm{drv}} = \left(\frac{\beta_{\mathrm{d}}^{\mathrm{tot}}}{\beta_{\mathrm{d}}} - 1 \right) \cdot \frac{J_{\mathrm{r}} + J_{\mathrm{g}}}{J_{\mathrm{r}}} \cdot k_{\mathrm{d}} \tag{5.9}$$

Due to the better phase behaviour of the configuration with Kalman filter, it was allowed to apply a higher value of $\beta_{\mathrm{d}}^{\mathrm{tot}}$ for that option.

5.1.3 Time domain simulations

The simulations were calculated for a different but similar turbine as described in chapter 2 at above rated wind speed (16 $\mathrm{m/s}$).

The drive train model was dimensioned by a natural frequency ω_0^{d} = 16.3 $\mathrm{rad/s}$ (2.6Hz) and damping rate β_{d} of 0.005. Second order generator dynamics with bandwidth of 6 or 30 Hz and 0.7 damping rate were used.

The generator speed measurement was simulated with stochastic properties that agree with 4096 pulses per revolution of the generator shaft; a pulse-counting duration of 0.025 s had been assumed. Furthermore, digital control had been assumed to be based on control cycles of 0.025 s. Thus the digital control scheme for damping effectively causes a loop delay of 0.05 s (0.0125 average measurement delay, 0.025 s data processing delay and 0.0125 average hold delay of control signals).

Both feedback options have been considered in three simulation cases:

- speed option: straightforward feedback of the measured generator speed;
- Kalman filter option: feedback of the estimated speed difference between rotor and generator.

All curves with signal histories in the figures below are in percents of the nominal value; they concern variations around their mean values. If more curves are in one plot, they are shifted in order to not overlap.

Fig.(5.5) shows a short-term history of the shaft torque. The upper plot in the figure shows the shaft torque without damping control. The other two plots show the shaft torque with damping control included. The lower curve in both plots is the shaft torque history under feedback of the Kalman filter estimate of the speed difference between rotor and generator (Kalman filter option); the bandwidth of the generator torque servo behaviour amounted to 6 Hz. The upper curves in the middle and lower plot show the result of straightforward generator speed feedback (speed option); in the middle plot 30Hz torque-servo bandwidth applies and a design damping rate of 0.1, whereas 6 Hz and 0.3 respectively in the lower plot.

The middle plot shows that a bit more damping is achieved for the Kalman filter option than the speed option, even though the required torque servo bandwidth is five times lower. The lower plot shows that with an equal servo bandwidth of 6 Hz the Kalman filter option damps best by far. The speed option allows only such a low feedback gain that the torsion resonance is not signifcantly damped. At a higher feedback gain the phase margin would become far too small: only a slight increase in phase shift of the torque servo would then yield instability.

Long-term results are shown in figure fig.(5.6) for the speed option with 30 Hz servo bandwidth and the Kalman filter option with 6 Hz servo bandwidth. As a reference, the upper plot shows the shaft torque without damping control. The middle plot shows the controlled shaft torque (upper curve: speed option; lower curve: Kalman filter option). The lower plot shows the belonging generator torque variations for both control options. The middle plot shows that damping control significantly lowers the drive train loading in comparison with the upper plot. The Kalman filter option gives the best results. The equivalent 2.6 Hz loading has been determined for these three cases. The speed option lowers the shaft loading to 52.5% of the 'uncontrolled value' of 510 kNm, the Kalman filter option even to 46.4%. The lower plot in fig.(5.6) shows that the Kalman filter option needs significantly less control effort: it does not include the low-frequency contents of the generator torque as seen in the speed option, *though the same high pass filter had been used.*

Though not included in the figure, long-term load histories for the speed option with 6 Hz torque servo bandwidth had yet been determined (design damping rate 0.025). Postprocessing proved load reduction to only 80.8%.

Verifying calculations had been made that included the rotor speed influence on the aerodynamic torque as well as the quasi stationary torque/speed curve behaviour and tower naying. This low frequent turbine behaviour did not affect the drive train damping mechanism.

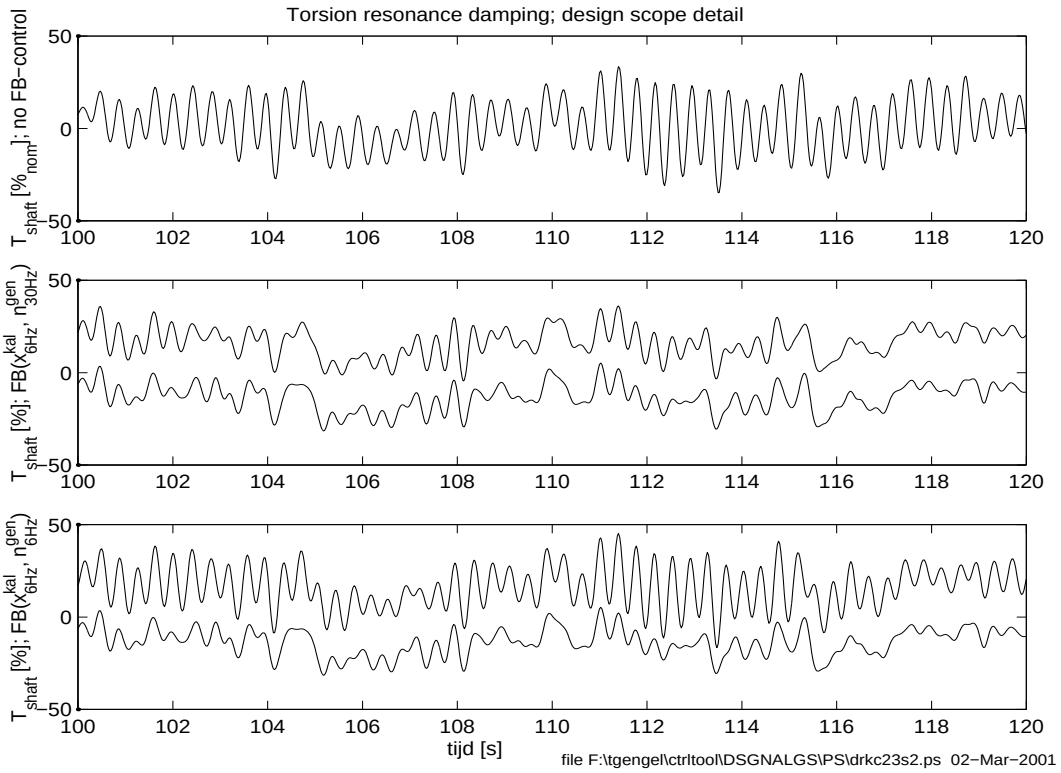

Figure 5.5: *Shaft torque variatons in 16 m/s mean wind speed; short-term history*

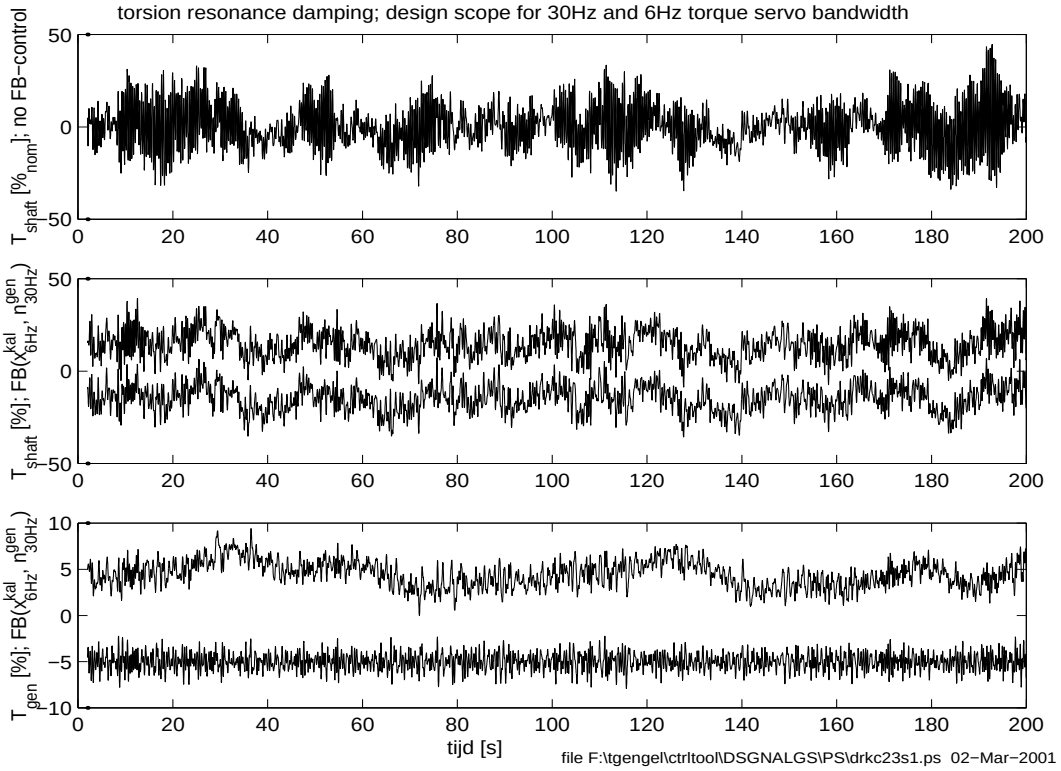

Figure 5.6: *Shaft torque variatons in 16 m/s mean wind speed; long-term history*

5.1.4 Evaluation

In the two examined damping mechanisms, the high-pass filtered generator speed measurement is fed back to the generator torque setpoint. The difference lays in the use of a Kalman filter for estimation of the deviation between the rotor and generator speed: either the estimated deviation is mapped to a torque setpoint or the measured generator speed.

The following conclusions can be drawn from scoping calculations on drive train damping control:

- The fatigue loading on the drive train can be reduced to 50% of the loading level without damping control (5% more reduction at Kalman filter use).
- Without a Kalman filter, 50% load reduction will coincide with disturbation of low frequent control for torque/speed-curve operation and sideward tower damping.
- For similar load reduction, the use of a Kalman filter strongly lowers the required bandwidth of the electric torque servo behaviour (6 Hz vs 30 Hz).
- Without a Kalman filter, load reduction to only 80% of the undamped level is allowed at 6 Hz torque servo bandwidth because of dynamic stability.

It has shown that the Kalman filter approach puts far weaker requirements on the control equipment than straightforward speed feedback. Though it concerns scoping results, practical limitations have been accurately taken into account in order to get a realistic view on the possibilities of the proposed approach.

5.2 Improved damping in fore-afterward direction

Reduction of fore-aft movements or 'nodding' of the turbine will become more relevant for larger offshore turbines, due to its lower frequency of the first bending resonance and the external excitations by waves. Active damping possibilities by pitch control will be discussed in the next subsections.

5.2.1 Damping approach

Tower top displacements, x_{nd} , are caused by interaction between the aerodynamic axial force, tower dynamics and existing external forces (waves).

Besides structural tower damping, β_{t} , as defined in eq.(2.19), both the (natural) aerodynamic behavior of the rotor and (active) feedback of tower top speed, $\dot{x}_{\mathrm{nd}}$, to the pitch angle, will cause similar damping effects.

$$\begin{aligned} \partial F_{\mathrm{a}} &= (F_{\mathrm{a}})'_{\theta} \cdot \theta + (F_{\mathrm{a}})'_{\dot{\mathrm{x}}_{\mathrm{nd}}} \cdot \dot{x}_{\mathrm{nd}} \\ &= \left((F_{\mathrm{a}})'_{\theta} \cdot K_{\mathrm{P}}^{\ddot{\mathrm{x}}_{\mathrm{nd}}} - (F_{\mathrm{a}})'_{\mathrm{V_w}} \right) \cdot \dot{x}_{\mathrm{nd}} \end{aligned} \tag{5.10}$$

The influence by the rotor speed sensitivity, $(F_{\mathrm{a}})'_{\Omega_{\mathrm{r}}}$, has been proven to be small and therefore neglected in eq.(5.10). In practice, the measured tower top acceleration $\tilde{\ddot{x}}_{\mathrm{nd}}$, will be used to determine an additional pitching speed setpoint component $\dot{\theta}^{*}_{\ddot{\mathrm{x}}_{\mathrm{nd}}}$, via a feed back gain $K_{\mathrm{P}}^{\ddot{\mathrm{x}}_{\mathrm{nd}}}$.

Substitution of eq.(2.17) and eq.(2.19) in eq.(5.10), results in a total damping, which consists of three components as supposed before: structural damping, β_{t} , aerodynamic damping, $\beta_{\mathrm{t}}^{\mathrm{aero}}$, and active damping $\beta_{\mathrm{t}}^{\mathrm{ctrl}}$:

$$\begin{aligned} \beta_{\mathrm{t}}^{\mathrm{tot}} &= \frac{1}{2\sqrt{m_{\mathrm{t}} c_{\mathrm{t}}}} \left(k_{\mathrm{t}} + (F_{\mathrm{a}})'_{\mathrm{V_w}} - K_{\mathrm{P}}^{\ddot{\mathrm{x}}_{\mathrm{nd}}} \cdot (F_{\mathrm{a}})'_{\theta} \right) \\ &= \beta_{\mathrm{t}} + \beta_{\mathrm{t}}^{\mathrm{aero}} + \beta_{\mathrm{t}}^{\mathrm{ctrl}} \end{aligned} \tag{5.11}$$

A simple second order system as given in eq.(5.12) appears to be sufficient to analyse active damping of tower vibrations [5]

$$\ddot{x}_{\mathrm{nd}} + \left(2\beta_{\mathrm{t}}^{\mathrm{tot}}\omega_0^{\mathrm{t}}\right) \cdot \dot{x}_{\mathrm{nd}} + \left(\omega_0^{\mathrm{t}}\right)^2 \cdot x_{\mathrm{nd}} = F_{\mathrm{nd}}^{\mathrm{top_{eq}}}/m_{\mathrm{t}}, \tag{5.12}$$

where $F_{\mathrm{nd}}^{\mathrm{top_{eq}}}$ is defined as tower top equivalent excitation force eq.(2.20) and ω_0^{t} the resonance frequency of the first (fore-aft) tower bending mode.

5.2.2 Feedback structure

The proposed feedback structure aims to avoid turbine shut down (safety system) due to exceeding a critical tower top acceleration level, $\ddot{x}_{\mathrm{nd}}^{\mathrm{lim}}$, and to reduce the fatigue loading by tower top displacements. This should be realised by improving the total damping rate $\beta_{\mathrm{t}}^{\mathrm{tot}}$ to a maximum constant level for the whole turbine operation area, while causing as little as possible loss of power production.

Due to additional system restrictions and practical requirements, a simple proportional feedback will be not sufficient to achieve this objective:

- maximum allowable pitch speed during normal operation, $\dot{\theta}^{\mathrm{full}}$, and emergency operation, $\dot{\theta}^{\mathrm{emg}}$;
- disturbing components in the measured tower top acceleration (3p, flapwise), $\tilde{\ddot{x}}_{\mathrm{nd}}$;
- stability must be guaranteed;
- working point dependent sensitivities, $(F_{\mathrm{a}})'_{\mathrm{V_w}}$ and $(F_{\mathrm{a}})'_{\theta}$.

Conditional operation of the feedback loop will be a possible solution to deal with the first item and makes it possible to avoid power production loss caused by pitch corrections from non-significant tower top accellerations. A narrow bandpass filter around the resonance frequency [2] will introduce restrictions to the feedback gain for stability reasons. Additionally, its sensitive phase behaviour will have to much effect on the damping performance. Because the tower resonance frequency hardly changes, a solution has been found in on-line determination of the required phase correction (delay) to ensure increase of damping as intended originally by proportional feedback [5]. Because this correction implies quasi-proportional feedback of a pure second order system, stability requirements can be omitted. Scheduling functions will be a solution to deal with non-linear aerodynamic sensitivities. Design of the proposed structure, as shown in fig.(5.7) is separated in three parts: phase corrected band pass filtering, conditional feedback gain and non-linear scheduling.

Phase corrected band pass filtering: Because of its moderate phase slope within the pass band and its guaranteed reduction outside this band, a fourth order inverse Chebychev filter with 40dB reduction proved to be the most suitable bandpass filter. At its center frequency, ω_0^{t} , the phase shift is exactly zero, fig.(5.8). Deviations cause phase shifts, which will be fitted in a polynomial as a priori knowledge to enable phase shift corrections in case of actual tower resonances (which vary slightly in practice around its resonance frequency ω_0^{t}). Observation of the actual tower resonance frequency, $\hat{\omega}^{0\mathrm{t}}$, is based on time recording between zero crossings of the filtered tower top accelleration, $\tilde{\ddot{x}}_{\mathrm{nd}}^{\mathrm{f}}$. The calculated actual phase shift at this frequency is converted to a discrete number of control 'delay' cycles. As the recent history of the filtered tower top acceleration values is stored in a register, an accurate correction can be determined easily.

Conditional feedback gain: The feedback gain factor, $K_{\mathrm{P}}^{\ddot{\mathrm{x}}_{\mathrm{nd}}}$, shall be limited in order to not exceed the maximum allowable pitch speed, $\dot{\theta}^{\mathrm{full}}$ or $\dot{\theta}^{\mathrm{emg}}$. Emergency operation for nodding damping will be required to avoid shut down by the turbine safety system, as soon as the

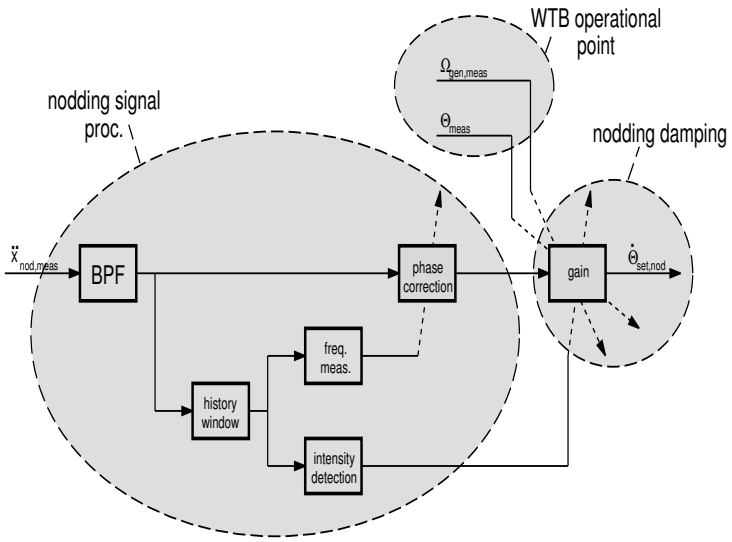

Figure 5.7: *Feedback control structure for improved damping of tower top nodding*

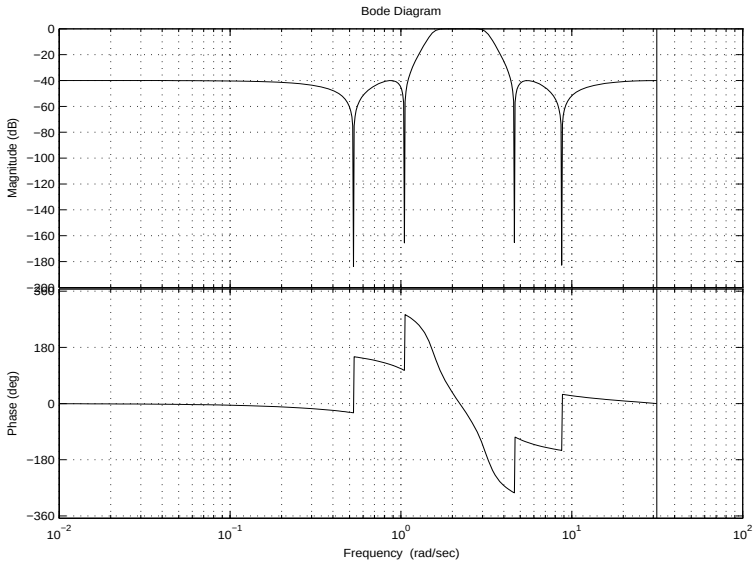

Figure 5.8: *Amplitude and phase diagram of 4^{th} order Inverse Chebychev band pass filter*

actual tower top accelleration, $\ddot{x}_{\rm nd}^{\rm cmp}$, exceeds a critical tower top acceleration level $\ddot{x}_{\rm nd}^{\rm lim}$. The following scheme is used for feedback gain in order to achieve pitch rates up to $\dot{\theta}^{\rm emg}$

$$\begin{cases} K_{\rm P}^{\ddot{x}_{\rm nd}} & \leq \frac{\dot{\theta}^{\rm full}}{\ddot{x}_{\rm nd}^{\rm cmp}}, \quad \text{if} \quad \ddot{x}_{\rm nd}^{\rm cmp} \leq \xi \cdot \ddot{x}_{\rm nd}^{\rm lim} \\ K_{\rm P}^{\ddot{x}_{\rm nd}} & \leq \frac{\dot{\theta}^{\rm emg}}{\ddot{x}_{\rm nd}^{\rm cmp}}, \quad \text{if} \quad \ddot{x}_{\rm nd}^{\rm cmp} > \xi \cdot \ddot{x}_{\rm nd}^{\rm lim} \end{cases} \tag{5.13}$$

The introduced quantity, $\ddot{x}_{\rm nd}^{\rm cmp}$, is defined as maximum level of the mean value (for two nodding periods) of the filtered tower top accelleration, while ξ is an arbitrary fraction (e.g. 90%) of $\ddot{x}_{\rm nd}^{\rm lim}$.

In addition, at an allowable tower top accelleration level ζ, at which $\ddot{x}_{\rm nd}^{\rm cmp} = 0.2 \cdot \ddot{x}_{\rm nd}^{\rm lim}$, active tower damping will not be effectuated to avoid loss of power production. The following scheme

is used for feedback gain in order to achieve pitch rates up to $\dot{\theta}^{\text{full}}$

$$\begin{cases} K_{\text{P}}^{\ddot{x}_{\text{nd}}} = 0, & \text{if } \ddot{x}_{\text{nd}}^{\text{cmp}} \leq \zeta \cdot \ddot{x}_{\text{nd}}^{\text{lim}} \\ K_{\text{P}}^{\ddot{x}_{\text{nd}}} = \frac{K_{\text{P}}^{*,\ddot{x}_{\text{nd}}}}{\ddot{x}_{\text{nd}}^{\text{lim}}} \cdot \left(\ddot{x}_{\text{nd}}^{\text{cmp}} - \ddot{x}_{\text{nd}}^{\text{lim}}\right) & \text{if } \zeta \cdot \ddot{x}_{\text{nd}}^{\text{lim}} < \ddot{x}_{\text{nd}}^{\text{cmp}} \leq 2\zeta \cdot \ddot{x}_{\text{nd}}^{\text{lim}} \\ K_{\text{P}}^{\ddot{x}_{\text{nd}}} = K_{\text{P}}^{*,\ddot{x}_{\text{nd}}} & \text{if } \ddot{x}_{\text{nd}}^{\text{cmp}} > 2\xi \cdot \ddot{x}_{\text{nd}}^{\text{lim}} \end{cases} \tag{5.14}$$

Fig.(5.9) shows the conditional gain factor for a normalised operation range $\ddot{x}_{\text{nd}}^{\text{cmp}}$ / $\ddot{x}_{\text{nd}}^{\text{lim}}$. The limiting 'curves' are described by eq.(5.13) for $\dot{\theta}^{\text{full}}$ = 4 $^{\text{o}}/\text{s}$ and $\dot{\theta}^{\text{emg}}$ = 10 $^{\text{o}}/\text{s}$). Eq.(5.14) defines the left area, until it is limited at χ, where $K_{\text{P}}^{*,\ddot{x}_{\text{nd}}}$ crosses $\ddot{x}_{\text{nd}}^{\text{lim}}$ at $\ddot{x}_{\text{nd}}^{\text{cmp}}$ = 0.5. Above the critical nodding level, $\ddot{x}_{\text{nd}}^{\text{lim}}$, the maximum (emergency) gain value shall be used to achieve maximal damping. A linear transition zone is used for gradual connection of the limiting curves.

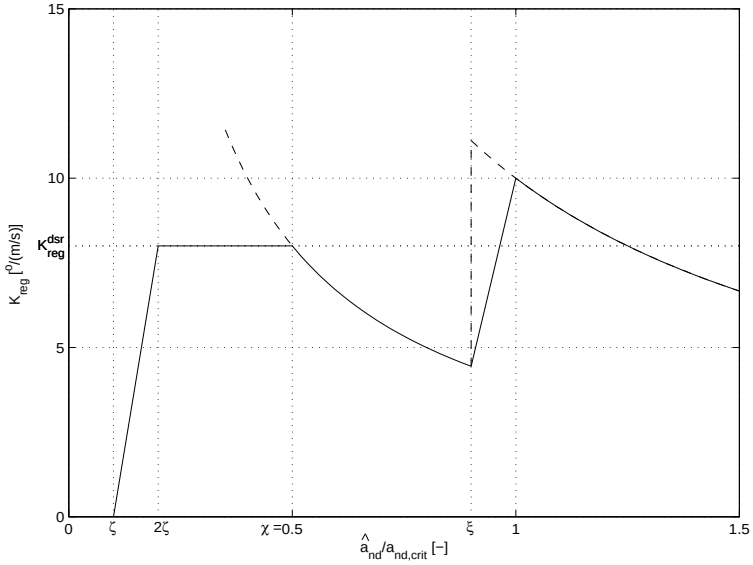

Figure 5.9: *Conditional limits of feed back gain factor,* $K_{\text{P}}^{\ddot{x}_{\text{nd}}}$

Scheduling: Eq.(5.10) shows that two aerodynamic gains are of relevance: $(F_{\text{a}})'_{\text{V}_{\text{w}}}$, and $(F_{\text{a}})'_{\theta}$. Both are dependent of the rotor speed, wind speed and pitch angle. If a constant damping ratio β_{t}^{*} in the whole operation region ($\zeta < \ddot{x}_{\text{nd}}^{\text{cmp}}/\ddot{x}_{\text{nd}}^{\text{lim}} < \chi$) is aimed, $K_{\text{P}}^{*,\ddot{x}_{\text{nd}}}$ will be also non-linear and operation point dependent: $K_{\text{P}}^{*,\ddot{x}_{\text{nd}}}$ (θ ,Ω_{r}); the dependancy of the wind speed is not taken into account.

A feasible damping ratio β_{t}^{*} is determined in advance from eq.(5.11) by using mean operation values $\overline{\Omega}_{\text{r}}$, $\overline{\theta}$ and the accompanying value of $K_{\text{P}}^{*,\ddot{x}_{\text{nd}}}$ at ξ. A non-linear expression for $K_{\text{P}}^{*,\ddot{x}_{\text{nd}}}(\theta,\Omega_{\text{r}})$ can be determined by using β_{t}^{*} in eq.(5.15)

$$K_{\text{P}}^{*,\ddot{x}_{\text{nd}}}(\theta,\Omega_{\text{r}}) = \frac{k_{\text{t}} + (F_{\text{a}})'_{\text{V}_{\text{w}}} - \beta_{\text{t}}^{*} \cdot 2\sqrt{m_{\text{t}} c_{\text{t}}}}{(F_{\text{a}})'_{\theta}} \tag{5.15}$$

Eq.(5.15) is shown in fig.(5.10) for the whole operation range. The grid is a fit by a 2D polynomial function, eq.(5.16), which will be used to pursue a constant damping ratio in the whole operation region.

$$K_{\text{P}}^{*,\ddot{x}_{\text{nd}}}(\tilde{\theta}^{\text{f}},\tilde{\Omega}_{\text{r}}^{\text{f}}) = \sum_{\text{i}=1}^{\text{N}_{\theta}+1} \sum_{\text{j}=1}^{\text{N}_{\Omega_{\text{r}}}+1} C_{\text{K}_{\text{P}}^{*,\ddot{x}_{\text{nd}}}}(i,j) \cdot \Omega_{\text{r}}^{(i-1)} \cdot \theta^{(j-1)} \tag{5.16}$$

A damping ratio $\beta_{\text{t}}^{*} \approx 0.15$, has appeared possible.

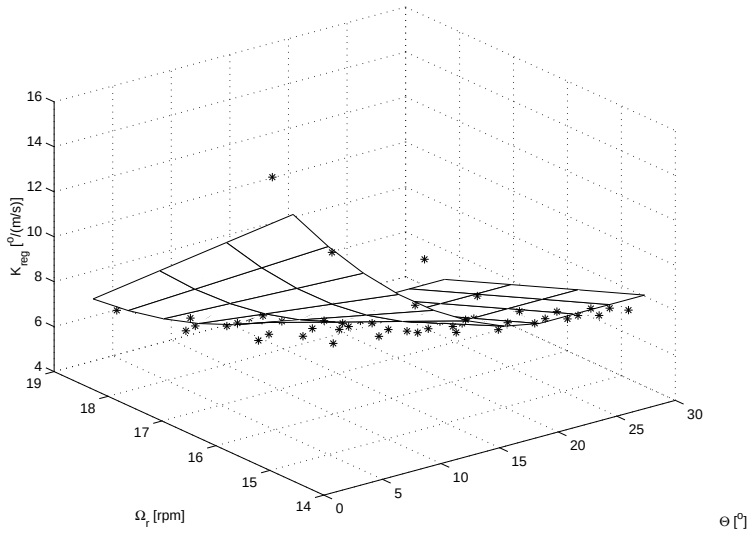

Figure 5.10: *Polynomial fit for $K_{\mathrm{P}}^{*,\ddot{x}_{\mathrm{nd}}}$,eq.(5.15)*

5.2.3 Time domain simulation and evaluation

Time domain simulation will show the behaviour of the improved damping structure as proposed before. To introduce considerable tower top accelleration, external forces by waves (subsection 2.3.2) were added and the simulation was calculated around cut-off wind speed. During simulation all pitch control features were incorporated (section 3.2), conventional generator control was applied (subsection 3.4.1) and drive train damping was included (section 5.1). Fig.(5.11) shows the nodding displacement, the pitch angle and pitch speed control with (dashed line) and without (solid line) the proposed structure. In the upper window the damping

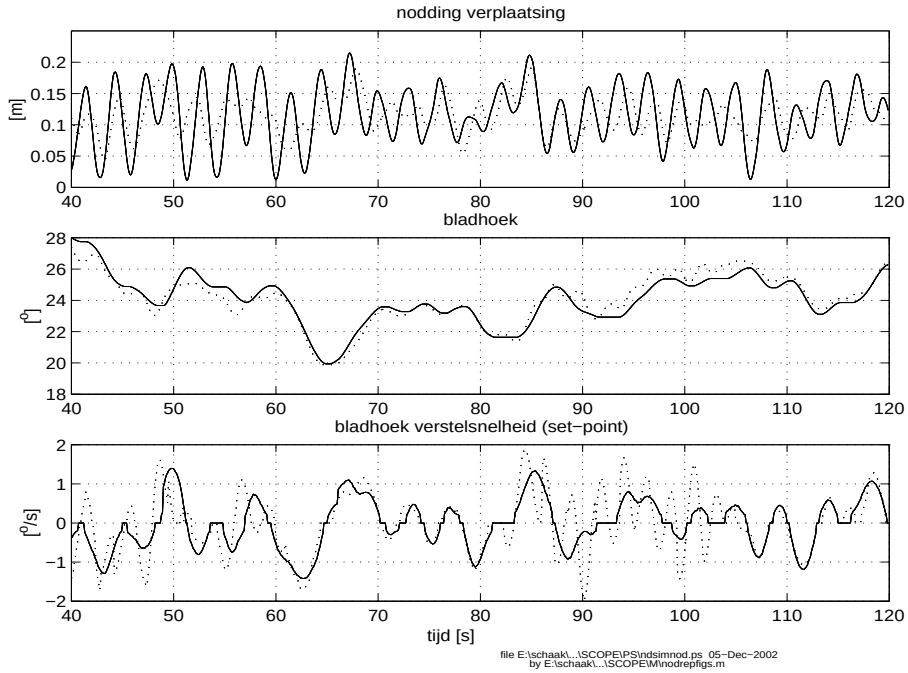

Figure 5.11: *Damping results of proposed damping feedback structure; with control (dashed line) and without control (solid) line)*

possibilities are proved and the additional pitch actuations (tower frequency) are clearly visible during the time intervals at which the conditional feedback loop is activated.

Fig.(5.12) shows the rotor speed and power production consequences as variations around rated ,with (dashed line) and without (solid line) the proposed structure. Although, difference in

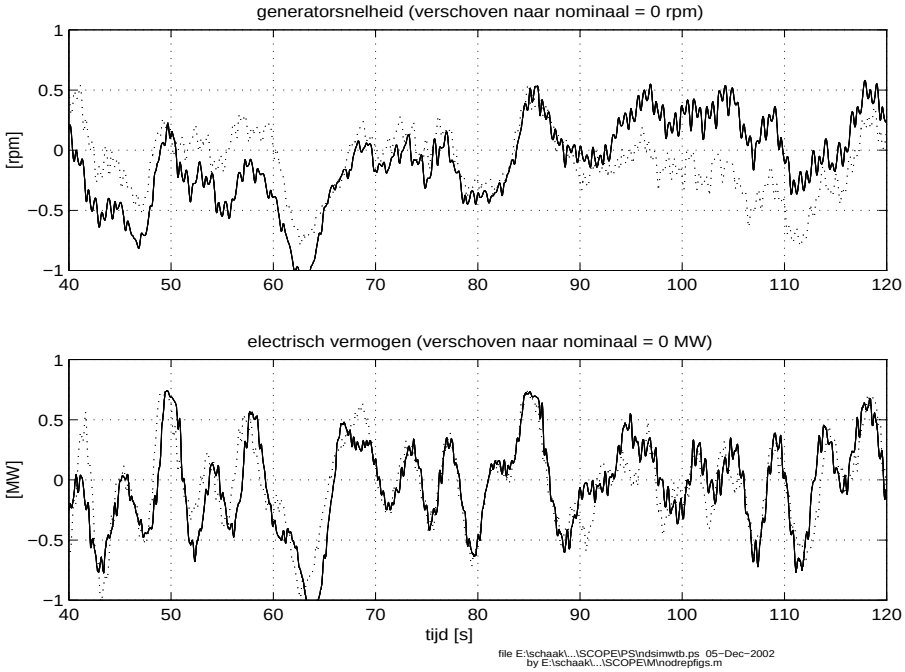

Figure 5.12: *Rotor speed and power variations of the proposed damping feedback structure; with control (dashed line) and without control (solid line)*

rotor speed is observed, control toward rated is maintained by the pitch control and generator control, just as power production. The shown deviations are attributed to the non-linear nature of the wind turbine; cumulation of small differences lead to different time realisations with preservation of 'typical' behaviour.

Promising results of the damping feedback structure for fore-aft tower movements have been achieved. Although, implementation and analysis in an aerodynamic code (Phatas) will be necessary to verify the control approach towards coupled system modes (tower, blades, drive train).

5.3 Improved damping in sideward direction

Reduction of sideward tower movements or 'naying' of the turbine will be important because they are naturally badly damped, due to the absence of aerodynamic rotor damping. Active damping possibilities by actuation of electric torque will be discussed in the next subsections.

5.3.1 Damping approach

Tower top displacements in sideward direction, are caused by drive train torque reactions and external forces of waves. Only structural damping $\beta_{\rm t}$ will reduce vibrations; because this is usually very small (0.005), additional damping is desired.

Similar to the approach on increase of damping in fore-aft direction, a velocity feedback loop from naying speed $\dot{x}_{\rm ny}$ to an additive electric torque setpoint $T^*_{\rm e,ny}$ will be clear. In practice, the measured tower top accelleration, $\tilde{\ddot{x}}_{\rm ny}$, will be used to determine an additive electric torque setpoint $T^*_{\rm e,ny}$, via a feedback gain $K_{\rm P}^{\ddot{x}_{\rm ny}}$. Therefore, $\tilde{\ddot{x}}_{\rm ny}$ should be (numerically) be integrated, which fortunately results in a smoothened signal. Fig.(5.13) illustrates the feedback approach in relation to existing control loops and relevant turbine dynamics:

- rotor speed control by pitch actuation, subsection 3.2.1;
- power production by generator control, subsection 3.4.1;
- first bending mode tower dynamics, eq.(2.18);
- tower excitation force, eq.(2.21).

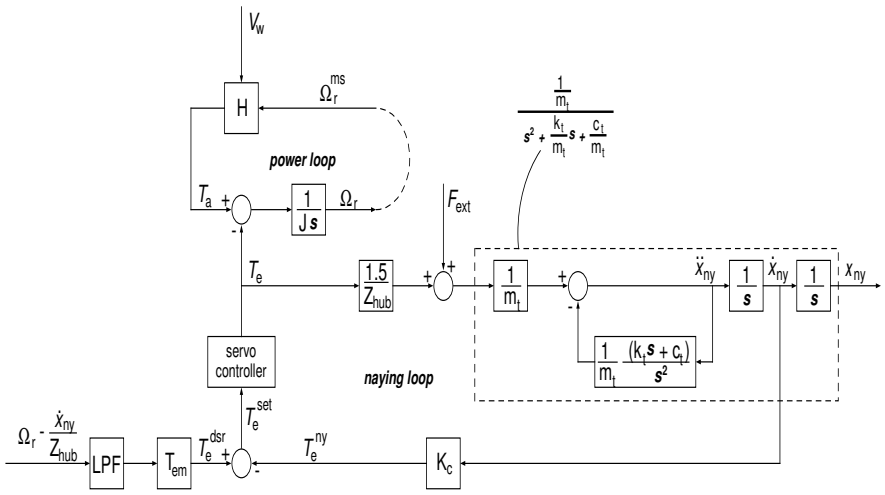

Figure 5.13: *Feedback control structure for improved damping of sideward tower vibrations.*

From eq.(2.18), eq.(2.21) and eq.(2.19) into the standard notation of a second order system, it can be easily found that:

$$\begin{aligned}\beta_{\rm t}^{\rm tot} &= \frac{1}{2\sqrt{m_{\rm t}c_{\rm t}}}\left(k_{\rm t}+\tfrac{3}{2}\frac{K_{\rm P}^{\ddot{x}_{\rm ny}}}{Z_{\rm t}}\right)\\ &= \beta_{\rm t}+\beta_{\rm t}^{\rm ctrl}\end{aligned} \tag{5.17}$$

In terms of a damping multiplication factor $\beta_{\rm t}^{\rm F}$ this can also be written as:

$$\beta_{\rm t}^{\rm tot} = \beta_{\rm t}^{\rm F}\cdot\beta_{\rm t} \tag{5.18}$$

$$\beta_{\rm t}^{\rm F} = 1+\tfrac{3}{2}\frac{K_{\rm P}^{\ddot{x}_{\rm ny}}}{k_{\rm t}Z_{\rm t}} \tag{5.19}$$

Similar to 'nodding', a simple second order system as given in eq.(5.20) appears to be sufficient to analyse active damping of tower vibrations [4]

$$\ddot{x}_{\mathrm{ny}} + \left(2\beta_{\mathrm{t}}^{\mathrm{tot}}\omega_0^{\mathrm{t}}\right) \cdot \dot{x}_{\mathrm{ny}} + \left(\omega_0^{\mathrm{t}}\right)^2 \cdot x_{\mathrm{ny}} = F_{\mathrm{ny}}^{\mathrm{top_{eq}}}/m_{\mathrm{t}}, \tag{5.20}$$

where $F_{\mathrm{ny}}^{\mathrm{top_{eq}}}$ is defined as tower top equivalent excitation force eq.(2.21) and ω_0^{t} the resonance frequency of the first (sideward) tower bending mode.

5.3.2 Feedback structure

The proposed feedback structure aims to improve the badly damped sideward tower resonances in order to reduce fatigue loading and to prevent turbine shut-down by the turbine safety system. This should be realised by improving the damping rate $\beta_{\mathrm{t}}^{\mathrm{tot}}$ to a maximum level, while causing as little as possible influences to power control and quality (fluctuation).

Stability analysis has been considered by comparison of the rotor speed loop with and without naying feedback loop. It has been proved that additional damping with realistic values of $\beta_{\mathrm{t}}^{\mathrm{F}}$ (10 ..100) have hardly influence on stability. It has also been proved that operation point dependency is not an issue; there's barely any relationship with the non-linear aerodynamics [4].

A restriction to the value of $K_{\mathrm{P}}^{\ddot{x}_{\mathrm{ny}}}$ is found in the maximum allowable power and torque fluctuations. A value of 10% seems to be practical due to drive train loading.

To deal with disturbing components, two filters are needed for proper damping effects

- a band pass filter in the feedback loop;
- a low pass filter in the torque setpoint loop for power production;

The band pass filter is implemented to intensify the natural concentration of velocity feedback around the eigenfrequency, ω_0^{t} . Be conscious that the tower naying itself act as a band pass filter around its eigen frequency. A first order elliptic filter with a passband $\omega_0^{\mathrm{t}} \pm 0.25\mathrm{rad/s}$, 20dB reduction and 2 dB ripple has emperically shown satisfied behaviour, because of less phase shift around ω_0^{t} .

The 'very low pass filter' in the torque setpoint loop should avoid any 'high' frequent effect to power production (setpoint raising) while phase shift is to be avoided for low frequencies (shift between rotor speed and torque). A high order invers Chebychev filter with cut-off frequency ω_0^{t}-0.5 rad/s and 10dB reduction gave good performance.

5.3.3 Evaluation

To evaluate the proposed feedback structure, the time domain performance with and without active damping was compared by (linear) simulation. The simulation was calculated for a different but similar turbine as described in chapter 2 at above rated wind speed (16m/s) and 'worst case' waves (20 depth) that hits the turbine with maximum energy at ω_0^{t} (see subsection 2.3.2). The feedback factor $K_{\mathrm{P}}^{\ddot{x}_{\mathrm{ny}}}$ was set to a value which results in $\beta_{\mathrm{t}}^{\mathrm{F}}$=15 (eq.(5.19)) and maximum allowable torque fluctuations of 10%.

Fig.(5.14) illustrates this comparison by showing the rotor speed, electric torque and naying acceleration (proportional with the in plane forces as experienced by the tower). The upper window proves that the rotor speed is hardly affected. The middle window visualises clearly the additional torque variations $T_{\mathrm{e,ny}}^{*}$ around the setpoint for power production (dotted line). The lower window shows that the absolute maximum of the naying acceleration is decreased by a factor 2.5 (60%).

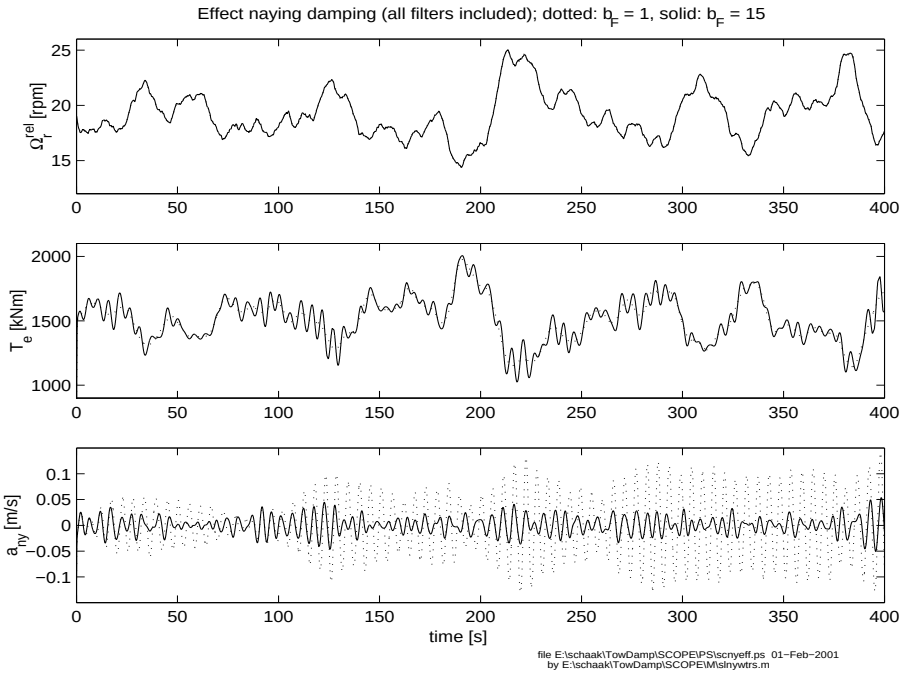

Figure 5.14: *Resulting time domain simulation with (solid line) and without (dotted line) naying feedback loop; tower excitation by waves at 16m/s mean wind speed*

6 CONCLUSIONS

DOWEC workpackage 1, task 3 has contributed to the

- set-up of a modular control structure based on theoretical analysis and industrial needs;
- increase of turbine performance (power production, load reduction) by additional control features and actions.

It can be concluded that the control structure is superior to ordinary PD feedback control of the rotor speed. An independent comparison study for the DOWEC turbine, using an aerodynamic code with a state-of-the-art control structure has resulted in improvements concerning:

- extreme fore-aft tower bending moment (-40%);
- fatigue fore-aft tower bottom bending equivalent moment (-50%);
- variations in blade pitch rate (standard dev. -0.65 dg/s);
- tilt moment (-10%).

The mean power production (10min) in above rated wind speeds was over 99% of its rated value. Opposite to the improvements it has brought about larger variations in generator speed (standard dev. +0.5 rpm), increase of yaw moment (12%) and radial blade forces (14%).

Increase of turbine performance can be particularly attributed to the following control features:

- dynamic inflow compensation (wake behaviour);
- enlarged control gain by advanced gain scheduling;
- improvement of full load power production and behaviour to wind gusts by wind speed feed forward control;
- smooth and production effective mode transition around rated conditions by mutual interaction between electric torque and pitch control;
- reduction of drive train vibrations by high frequent electric torque variations based on the estimated shaft distorsion speed (Kalman filter).

Optimisation of the control mode transition around rated by using small electric torque variations ($\pm$ 6%) gives a considerable improvement to the energy yield (+0.8%) *).

It has been shown that *wind speed feed forward control* enables an increase of energy yield of 0.9% (without optimisation around rated) *).

The use of a Kalman filter, which estimates the main shaft distorsion from the generator speed, has resulted in a reduction of the shaft loading by 50%, using a torque servo bandwidth of only 6Hz.

In addition, promising examinations on suppression of tower resonances in both fore-aft and sideward directions were made by pitch angle and electric torque variations, respectively.

*) these improvements are related to de-activation of the concerning control action with respect to its active situation.

REFERENCES

[1] Int. Electrotechnical Commission. Wind turbine generator systems - part 1: Safety requirements. Technical Report IEC 61400-1, IEC, February 1999.

[2] E.L. van der Hooft. Actieve demping via bladhoek van voor- en achterwaartse torentrillingen. Technical Report Internal document, ECN Petten, April 2000.

[3] E.L. van der. Hooft. Dowec blade pitch control algoriths for blade optimisation purposes. Technical Report ECN-CX–00-083, ECN Petten, February 2001.

[4] P. Schaak. Demping van zijwaartse torenbuiging via generatorkoppel. Technical Report Internal document, ECN Petten, June 2001.

[5] P. Schaak. Bladhoek geregelde demping van axiale torentrillingen bij windturbines. Technical Report ECN-C–03-134, ECN Petten, December 2003.

[6] P. Schaak. Koppelregeling van variabel-toeren windturbines. Technical Report ECN-C–03-136, ECN Petten, December 2003.

[7] H. Schepers J.G. Snel. Engineering models for dynamic inflow phenomena. Technical Report Journal of Wind Engineering and Industrial Aerodynamics, 39, p267-p281, Elsevier Science Publishers B.V. Amsterdam, 1992.

[8] P. Schaak T.G. van Engelen E.L. van der Hooft and E.J. Wiggelinkhuizen. Ontwikkeling van een gereedschap voor het ontwerpen van windturbine regelingen - fase 1. Technical Report ECN-C–03-133, ECN Petten, In preparation to issue 2004.

[9] T.G. van Engelen P. Schaak and C. Lindenburg. Control for damping the fatigue relevant deformation modes of offshore wind turbines. Technical Report ECN-C–03-136, ECN Petten, December 2003.

[10] James F. Wilson. Dynamics of offshore structures. Technical Report ISBN 0-471-87568-6, John Wiley and Sons, 1984.

	Date: December 2003	**Report No.:** ECN-C--03-111
Title	Wind turbine control algorithms	
Author	E.L. van der Hooft; P. Schaak; T.G. van Engelen	
Principal(s)	DOWEC	
ECN project number	7.4218	
Principal's order number	EETK98031/398410-0810	
Programmes	EET	

Abstract

The objective of DOWEC task 3 of work package 1 has been defined as 'research and development of wind turbine (power) control algorithms to maximize energy yield and reduction of turbine fatigue load, and its optimisation for offshore operation'. In accordance with the DOWEC baseline turbine and the related DOWEC turbine all activities were focused on active pitch to vane, variable speed concept. The results of this task contribute to the:

- set-up of a modular control structure based on theoretical analysis and industrial needs;
- increase of turbine performance (power production, load reduction) by additional control features and actions.

It can be concluded that the control structure is superior to ordinary PD feedback control of the rotor speed. An independent comparison for the DOWEC turbine using an aerodynamic code, with a state-of-the-art control structure, has resulted in improvements concerning:

- extreme fore-aft tower bending moment (-40%);
- fatigue fore-aft tower bottom bending equivalent moment (-50%);
- variations in blade pitch rate (standard dev. -0.65 dg/s);
- tilt moment (-10%).

The mean power production (10min) in above rated wind speeds was over 99% of its rated value. Opposite to the improvements it has brought about larger variations in generator speed (standard dev. +0.5 rpm), increase of yaw moment (12%) and radial blade forces (14%).

The underlying approach of the control structure divides the multivariable wind turbine system into different independent scalar subsystems by band filtering. As a consequence the resulting setpoints, the pitch rate and electric torque, consist of additive contributions of the different control actions.

Concerning power control, ordinary rotor speed feedback has proved to be a robust core. However, valuable extensions were developed by wind speed feed forward control (pitch control) and optimisation around rated condition (electric torque control).

Promising results have been achieved on fore-aft tower damping by pitch control. Electric torque control has enabled considerable damping results of (collective) drive train resonances and possibilities for badly damped sideward tower vibrations.

Keywords

DOWEC, Wind turbine control, Pitch Control, Power Control, Torque Control, Variable speed control

Authorization	**Name**	**Signature**	**Date**
Checked	T.G. van Engelen		
Approved	H.B. Hendriks		
Authorised	H.J.M Beurskens		